MOLECULAR MECHANISMS OF NUCLEATION AND GROWTH OF CLATHRATE HYDRATES

by

Liam Christopher Jacobson

A dissertation submitted to the faculty of
The University of Utah
in partial fulfillment of the requirements for the degree of

Doctor of Philosophy

Department of Chemistry

The University of Utah

August 2011

The University of Utah Graduate School

STATEMENT OF DISSERTATION APPROVAL

The dissertation of **Liam Christopher Jacobson**

has been approved by the following supervisory committee members:

Valeria Molinero	, Chair	**5/23/2011** Date Approved
Jack Simons	, Member	**5/23/2011** Date Approved
Michael D. Morse	, Member	**5/23/2011** Date Approved
Jennifer Shumaker-Parry	, Member	**5/23/2011** Date Approved
Thomas Cheatham	, Member	**5/23/2011** Date Approved

and by **Henry White**, Chair of the Department of **Chemistry**

and by Charles A. Wight, Dean of The Graduate School.

ABSTRACT

Clathrate hydrates are a crystalline phase of water in which the hydrogen bond network forms polyhedral cages that can trap nonhydrogen bonding molecules such as methane and carbon dioxide. Methane clathrate hydrates occur naturally on the ocean floor and are so abundant that it is estimated they contain more energy than the rest of the world's hydrocarbon reserves combined. As a result, methods to promote and inhibit the formation of clathrates are highly sought after. However, a detailed understanding of the microscopic mechanism of clathrate nucleation remains elusive. Experimental techniques are unable to resolve the structure of clathrate nuclei. Simulations provide an alternative, but nucleation is a stochastic event and the computational cost to observe nucleation events can be prohibitive.

In this work we studied the mechanism of clathrate hydrate nucleation with molecular simulations using an efficient coarse-grained model mW that represents water as a single site that is encouraged to form "hydrogen-bonded" configurations without the use of hydrogen atoms. The coarse-grained model allows the observation of many more nucleation events than is possible with atomistic models.

Using the coarse-grained water model and guest potentials, we studied the nucleation of clathrate hydrates at supercooled conditions. The nucleation mechanism we observed is a multistep mechanism with an amorphous intermediate that we call "the blob." The first step in the nucleation is the densification of guest molecules in solution to form long-lived solvent-separated configurations. These persist in solution and give rise to the formation and

dissolution of individual cages. Once "the blob" is large enough, it eventually forms persistent polyhedral cages. The critical nucleus is defined by the solvent-separated guest molecules and polyhedral water cages. The clathrate at this point is amorphous and lacks the symmetry of the crystalline clathrate, but is made of the same building blocks. We find that an amorphous clathrate seed is able to nucleate the formation of crystalline clathrates. We develop order parameters for the densification of guest molecules in solution, the identification of polyhedral cages, and the crystallinity of the clathrate phase. These order parameters will be useful for describing the reaction coordinate of clathrate nucleation at low driving force.

TABLE OF CONTENTS

ACKNOWLEDGEMENTS

I would like to thank my advisor Valeria Molinero for allowing me to join her group even though I was in a different school in another state, and then letting me change my research topic to something completely new. I am especially thankful to Waldemar Hujo for writing the code that enabled us to find the clathrate cages. I would also like to thank my fellow group members who helped me with technical issues as well as moral support: Emily Moore, Noah Kastelowitz, Robert Demille, Diane Neff, and Jessica Johnston. I also greatly appreciate the expert technical assistance of the CHPC staff. Finally, I'd like to thank my parents for support throughout my academic career and my brother Michael Jacobson who led the way and showed me that graduate school was even an option.

CHAPTER 1

INTRODUCTION AND OVERVIEW

Clathrate hydrates are a crystalline phase of water in which the hydrogen bond network forms polyhedral cages that can trap nonpolar molecules such as methane and carbon dioxide to form nonstoichiometric solids. In general, the guest molecules enclathrated by the water lattice do not compete with the hydrogen bonding interactions that form the tetrahedrally coordinated water lattice, with the exception of semiclathrates, in which the guests are also part of the hydrogen-bonded network.[1,2] Just as in ice, each water molecule in the clathrate hydrate lattice is four-coordinated to neighboring water molecules. Clathrates are stable at high pressures, and only form in the presence of guest molecules. Even though hydrophobic guest molecules such as methane are only slightly soluble in water, they form clathrate crystals in which the concentration of methane in the clathrate is 1000 times greater than it is in solution. Therefore, a fundamental question addressed in this dissertation is how clathrate hydrates form if the guest molecules are so insoluble.

Methane clathrates form naturally on the ocean floor and represent the most abundant source of hydrocarbon energy on the planet, with some estimates suggesting that there is more energy stored in clathrates than in all other hydrocarbon sources on the planet combined.[3] Clathrate plug formation in high-pressure pipelines presents a major challenge to the petroleum industry that results in lost revenue from work stoppage and safety issues.[4] Clathrates are also being considered for carbon sequestration,[5] through injection of carbon dioxide in natural gas clathrates, as the carbon dioxide clathrate is more stable than the

methane clathrate. A major impediment to harnessing the promise of clathrate hydrates is the slow formation kinetics[6,7] and a lack of understanding of the mechanisms of clathrate crystallization.[8-10]

Van der Waals and Platteeuw developed a statistical mechanical model to study the equilibrium thermodynamics of clathrate hydrates.[11] The statistical mechanical approach of van der Waals and Platteeuw was modified and extended to accurately determine the chemical potential of clathrates of a variety of guest molecules and has been implemented into the software package CSMGem to accurately predict the phase diagram of clathrates.[12] Although the thermodynamics of clathrates are well established, the kinetics and mechanism of clathrate formation are still poorly understood.[10] As such there is a great amount of interest to better understand the mechanism of clathrate nucleation in order to both prevent and promote clathrate formation.

Before the work presented in this dissertation, there were two primary hypotheses in the literature on the microscopic mechanism of nucleation of clathrates. The first was the Labile Cluster Hypothesis (LCH) proposed by Sloan and coworkers,[10] which describes the mechanism of clathrate nucleation as taking place through the formation of individual polyhedral cages around the dissolved guest molecules. LCH postulates that these individual polyhedral water cages are stable enough in solution to diffuse and agglomerate to form a critical nucleus that then allows for the growth of the clathrate phase. Molecular simulations, performed after LCH was proposed, indicate that the individual cages are not stable in solution[13] and do not survive long enough to agglomerate.[14]

The Local Structuring Hypothesis (LSH) described by Trout and coworkers[13] and similarly by Rodger and coworkers[15] proposes that fluctuations of guest molecules in solution create clusters in which the guest molecules are in configurations that are close

enough to the positions that they have in the clathrate crystals that the water molecules quickly reorganize to form the critical nucleus. However, observations of clathrate nucleation in molecular dynamics simulations show that the clathrate nuclei do not have the same symmetry as the stable crystal, but rather they are an amorphous mixture of polyhedral cages with structural motifs from both clathrate structures.[16-18] Clathrate hydrates primarily form two cubic structures known as sI and sII. The sI crystal is stable with respect to the sII crystal for methane hydrate. Even so, experimental observations show that both sI and sII crystals form in the initial stages of methane hydrate growth.[19,20] Simulations indicate that $5^{12}6^3$ cages form at the interface between these two crystals.[19]

Current state of the art experimental techniques are unable to resolve the nascent clathrate nuclei.[20] Therefore, molecular simulations represent an effective alternative to understand the pathway of nucleation for the clathrates. Although molecular simulations have given great insight into the structure,[19,21-24] thermodynamic stability,[25-32] thermal conductivity,[33,34] mobility,[35,36] growth,[37-39] decomposition,[40-42] and nucleation[13,15,16,43-46] of clathrate hydrates, a thorough understanding of the mechanism of nucleation remains elusive because of the stochastic nature of nucleation and long timescales needed to observe nucleation events in simulations. Nucleation is a stochastic event and as a result, the resources needed to observe a nucleation event in a simulation can be prohibitive, especially when multiple nucleation events are needed for a statistical analysis. For instance, one nucleation event in an atomistic simulation required more than a microsecond of simulation time, which represented several months of CPU time on a supercomputer.[17]

To address the limitations of atomistic force fields in observing stochastic nucleation events, we use a coarse-grained model of water, the monatomic water model mW, in which the water molecules are represented as single sites that are encouraged to form "hydrogen-

bonded" tetrahedral configurations by including a three-body interaction.[47] The mW water model has proven successful in reproducing the structure of liquid water and ice, as well as the melting temperature and enthalpy of melting of ice with the same or better accuracy than the most popular atomistic models of water.[47,48]

Substances such as H_20, SiO_2, Si and Ge that form tetrahedral crystals also form clathrates.[49] Although a guest-free clathrate has not been observed for water, guest-free clathrates have been made with Ge[50] and Si.[51] Since water, silicon and germanium form similar structures and have related phase diagrams,[47,52,53] empty water clathrates may also be possible to produce experimentally. An empty water clathrate lattice would be the lowest density ice phase of water. Such a low-density phase would only be thermodynamically favored by low or negative pressures; thus the empty water clathrates may be a stable crystal of water under extension. Water can undergo extension to negative pressures until it reaches the cavitation limit, but such conditions are difficult to attain in experiment.[54] In Chapter 2, we use the coarse-grained mW model to calculate the regions of stability of the empty sII clathrate lattice. We also determined the equilibrium melting temperatures of the empty sI and sII clathrates for the first time. We find that he empty clathrates are metastable with respect to ice at positive pressures and at negative pressures they become the stable phase. Conde et al. calculated the phase diagram of the empty clathrates with an all-atom potential for water and also found that at negative pressures, the empty sII lattice becomes the stable phase of water.[31] The implications of the work in Chapter 2 suggest that the clathrates do not need guest molecules present in the cages to grow at temperatures at which the empty clathrates are stable, but require the guest molecules to nucleate from solution. We propose two experimental avenues to produce the empty clathrates in the laboratory. The first method involves producing a (filled) hydrogen clathrate hydrate and allowing the hydrogen

guest molecules to diffuse out at low temperature and pressure. The second method to produce empty clathrates involves the vapor deposition of water molecules on a template of filled clathrates.

In Chapter 3, we present the development of a coarse-grained methane potential and parameterize the water-methane and methane-methane interactions. The coarse-grained potential is about 200 to 1000 times computationally more efficient than atomistic potentials with Ewald sums. Typically when someone performs a simulation of water and methane, they use existing water and methane potentials and employ Lorentz-Berthelot combination rules for the water-methane interaction potentials without validating them with experimental observables such as solubility, hydration number, enthalpy of melting and melting temperature of the clathrate. Docherty et al. showed that using combination rules to determine water-methane interactions is unable to reproduce the chemical potential of methane in solution, using even the most accurate water and methane potentials.[55] The melting temperature of sI methane hydrate is known for only a few atomistic force-fields,[58-60] and in these instances the melting temperature of the sII methane clathrate remains unknown. The methane-water potential developed in Chapter 3 accurately reproduces the experimental solubility and hydration number of methane in solution. In addition, another important factor that is commonly overlooked when using interaction potentials to model clathrate nucleation and growth is the identity of the stable clathrate phase. When the work in Chapter 3 was first published, it was the first instance of determining the absolute and relative stability of the sI and sII clathrate crystals in molecular simulations. The methane-water potential of Chapter 3 correctly predicts that sI is the stable structure. This is important to know when studying the nucleation and growth so that the effect of metastable

phases can be considered. The methane-water potential developed in chapter 3 should be useful not only for clathrates, but for studies of hydrophobic hydration as well.

Molecular simulations have been used to ascertain the viability of the Labile Cluster Hypothesis and the Local Structuring Hypothesis. Guo et al. searched simulations of methane in solution for polyhedral cages surrounding single methane molecules that would make up the labile clusters and found that they only form with a probability of 10^{-6}.[14] In a separate study, they showed that the lifetime of a dodecahedral cage in solution increases exponentially with the number of methane molecules surrounding it.[46] Rodger and coworkers[15,16,43-45] and, more recently, Walsh et al.[17] observed spontaneous methane hydrate nucleation in atomistic molecular dynamics simulations using conditions of high driving force. In each case, the result is an amorphous clathrate nucleus.

In Chapter 4, we investigate the mechanism of nucleation of clathrates, and unravel a multistep pathway of clathrate nucleation involving a long-lived amorphous intermediate that we call "the blob." The multistep mechanism of clathrate nucleation is a departure from classical nucleation mechanisms in which the nucleus already has the structure of the stable phase, and has strong commonalities with multistep mechanisms for the crystallization of proteins, colloids, and $CaCO_3$.[56-59] The "blob hypothesis," as we call it, is a novel mechanism for the nucleation of clathrate hydrates that synthesizes elements from both the labile cluster and local structuring hypotheses. The first step of the blob mechanism involves the densification of guest molecules in solution to form solvent-separated clusters of guests. These clusters of solvent-separated guests (the blobs) are long-lived, on the order of several nanoseconds, and the reordering of the water molecules within the blob gives rise to the formation of polyhedral water cages. Initially, the cages are transient, but as the blob intermediate gets bigger, the cages persist and eventually the nucleus reaches a critical size

and growth of the clathrate phase occurs. Our simulations indicate that the stability of the blob arises from guest molecules in solvent-separated configurations. This is supported by work of Matsumoto, who computed the multi-body potentials of mean force between methane molecules in water and showed that for clusters containing four methane molecules, the solvent-separated configurations are more stable than configurations with the methane molecules in contact.[60] The resulting clathrates of this initial study at high supercooling were amorphous, and there was no reorganization to the crystalline phase on the timescale of the simulations. Since the publication of the work in Chapter 4, Vatamanu and Kusalik also observed a multistep mechanism of crystallization involving amorphous clathrate intermediates using a different model and methods.[18] The reorganization of amorphous clathrates to crystalline clathrates at highly supercooled temperatures is too slow to be observed in molecular dynamics simulations, but can be observed after annealing the system at higher temperatures.[61]

Previously, molecular simulations have only been used to study the nucleation of clathrates with methane or carbon dioxide guest molecules. In Chapter 5, we investigate the effect of the size and solubility of the guests in the pathways of clathrate nucleation. We found that the main difference in the pathway to nucleation of the hydrophilic compared to the hydrophobic guest molecules is that the hydrophobic guest molecules rely on the rare event of the insoluble guest molecules finding each other in solution versus the hydrophilic guest molecules waiting for the rare event of being pulled apart into solvent-separated configurations. An important finding of our work presented in Chapter 4 is that kinetic factors promote the formation of cages in a ratio that is not predicted by the Boltzmann statistics using equilibrium stabilization energies of guests filling the cages. We find that the formation of dodecahedral cages dominates for all solutes regardless of which is the most

stable cage. The most novel contribution of the work presented in Chapter 5 is the important role of empty dodecahedral cages in the nucleation of the clathrate phase. Solvent-separated clusters of guest molecules that are too large to fit in the dodecahedral cages result in the formation of networks of face-sharing empty dodecahedra surrounded by guest molecules rather than filled larger cages. This is in accordance with other studies that find the nucleation of hydrates of small guests is initiated primarily through the formation of dodecahedral cages.[15-17,45]

Simulations of nucleation of colloids and globular proteins with attractive, short-ranged interactions show a multistep mechanism of nucleation with an amorphous intermediate that form below a fluid-fluid coexistence line, where the free energy of the dense, disordered intermediate form is lower than for the solution.[57,62] Recent simulations indicate that the dense, disordered phase could also be an intermediate above the fluid-fluid coexistence line where it is unstable.[58,63] This suggests that amorphous intermediates could form in the nucleation pathway at low driving force. Therefore, it is important to elucidate the stability of amorphous nuclei and determine whether amorphous clathrates can grow the crystal phase. In Chapter 6, we determined the size of the critical crystalline and amorphous clathrate nuclei as a function of temperature. We found that the relation between radius of the nucleus and temperature of dissociation and growth follows the Gibbs-Thomson relation for spherical particles. Using the Gibbs-Thomson relation and the enthalpies of melting, we determined the solid-liquid surface tension for both the crystalline and amorphous clathrates. We found that at any given temperature, the radii of the critical amorphous nuclei are always larger than for the crystalline nuclei, the difference being the most pronounced for lower driving forces. This finding is substantial, considering that the products of clathrate nucleation observed in simulations at high driving force are not

crystalline, but amorphous. This suggests that at high driving force lower kinetic barriers favor a pathway to nucleation through the formation of the larger amorphous clathrates. The importance of the amorphous clathrates in the nucleation of the clathrates is something that was not discussed prior to the work put forth in this thesis. One of the important questions raised as a result of the work in Chapter 4 is how does the amorphous clathrate intermediate transform into a crystalline clathrate. The work in Chapter 6 demonstrates that crystalline clathrates can grow from an amorphous seed.

Finally, in Chapter 7, we develop novel order parameters (OP) to follow the nucleation and growth of clathrate hydrates. These order parameters include the number of polyhedral cages, the crystallinity of the clathrate phase, and the clustering and connectivity of the guest molecules in solution. Through the use of an order parameter to identify clusters of guest molecules in solution in solvent-separated configurations, we determine that the formation of the clusters of solvent-separated guests precedes the formation of clathrate cages. The use of order parameters that can distinguish between the different crystalline structures of clathrates (i.e., sI, sII, and amorphous) is important if the role of metastable structures in the nucleation pathway of clathrate hydrates is to be understood. In this work we develop the first order parameters able distinguish between sI, sII and amorphous clathrates. These OP can be implemented both as local or global variables, and should be an asset in subsequent studies of the mechanisms of nucleation and growth of clathrate hydrates and the underlying mechanisms of polymorph selection in hydrates.

The use of a very efficient coarse-grained model has enabled a better understanding of the mechanism of clathrate nucleation. However, in this work we only investigated clathrate nucleation at high driving force. Further work is still needed to completely understand the pathway to nucleation, especially at low driving forces. To do so, it will be

necessary to use enhanced sampling techniques such as transition path sampling,[69-72] aimless shooting,[64,65] transition interface sampling,[66,67] forward flux sampling[68-70] or metadynamics.[71,72] Such methods require the use of various order parameters in order to accurately describe the reaction coordinate, and the efficiency of the methods is dependent on the choice of order parameters.[68,69,73,74] The order parameters developed and discussed in this thesis should provide a valuable set of analysis tools for further study of clathrate nucleation. Order parameters have been previously proposed to characterize the crystallization of clathrates from aqueous solutions.[13,15,16,75-77] Although some of these order parameters are able to identify regions of solid clathrate, they are unable to distinguish between amorphous and crystalline clathrate as well as the different crystal polymorphs. The order parameters described in Chapter 7 are able to differentiate the dilute solution, crystalline clathrate and amorphous intermediate clathrate, which represent the basins of configurational space that correspond to the reactants, products and intermediates in the pathway of clathrate nucleation.

Coarse-grained models evolve in smoother potential energy surfaces than fully atomistic models. As a result, an accurate pathway to nucleation can be extracted using a coarse-grained model, but the rates will not be accurate. A multiscale approach that bridges the coarse-grained and atomistic potential energy surfaces may provide an efficient route to first discover the reaction coordinate of clathrate nucleation and then further refine the sampling of the important regions of the potential energy surface with increasing atomistic detail.

In addition to working with my advisor Valeria Molinero, I was also aided by two additional coauthors for several papers written during the coarse of my graduate career. Waldemar Hujo is a coauthor of the work published in Chapters 2, 4, and 5. He wrote the

algorithm to identify the polyhedral cages in molecular configurations. Masakazu Matsumoto is a coauthor in Chapter 7. He identified the unique chemical environments that water molecules occupy in each clathrate crystal. He also wrote the original ring identification algorithm that Waldemar Hujo based his cage identification algorithm on.

References

(1) McMullan, R.; Jeffrey, G. A. *J. Chem. Phys.* **1959**, *31*, 1231.

(2) Shin, K.; Kim, Y.; Strobel, T. A.; Prasad, P. S. R.; Sugahara, T.; Lee, H.; Sloan, E. D.; Sum, A. K.; Koh, C. A. *J. Phys. Chem. A* **2009**, *113*, 6415.

(3) Sloan, E. D. *Nature* **2003**, *426*, 353.

(4) Koh, C. A.; Sum, A. K.; Sloan, E. D. *J. Appl. Phys.* **2009**, *106*, 061101.

(5) Brewer, P. G. *Ann. N. Y. Acad. Sci.* **2000**, 195.

(6) Abbondondola, J. A.; Fleischer, E. B.; Janda, K. C. *J. Phys. Chem. C* **2009**, *113*, 4717.

(7) Gulluru, D. B.; Devlin, J. P. *J. Phys. Chem. A* **2006**, *110*, 1901.

(8) Koh, C. A. *Chem. Soc. Rev.* **2002**, *31*, 157.

(9) Wang, X.; Schultz, A. J.; Halpern, Y. *J. Phys. Chem. A* **2002**, *106*, 7304.

(10) Sloan, E. D.; Koh, C. A. *Clathrate Hydrates of Natural Gases*, 3rd ed.; CRC Press/Taylor-Francis: Boca Raton, 2007.

(11) van der Waals, J. H.; Platteeuw, J. C. *Adv. Chem. Phys.* **1959**, *2*, 1.

(12) Ballard, A. L.; Sloan, E. D. *J. Supramol. Chem.* **2002**.

(13) Radhakrishnan, R.; Trout, B. L. *J. Chem. Phys.* **2002**, *117*, 1786.

(14) Guo, G. J.; Zhang, Y. G.; Li, M.; Wu, C. H. *J. Chem. Phys.* **2008**, *128*, 8.

(15) Moon, C.; Taylor, P. C.; Rodger, P. M. *J. Am. Chem. Soc.* **2003**, *125*, 4706.

(16) Hawtin, R. W.; Quigley, D.; Rodger, P. M. *Phys. Chem. Chem. Phys.* **2008**, *10*, 4853.

(17) Walsh, M. R.; Koh, C. A.; Sloan, E. D.; Sum, A. K.; Wu, D. T. *Science* **2009**, *326*, 1095.

(18) Vatamanu, J.; Kusalik, P. G. *Phys. Chem. Chem. Phys* **2010**, *12*, 15065.

(19) Vatamanu, J.; Kusalik, P. G. *J. Am. Chem. Soc.* **2006**, *128*, 15588.

(20) Sum, A. K.; Koh, C. A.; Sloan, E. D. *Ind. Eng. Chem. Res.* **2009**, *48*, 7457.

(21) Koga, K.; Tanaka, H.; Nakanishi, K. *J. Chem. Phys.* **1994**, *101*, 3127.

(22) Alavi, S.; Ripmeester, J. A.; Klug, D. D. *J. Chem. Phys.* **2006**, *124*.

(23) Jiang, H.; Jordan, K. D.; Taylor, C. E. *J. Phys. Chem. B* **2007**, *111*, 6486.

(24) Anderson, B. J. *Fluid Phase Equilib.* **2007**, *254*, 144.

(25) Susilo, R.; Alavi, S.; Ripmeester, J.; Englezos, P. *Fluid Phase Equilib.* **2008**, *263*, 6.

(26) Ota, M.; Ferdows, M. *Jsme International Journal Series B-Fluids and Thermal Engineering* **2005**, *48*, 802.

(27) Okano, Y.; Yasuoka, K. *J. Chem. Phys.* **2006**, *124*.

(28) Miyoshi, T.; Imai, M.; Ohmura, R.; Yasuoka, K. *J. Chem. Phys.* **2007**, *126*, 234506.

(29) Katsumasa, K.; Koga, K.; Tanaka, H. *J. Chem. Phys.* **2007**, *127*.

(30) Alavi, S.; Klug, D. D.; Ripmeester, J. A. *J. Chem. Phys.* **2008**, *128*.

(31) Conde, M. M.; Vega, C.; Tribello, G. A.; Slater, B. *J. Chem. Phys.* **2009**, *131*, 034510.

(32) McCarthy, V. N.; Jordan, K. D. *Chem. Phys. Lett.* **2006**, *429*, 166.

(33) Jiang, H.; Myshakin, E. M.; Jordan, K. D.; Warzinski, R. P. *J. Phys. Chem. B* **2008**, *112*, 10207.

(34) Inoue, R.; Tanaka, H.; Nakanishi, K. *J. Chem. Phys.* **1996**, *104*, 9569.

(35) Peters, B.; Zimmermann, N. E. R.; Beckham, G. T.; Tester, J. W.; Trout, B. L. *J. Am. Chem. Soc.* **2008**, *130*, 17342.

(36) Alavi, S.; Ripmeester, J. A. *Angewandte Chemie International Edition* **2007**, *46*, 6102.

(37) Luis A, B.; Paulette, C. *Ann. N. Y. Acad. Sci.* **1994**, *715*, 177.

(38) Vatamanu, J.; Kusalik, P. G. *J. Phys. Chem. B* **2008**, *112*, 2399.

(39) Nada, H. *J. Phys. Chem. B* **2006**, *110*, 16526.

(40) Rodger, P. M.; Forester, T. R.; Smith, W. *Fluid Phase Equilib.* **1996**, *116*, 326.

(41) Ding, L. Y.; Geng, C. Y.; Zhao, Y. H.; Wen, H. *Mol. Simul.* **2007**, *33*, 1005.

(42) English, N. J.; Johnson, J. K.; Taylor, C. E. *J. Chem. Phys.* **2005**, *123*, 12.

(43) Moon, C.; Taylor, P. C.; Rodger, P. M. *Can. J. Phys.* **2003**, *81*, 451.

(44) Moon, C.; Hawtin, R. W.; Rodger, P. M. *Faraday Discuss.* **2007**, *136*, 367.

(45) Zhang, J. F.; Hawtin, R. W.; Yang, Y.; Nakagava, E.; Rivero, M.; Choi, S. K.; Rodger, P. M. *J. Phys. Chem. B* **2008**, *112*, 10608.

(46) Guo, G. J.; Zhang, Y. G.; Liu, H. *J. Phys. Chem. C* **2007**, *111*, 2595.

(47) Molinero, V.; Moore, E. B. *J. Phys. Chem. B* **2009**, *113*, 4008.

(48) Moore, E. B.; Molinero, V. **2010**, *to be submitted.*

(49) San-Miguel, A.; Toulemonde, P. *High Pressure Research* **2005**.

(50) Guloy, A. M.; Ramlau, R.; Tang, Z. J.; Schnelle, W.; Baitinger, M.; Grin, Y. *Nature* **2006**, *443*, 320.

(51) Nolas, G. S.; Beekman, M.; Gryko, J.; Lamberton, G. A.; Tritt, T. M.; McMillan, P. F. *Appl. Phys. Lett.* **2003**, *82*, 910.

(52) Molinero, V.; Sastry, S.; Angell, C. A. *Phys. Rev. Lett.* **2006**, *97*, 075701.

(53) Bhat, M. H.; Molinero, V.; Soignard, E.; Solomon, V. C.; Sastry, S.; Yarger, J. L.; Angell, C. A. *Nature* **2007**, *448*, 787.

(54) Zheng, Q.; Durben, D. J.; Wolf, G. H.; Angell, C. A. *Science* **1991**, *254*, 829.

(55) Docherty, H.; Galindo, A.; Vega, C.; Sanz, E. *J. Chem. Phys.* **2006**, *125*, 074510.

(56) Savage, J. R.; Dinsmore, A. D. *Phys. Rev. Lett.* **2009**, *102*, 198302.

(57) Wolde, P. R. t.; Frenkel, D. *Science* **1997**, *277*, 1975.

(58) Liu, H.; Kumar, S. K.; Douglas, J. F. *Phys. Rev. Lett.* **2009**, *103*, 018101.

(59) Pouget, E. M.; Bomans, P. H. H.; Goos, J. A. C. M.; Frederik, P. M.; de With, G.; Sommerdijk, N. A. J. M. *Science* **2009**, *323*, 1555.

(60) Matsumoto, M. *Journal of Physical Chemistry Letters* **2010**, *1*, 1552.

(61) Liang, S.; Kusalik, P. G. *Chemical Science* **2011**, *In Press*.

(62) Vekilov, P. G. *J. Cryst. Growth* **2005**, *275*, 65.

(63) Whitelam, S. *J. Chem. Phys.* **2010**, *132*, 194901.

(64) Peters, B.; Trout, B. L. *J. Chem. Phys.* **2006**, *125*, 054108.

(65) Peters, B.; Beckham, G. T.; Trout, B. L. *J. Chem. Phys.* **2007**, *127*, 034109.

(66) van Erp, T. S.; Moroni, D.; Bolhuis, P. G. *J. Chem. Phys.* **2003**, *118*, 7762.

(67) van Erp, T. S.; Bolhuis, P. G. *J. Comput. Phys.* **2005**, *205*, 157.

(68) Allen, R. J.; Frenkel, D.; ten Wolde, P. R. *J. Chem. Phys.* **2006**, *124*, 024102.

(69) Allen, R. J.; Warren, P. B.; ten Wolde, P. R. *Phys. Rev. Lett.* **2005**, *94*, 018104.

(70) Valeriani, C.; Allen, R. J.; Morelli, M. J.; Frenkel, D.; ten Wolde, P. R. *J. Chem. Phys.* **2007**, *127*, 114109.

(71) Laio, A.; Rodriguez-Fortea, A.; Gervasio, F.; Ceccarelli, M.; Parrinello, M. *J. Phys. Chem. B* **2005**, *109*, 6714.

(72) Laio, A.; Gervasio, F. L. *Rep. Prog. Phys.* **2008**, *71*, 126601.

(73) Dickson, B. M.; Makarov, D. E.; Henkelman, G. *J. Chem. Phys.* **2009**, *131*, 074108.

(74) Fernando, A. E.; et al. *J. Phys.: Condens. Matter* **2009**, *21*, 333101.

(75) Rodger, P. M. *Ann. N. Y. Acad. Sci.* **2000**, *912*, 474.

(76) Steinhardt, P. J.; Nelson, D. R.; Ronchetti, M. *Phys. Rev. B* **1983**, *28*, 784.

(77) Errington, J. R.; Debenedetti, P. G. *Nature* **2001**, *409*, 318.

CHAPTER 2

THERMODYNAMIC STABILITY AND GROWTH OF GUEST-FREE CLATHRATE HYDRATES: A LOW-DENSITY CRYSTAL PHASE OF WATER

Reprinted with permission from the American Chemical Society

Jacobson, L. C.; Hujo, W.; Molinero, V. *J. Phys. Chem. B* **2009**, *113*, 10298.

10298 *J. Phys. Chem. B* **2009,** *113,* 10298–10307

Thermodynamic Stability and Growth of Guest-Free Clathrate Hydrates: A Low-Density Crystal Phase of Water

Liam C. Jacobson, Waldemar Hujo, and Valeria Molinero*

Department of Chemistry, University of Utah, 315 South 1400 East, Salt Lake City, Utah 84112-0850

Received: April 14, 2009; Revised Manuscript Received: June 15, 2009

We use molecular dynamics simulations with the monatomic water (mW) model to investigate the phase diagram, metastability, and growth of guest-free water clathrates of structure sI and sII. At 1 atm pressure, the simulated guest-free water clathrates are metastable with respect to ice and stable with respect to the liquid up to their melting temperatures, 245 ± 2 and 252 ± 2 K for sI and sII, respectively. We characterize the growth of the sI and sII water crystals from supercooled water and find that the clathrates are unable to nucleate ice, the stable crystal. We computed the phase relations of ice, guest-free sII clathrate, and liquid water from −1500 to 500 atm. The resulting phase diagram indicates that empty sII may be the stable phase of water at pressures lower than approximately−1300 atm and temperatures lower than 275 K. The simulations show that, even in the region of stability of the empty clathrates, supercooled liquid water crystallizes to ice. This suggests that the barrier for nucleation of ice is lower than that for clathrates. We find no evidence for the existence of the characteristic polyhedral clathrate cages in supercooled extended water. Our results show that clathrates do not need the presence of a guest molecule to grow, but they need the guest to nucleate from liquid water. We conclude that nucleation of empty clathrates from supercooled liquid water would be extremely challenging if not impossible to attain in experiments. We propose two strategies to produce empty water clathrates in laboratory experiments at low positive pressures.

I. Introduction

Most pure substances that form tetrahedrally coordinated crystals—H_2O, SiO_2, Si, Ge, even Sn—also form clathrate structures in the presence of an appropriate solute.[1] In these binary crystals, the tetrahedral substance makes a three-dimensional lattice with empty polyhedral cages that can host small guest molecules or atoms. A commonality of these binary clathrate crystals is that the guests generally do not compete with the interactions that keep together the tetrahedrally coordinated lattice formed by the host. In the case of water, this is the hydrogen bonding interaction. A notable exception is semiclathrates, in which the guests are simultaneously enclathrated and part of the hydrogen-bonded network.[2,3]

Clathrate hydrates are a solid phase of water that encages small guest molecules that do not form hydrogen bonds with water, such as CH_4, H_2, Ar, Xe, CO_2, and tetrahydrofurane (THF). When the guest molecule has low solubility in water, high pressures are required to stabilize the clathrate crystal.[4] Most hydrate compounds come in the form of cubic structures I (sI) and II (sII). The clathrate lattices are formed by the hydrogen-bond networks of the water molecules. The sI clathrates consist of two 5^{12} cages (dodecahedrons with 12 pentagonal faces) and six of the larger $5^{12}6^2$ cages per unit cell. The sII clathrates consist of 16 5^{12} cages and 8 $5^{12}6^4$ cages per unit cell. The structures of these cages are shown in Figure 1.

From the point of view of their use and applications, clathrate hydrates of hydrophobic guest molecules have garnered much attention lately because of their potential use as an abundant energy source as well as a possible solution to excess atmospheric carbon.[5] By some estimates, there is more than twice as much energy trapped in methane hydrates than there is in all

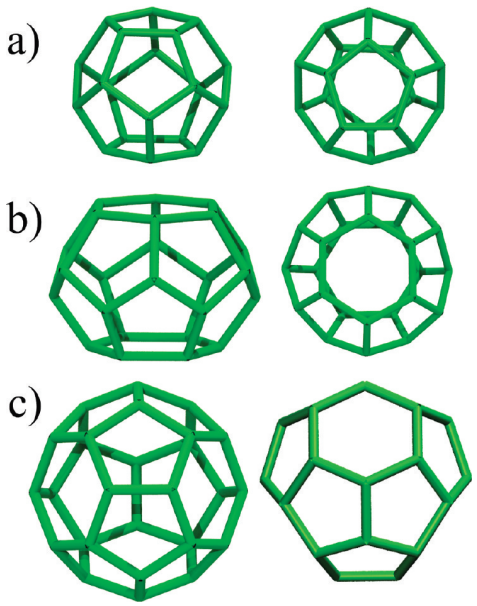

Figure 1. Water structures present in the cubic clathrates with structures sI and sII. (a) 5^{12} cage, a dodecahedron formed with 12 pentagonal faces. It contains 20 water molecules. (b) $5^{12}6^2$ cage, a tetrakaidecahedron, formed by 12 pentagonal and 2 hexagonal faces, containing 24 water molecules. (c) $5^{12}6^4$ cage, a hexakaidecahedron, formed by 12 pentagonal faces and 4 hexagonal faces, containing 28 water molecules. The water molecules are in the vertices of the cages. Each water molecule is four-coordinated in the clathrate crystals; see Figure 2.

* Corresponding author. E-mail: Valeria.Molinero@utah.edu. Phone: 1-801-585-9618. Fax: 1-801-581-4353.

10.1021/jp903439a CCC: $40.75
Published on Web 07/08/2009

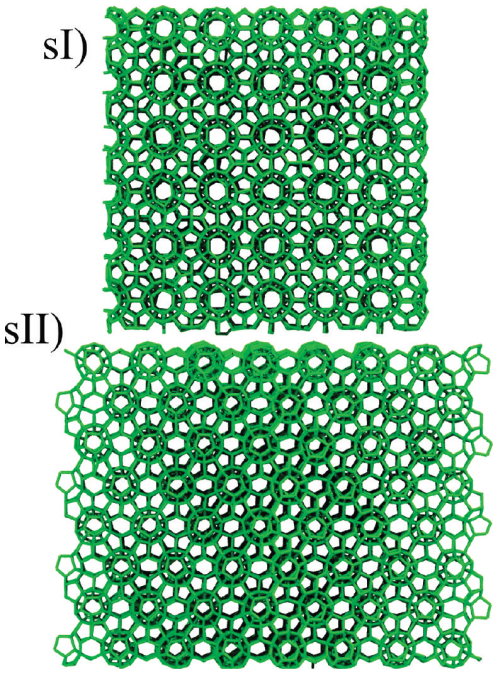

Figure 2. Crystal structures of the cubic water clathrates sI and sII. The "hydrogen-bonded" network (there are no H atoms in mW) is represented by green tubes connecting water molecules that are within 3.5 Å of each other. The snapshots show a 6 × 6 × 6 unit cell lattice for sI and a 4 × 4 × 4 one for sII.

other conventional natural gas reserves combined.[6] It has been also suggested that water clathrates could be adequate for hydrogen storage.[7] Molecular hydrogen alone is not stabilizing enough to the clathrate lattice, so various strategies have been investigated to store hydrogen gas in clathrates such as using binary guest molecules, semiclathrates, and other more complex clathrate lattice structures.[8] Gas hydrates are also of great interest to the petroleum industry because of their propensity to clog natural gas pipelines, leading to production downtime and huge economic losses.[9]

All known water clathrates contain guest molecules that contribute to the stabilization of the crystal structure. Small guests can occupy all the available cages, while bigger guest molecules may only fill the larger ones, leaving the dodecahedra empty.[4] A pure water clathrate crystal in which all the cages are empty has not been synthesized to date. These guest-free clathrate structures have been produced, however, for Ge[10] and Si.[11] As water, silicon, and germanium form similar structures and have related phase diagrams,[12−15] empty water clathrates may also be realized in laboratory conditions.

Water has an extremely rich phase diagram: at positive pressures, it has more than a dozen known crystal phases and two distinct glasses (low- and high-density amorphous ice) that suggest the existence of two liquid phases![16−18] A water clathrate devoid of guest molecules would constitute the lowest-density ice phase of water. Low-density phases are thermodynamically favored by low or negative pressures, so empty clathrates may be a stable crystal of water under extension. Water is able to undergo extension to negative pressures until it reaches the cavitation limit at 313 K and −1400 atm, but these conditions are difficult to reach experimentally.[19] Due to the challenge involved in performing experiments under extension, the thermodynamics and phase relations of water at $p < 0$ are not yet fully elucidated.

In this work we use coarse-grained molecular simulations to investigate the regions of stability and metastability of empty clathrates. We investigate the growth, melting temperatures, and thermodynamics of empty clathrate hydrate lattices for sI and sII structures from −1500 to 500 atm. Using the results from the simulations and experimental data available in the literature, we evaluate the feasibility of crystallizing these low-density water crystals from supercooled water and present two possible strategies to produce them in experiments in accessible laboratory conditions. We also discuss possible implications of the metastability of empty clathrates for the mechanism of growth of gas hydrate clathrates.

II. Methods

A. Water Model. Water was modeled with the monatomic potential mW recently developed in our group.[12] In the mW model, water is represented by a single particle able to form "hydrogen bonded" structures through three-body nonbond interactions that encourage the formation of tetrahedrally coordinated structures. The water model is based upon the Stillinger−Weber (SW) silicon potential;[20] that consists of a sum of pairwise $v_2(r)$ and three-body $v_3(r,\theta)$ contributions, $v = v_2(r) + \lambda v_3(r,\theta)$. The three-body term adds an energy penalty to configurations with nontetrahedral angles. The parameter λ determines how tetrahedral the potential is. The full expression of the mW potential as a function of the intermolecular distance and the three-body angles is given by

$$E = \sum_i \sum_{j>i} \phi_2(r_{ij}) + \sum_i \sum_{j\neq i} \sum_{k>j} \phi_3(r_{ij}, r_{ik}, \theta_{ijk})$$
$$\phi_2(r_{ij}) = A\varepsilon\left[B\left(\frac{\sigma}{r_{ij}}\right)^{p_{ij}} - \left(\frac{\sigma}{r_{ij}}\right)^{q_{ij}}\right]\exp\left(\frac{\sigma}{r_{ij} - a\sigma}\right)$$
$$\phi_3(r_{ij}, r_{ik}, \theta_{ijk}) = \lambda\varepsilon[\cos\theta_{ijk} - \cos\theta_0]^2 \exp\left(\frac{\gamma\sigma}{r_{ij} - a\sigma}\right) \times \exp\left(\frac{\gamma\sigma}{r_{ik} - a\sigma}\right) \quad (1)$$

where $A = 7.049556277$, $B = 0.6022245584$, $p = 4$, $q = 0$, $\gamma = 1.2$, $a = 1.8$, $\theta_o = 109.47°$, $\sigma = 2.3925$ Å, $\varepsilon = 25.895$ kJ/mol, and $\lambda = 23.15$. Only the tetrahedrality λ, the diameter σ, and energy scale ε need to be tuned to transmute SW silicon to the monatomic water model mW. Note that the SW potential can be represented in reduced units independent of σ and ε; thus the main difference between water and silicon is the tetrahedrality. In terms of its thermodynamics and the strucure of the condensed phases, water behaves as a more tetrahedral silicon atom.[12] We will use these reduced units to compare clathrates of Si and water.

The mW potential does not have electrostatics and uses only short-ranged interactions, making it about 180 times faster than fully atomistic simulations. The monatomic water model reproduces the radial and angular structure of liquid water, ice I, and low-density amorphous ice, although no structural information was used for the force field development.[12,13] mW reproduces the thermodynamic and dynamic anomalies of water, and the existence of a phase transformation from a high- to low-density liquid in the supercooled region.[12] It also predicts correctly that hexagonal ice is the most stable crystal of water at room pressure, with a melting point T_m= 274 K. The

enthalpies of phase transformation (melting, vaporization, and sublimation) are predicted by mW with comparable or better accuracy than the most popular fully atomistic models of water.[12] The mW model has been extended to include ions (without the use of electrostatics)[21] and hydrophobic interfaces confined between which mW reproduces the phase behavior of atomistic water.[22] It should be noted that the mW potential was developed without any consideration for clathrate hydrate formation.

B. Simulation Methods. Molecular dynamics (MD) simulations were performed using LAMMPS, a massively parallel MD software program developed at Sandia National Laboratories by Plimpton et al.[23] All simulations were performed in systems with periodic boundary conditions. The equations of motion were integrated using the velocity-Verlet algorithm with a time step of 10 fs. The pressure and temperature were regulated with a Nose−Hoover barostat and thermostat with damping parameters 25 and 5 ps, respectively. In the simulation of crystals or systems with a crystal−liquid interface, each dimension was allowed to dilate and contract independently.

C. Preparation of the Initial Structures. Crystal structure unit cells of sI and sII hydrates were created from diffraction data.[24] These structures were equilibrated using the mW potential and used to build subsequent lattices containing 9936 and 8704 water particles for the sI and sII structures, respectively. The lattice of the sI system consisted of a $6 \times 6 \times 6$ unit cells, and for the sII system, a $4 \times 4 \times 4$ unit cells (Figure 2). The properties of hexagonal ice (Ih) were computed from simulations of crystals containing 4608 water molecules. The initial configuration of the systems used for the determination of the melting temperatures and crystal growth had twice the number of water particles, 19 872 for sI, 17 408 for sII, and 9216 for Ih, with approximately half of the atoms in the liquid and half in the solid phase.

D. Calculation of Thermodynamic Properties. ***Density.*** The density was calculated as $\rho = NM/(N_A\langle V\rangle)$, where N is the total number of molecules, $M = 18.015$ g/mol is the molar mass of water, N_A is Avogadro's number, and $\langle V\rangle$ is the time average of the volume of the simulation box.

Phase Diagram. The melting temperatures (T_m) of ice and clathrates were determined by the direct coexistence method.[25−27] In this method, a system that consists of a liquid and a crystal block, each containing about half of the molecules in the system (see Figures 3 and 4) is evolved at constant T and p. The growth of one phase at the expense of the other is monitored visually and through the evolution of the total energy. T_m was evaluated by determining the temperature for which there was no net advance or decomposition of the solid phase in systems consisting of half crystal and half liquid in thermal equilibrium. The melting temperatures of hexagonal ice and clathrates were determined at pressures from 500 atm to −1500 atm in steps of 500 atm. The liquid−ice−sII triple point was computed from the intersection of the melting lines of hexagonal ice Ih and sII clathrate. The ice−clathrate coexistence line was computed using the Clausius relation $(dp/dT)_{Ih-sII} = \Delta S/\Delta V$ and the liquid−Ih−sII triple point as a pivot.

Heat Capacity, Enthalpy, Excess Enthalpy, and Entropy of Liquid with Respect to the Crystals. Isobaric simulations of sI and sII clathrate cells were performed using a linear temperature ramp from 300 to 210 K at $p = 1$ atm. The rate of the temperature ramp was 0.5 K/ns, which is sufficiently slow for the mW potential to ensure that the system remains in a local equilibrium at each temperature.[12] The enthalpy, H, was calculated over the course of the simulation by the relationship $\langle H\rangle = \langle E + pV\rangle$, where E is the total energy per mole of water,

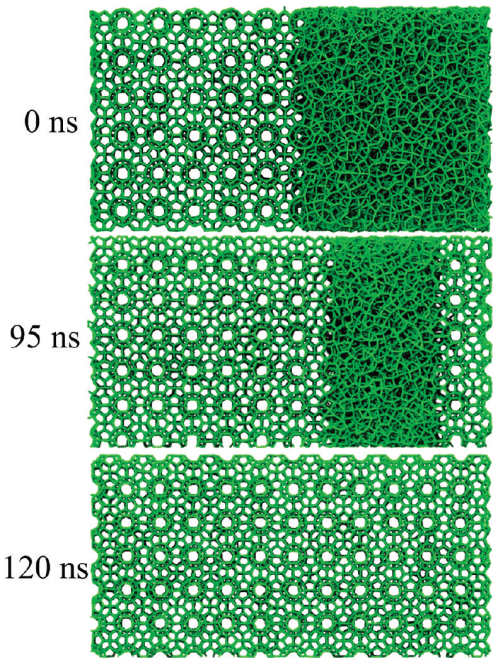

Figure 3. Growth of the sI lattice at 240 K, 5 K below the T_m of the empty sI lattice. The crystal plane exposed to the liquid is the one containing the planar hexagonal rings. The stepwise growth (see Figure 7) is limited by the formation of these 6-member rings.

p is the pressure, and V is the molar volume of water. The enthalpy of liquid and each solid were used to calculate the excess enthalpy of the liquid with respect to crystals as a function of temperature,

$$H^{ex} = H_{liquid} - H_{crystal} \tag{2}$$

The enthalpy data for the solid phases were fit to third-order polynomials to obtain analytical expressions for the enthalpy as a function of temperature. The analytical expression for the liquid and ice enthalpy was previously reported in ref 12. The isobaric heat capacity, C_p, was obtained by taking the analytical derivative of the fitted $H(T)$, $C_p = (dH/dT)_{p,N}$.

For the sake of verifying the quality of the computed heat capacities, we also computed the excess enthalpy from

$$H^{ex} = \Delta H_m(T_m) + \int_{T_m}^{T} \Delta C_p(T)\, dT \tag{3}$$

where $\Delta C_p(T)$ is the difference between the isobaric heat capacity of the liquid and the solid phases. Equations 2 and 3 produced the same result, validating the expression for C_p.

The excess entropy of the liquid with respect to each solid was determined from integration of the corresponding $\Delta C_p/T$ from the known values at the melting point of each crystal, $\Delta S_m = \Delta H_m/T_m$,

$$S^{ex}(T) = \frac{\Delta H_m(T_m)}{T_m} + \int_{T_m}^{T} \frac{\Delta C_p(T)}{T}\, dT \tag{4}$$

The excess enthalpy and excess entropy were combined to compute the Gibbs excess free energy, $G^{ex}(T) = H^{ex}(T) - TS^{ex}(T)$ of the liquid with respect to each crystal phase.

E. Identification of Clathrate Cages and Monitoring of Crystal Growth. The growth of the clathrates was monitored through the time evolution of two order parameters:

(i) The total energy of the system, that decreases as the crystal grows. This is a global order parameter that does not indicate where the growth occurs.

(ii) The number of polyhedral cages. We identified the cages (Figure 1) using the connectivity of water molecules and the topology of the rings they formed. We defined two water molecules to be connected if they are at a distance less than 3.5 Å; we then found all possible 5-member and 6-member rings formed by connected water molecules using the code by Matsumoto et al.[28] That algorithm uses only topological information, such as the connectivity of the particles by treating the waters as vertices in an undirected graph to identify the rings. After determining the connections between the rings, our algorithm searches for a five-membered ring that has five other pentagonal rings connected on each edge. This structure is half a dodecahedron cage that we refer to as a "cup". Through merging these cups we gain a full dodecahedron cage. This procedure was implemented to identify the 5^{12} cages (Figure 1a) as well as $5^{12}6^2$ (Figure 1b), where for the $5^{12}6^2$ cage the top of the cup is a six-membered-ring (hexagon) surrounded by six pentagons. A similar but more sophisticated method was implemented to identify the $5^{12}6^3$ and $5^{12}6^4$ cages (Figure 1c). Here we noticed that each $5^{12}6^4$ consists of four partly overlapped hexagon cups, where each hexagon shares an edge and two pentagons on three sides. This information is used to merge the four hexagon cups and identify the cage.

The total energy, along with visual inspection of the structures, was used to determine the advance or recession of crystals for the determination of the melting temperatures. The identification and counting of polyhedra was used to obtain insightful microscopic information on the growth of the clathrates and also allowed us to evaluate the existence of polyhedral cages in supercooled liquid water.

III. Results and Discussion

A. Melting Temperatures of Guest-Free Water Clathrates at Room Pressure. The structures for sI and sII clathrates in our study are the same as the experimental crystals. The density of the empty sII clathrate modeled with mW is 0.851 g/cm^3 at 1 atm and 274 K. The density of an hypothetical experimental empty sII clathrate may be estimated as the density of Ar clathrate hydrate considering only the water molecules, in which case the density is 0.818 g/cm^3. This is assuming a lattice parameter for the empty clathrate of 17.07 Å[29] and that Ar does not contract or expand the water lattice. In the same p and T conditions, the density of the empty sI structure is 0.860 g/cm^3 in the simulations. The density of ice at T_m in the mW model is 0.978 g/cm^3, larger than the experimental value, 0.917 g/cm^3. The density of the mW liquid water at T_m is 0.999 g/cm^3, in very good agreement with the 1.001 g/cm^3 of the experiment.[12] The overestimation of the density of the crystal phases between the mW model can be explained by the lack of hydrogens on the mW water molecules, which takes away the ability of the O−H bonds to extend upon freezing. As a result, the differences in molar volume between liquid on the one hand, and ice[12] and clathrate phases on the other, are smaller in the mW model than in the experiment.

We computed the liquid-crystal equilibrium melting temperature T_m for the guest-free clathrates of structure sI and sII. To calculate T_m we prepared systems that are half crystal phase and the other half liquid (Figures 3 and 4). We monitored the growth or decomposition of the lattice at different temperatures and determined the temperature T_m at which the ice and crystal phases remained in stationary equilibrium. T_m was determined for each clathrate lattice.

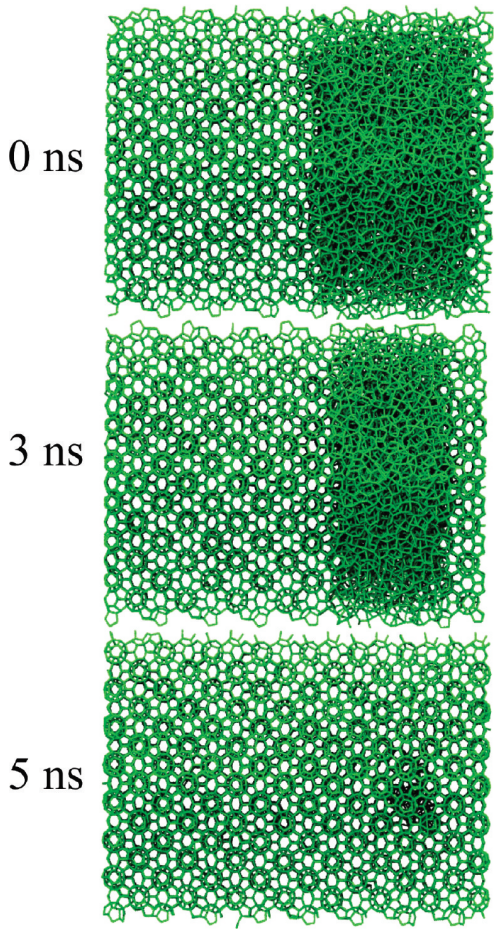

Figure 4. Growth of the sII crystal at 250 K, 2 K below the T_m of the empty sII lattice. The plane of the growth does not coincide with that of the 6-member rings, leading to a much faster growth compared to that displayed in Figure 3.

The melting temperatures of empty sI and sII clathrates at 1 atm were found to be 245 ± 2 and 252 ± 2 K, respectively. To our knowledge, this is the first time the T_m for empty water clathrate lattices has been calculated. In section IIID, we construct a thermodynamic cycle from which we assess the accuracy of the predicted T_m. The melting temperatures of the guest-free sI and sII crystal are well below the T_m of ice, 274 K for this model, but above the temperature of homogeneous nucleation of ice (200 K for mW;[12] 235 K in the experiment[30]). The low T_m of the empty clathrates may explain why they are not observed experimentally: any attempt to nucleate empty clathrates from supercooled water would most likely succumb to nucleation of hexagonal ice, the most stable phase.

The melting temperatures of our study indicate that below ~250 K the empty clathrates are more stable than liquid water

TABLE 1: Thermodynamics of Melting of Ice and Clathrates at 1 atm[a]

phase transition	T_m (K)	$\Delta H_m(T_m)$ (kJ/mol)	$\Delta S_m(T_m)$ (J/(mol K))
ice-liquid	274 (273)	5.27 (6.01)	19.3 (22.0)
sI-liquid	245	4.39	17.9
sII-liquid	252	4.63	18.5

[a] Enthalpy and entropy of melting, ΔH_m and ΔS_m, evaluated at their corresponding equilibrium melting temperatures T_m for the mW model at 1 atm. Experimental values, from ref 64 are shown in parentheses.

but less stable than hexagonal ice: guest-free water clathrates are a metastable crystal of water at room pressure. In section IIIC, we show that clathrates are not a good template for ice nucleation, so it may be expected that if an empty clathrate is formed (possible routes are discussed in section IIIG), it may survive up to its melting point as a mestastable crystal of water.

The energy of the empty sII clathrates is 0.17 kJ/mol lower than that of the empty sI clathrates (comparable to the difference between cubic and hexagonal ice[31]). The lower energy of sII is consistent with the observation that clathrates preferentially form the sII structure if the guest molecules are small enough (~4 Å).[4] Guest molecules that can fit in both the small 5^{12} cages and the larger $5^{12}6^4$ cages of sII clathrates preferentially form the sII structure. Guest molecules that are too big to fit in the 5^{12} cages preferentially form sI hydrates, because there are more large cages per number of water molecules in sI than in sII. Microscopically, the higher energy of the sI structure is due to a higher proportion of planar 6-member water rings that force the oxygen−oxygen−oxygen angle to 120°, away from the ideal tetrahedral value of 109°. Planar pentagons, with OOO angles of 108°, do not strain the hydrogen-bonded structure. The thermodynamic data for melting of clathrates and ice are summarized in Table 1.

B. Limit of Superheating of Empty Clathrates at Room Pressure. We now address what is the limit of superheating (one phase decomposition temperature T_d) of the empty clathrates. T_d is different and higher than the equilibrium melting temperature T_m between liquid and the corresponding crystal. To determine T_d, we performed simulations of hexagonal ice and the guest-free sI and sII clathrates at $p = 1$ atm and T ranging from 274 to 350 K. The systems consist of the crystals in a periodic cell without any interface that may help nucleate the liquid phase. The systems are simulated for 100 ns at each temperature. For hexagonal ice we find that the crystal decomposes to liquid at 340 K but not at 330 K in 100 ns simulations, in good agreement with the experimental limit of superheating, 330 ± 10 K.[32] The crystal has to be superheated considerably to nucleate the liquid phase. The sI and sII guest-free water clathrates remain in the crystalline state up to 340 K, but they both spontaneously decompose within 200 ps at 350 K. Below the limit of superheating, $T_d \approx 340 \pm 10$ K, we find no reorganization of the lattice during the 100 ns simulations. The limit of superheating T_d of sI and sII empty water clathrates is higher than T_m of ice and $p = 1$ atm.

It should be noted that the mW model explores the phase space faster than atomistic models of water, due to the absence of hydrogen atoms; the system evolves in a smoother potential energy surface. Thus we expect that a system that is metastable through a 100 ns simulation with the coarse-grained model will be metastable for a longer time if the simulations were performed with fully atomistic detail. Superheating of crystals is extremely challenging in experiments, where crystal interfaces that favor liquid nucleation cannot be avoided, so we do not expect empty clathrates to survive in experiments at temperatures higher than their melting points.

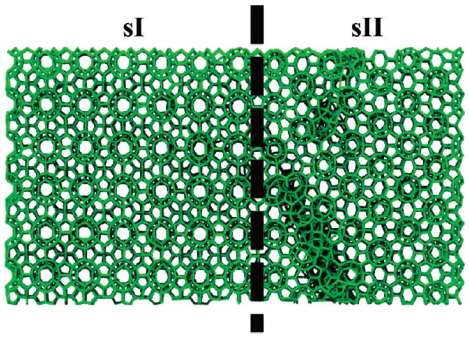

Figure 5. Final configuration after complete crystallization of deeply supercooled water starting from a sI-liquid configuration (as shown in the upper panel of Figure 3) at $T = 230$ K. The sI phase (left) nucleated the more stable sII phase (right). The dark areas in the sII phase are defects that resulted from the two advancing crystalline faces growing into each other.

An MD study of empty water clathrates modeled with the SPCE potential melted in a few picoseconds at 240 K.[33] It was determined that the excitation of low frequency modes related to the rotation of the water molecules, conspicuously absent in the coarse-grained model, were responsible for the destabilization of the SPCE water lattice.[33] Those MD simulations, it should be noted, were performed well above the T_m for hexagonal ice using the SPCE model, 215 K.[34] Also in agreement with the results of the mW model, an MD simulation of empty clathrates using the TIP4P potential for water found them to be mechanically stable for T as high as 300 K; this is about 28% higher than the melting point for hexagonal ice in that model.[35] Also in support of our claim of the metastability of the empty lattice at the equilibrium melting temperature of ice, recent simulations of empty sI and sII water crystals using the polarizable COS/G2 water model show no sign of instability for temperatures up to 260 K,[36] well above the melting point of hexagonal ice with that model, 236± 2 K.[37] A more appropriate comparison between the different water models would be made computing the ratio of the one-phase decomposition temperature (limit of superheating) of the empty clathrates to the equilibrium melting temperature of the same crystal, but the latter is not yet available for the atomistic models of clathrates.

C. Clathrate Structures Nucleate Each Other but They do not Nucleate Ice. Figure 4 shows a time sequence for the growth of empty sII clathrate from an initial system consisting of half sII empty clathrate and half liquid at $T = 250$ K $< T_m^{sII} = 252$ K. The empty sII clathrate lattice grew in supercooled water, nucleated by the already present clathrate lattice, until complete crystallization of the system occurred. The same is observed for sI in Figure 3. In deeply supercooled water, $T = 230$ K, starting with an sI crystal as a seed, we observed epitaxial growth of sI that in turn nucleated and grew the most stable sII crystal. A detail of the resulting composite sI/sII crystal is shown in Figure 5. These results show that clathrate structures can nucleate each other, a result that is not surprising taking into account the existence of common dodecahedron cages and identical planar pentagonal and hexagonal rings in the big $5^{12}6^2$ and $5^{12}6^4$ cages. In agreement with previous simulations of the crystalline structure of methane hydrates,[38] we find that regions of sI and sII are connected by layers of $5^{12}6^3$ cages. More interestingly, we find that the clathrates cannot nucleate ice,

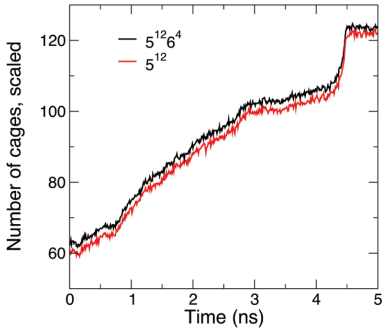

Figure 6. Number of polyhedral cages as a function of time for the growth sequence of the sII lattice at 250 K shown in Figure 4. The number of cages have been scaled by their stoichiometric ratio in the sII unit cell (16 5^{12}: 8 $5^{12}6^4$). The growth occurs via a steady addition of both types of cages. The rapid growth at the end results from the two crystal interfaces growing into each other. The final level section indicates that crystallization is complete.

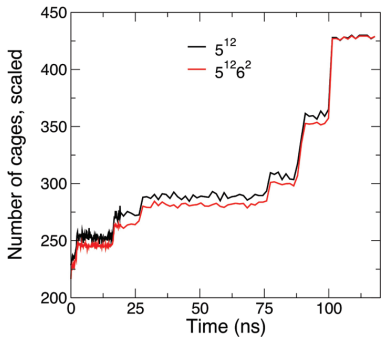

Figure 7. Number of polyhedral cages as a function of time for the growth sequence of the sI lattice at 240 K shown in Figure 3. The number of cages have been scaled by their stoichiometric ratio in the sI unit cell (2 5^{12}: 6 $5^{12}6^2$). Unlike the growth for the sII lattice, the growth in the sI lattice occurs in stochastic, discretized steps where the progression occurs layer by layer. The larger steps in the latter portion of the simulation are the result of multiple layers of growth that occur as the two crystalline faces encroach upon each other facilitating more rapid growth.

although the latter is the most stable phase. All water molecules in ice and clathrates are four-coordinated, but water is organized quite differently in these crystals. Ice contains only 6-member water rings, and these are not planar as in the clathrates.

It is observed experimentally that the crystal growth is slowest on planes with a preponderance of planar hexagonal rings, due to the unfavorable angles.[39] We observe the same in this work: the growth of the clathrate lattice is significantly faster when the exposed plane is the one with the fewest planar hexagonal rings. This is quantified in Figures 6 and 7 that display the number of polyhedral clathrate cages as a function of time for the growth of (i) empty sII at 250 K, illustrated in Figure 4, and (ii) empty sI at 240 K, illustrated in Figure 3. Although the degree of supercooling of the two crystals is essentially the same in Figures 6 and 7, the growth of the sI crystal is 20 times slower. The crystal plane exposed to the liquid in the sII simulation does not contain 6-member planar rings, and the growth occurs continuously. The crystal plane exposed to the liquid in the sI simulation, on the contrary, contains the planar 6-member rings leading to a stepwise growth that involves the

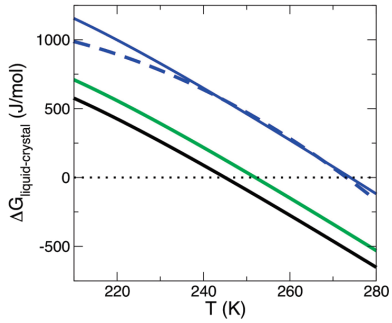

Figure 8. Excess free energy of liquid water with respect to hexagonal ice (blue), sII clathrate (green), and sI clathrate (black). The simulations predict an excess free energy for liquid with respect to ice that is in excellent agreement with the experiment (dashed blue), measured down to 235 K and extrapolated to lower temperatures.[41,42]

addition of a full new layer to the crystal, as shown in Figure 7. It should be noted that the time scale of the growth with the coarse-grained model is not predictive of the rate for a fully atomistic system, as the system evolves in a smoother potential energy surface due to the lack of hydrogen atoms.[12]

D. Region of Stability of Empty Clathrates in the Phase Diagram of Water. In this section, we investigate under which temperature and pressure conditions the empty clathrates are a thermodynamically stable phase of water. For this we built the phase diagram of water from the liquid−sII, liquid−Ih, and Ih−sII coexistence lines in $p-T$, and we also computed the excess free energy G^{ex} of supercooled liquid water with respect to each crystal and the free energy difference of clathrate with respect to ice, $\Delta G_{ice,clathrate}$. The latter quantity is an important part of thermodynamic cycles used to evaluate the free energy of gas hydrates. It cannot be directly determined, so it is normally computed from fitting experimental phase-change data such as enthalpy and heat capacity for clathrates containing guest molecules.[40]

Figure 8 shows the excess Gibbs free energy of liquid water with respect to hexagonal ice Ih and sI and sII clathrates computed with the mW model. The figure also displays the experimental Gibbs excess free energy of liquid with respect to Ih, measured down to 235 K and extrapolated at lower temperatures in ref 41 using data of ref 42. The agreement between the experimental and simulated G^{ex}_{Ih} is excellent.

The difference in free energy between the clathrate and Ih ice phase $\Delta G_{ice,clathrate}$ for the empty sII and sI clathrates at 274 K is 415 ± 6 and 537 ± 6 J/mol, respectively. Hexagonal ice is the phase of lowest free energy. We determined the enthalpy difference between the clathrate and ice phase $\Delta H_{ice,clathrate}$ for the empty sII and sI clathrates at $T = 274$ K to be 538 ± 6 and 714 ± 6 J/mol, respectively. Hexagonal ice is the phase of lowest enthalpy. The 176± 6 J/mol enthalpy difference between sI and sII is in excellent agreement with the 167 J/mol reported by Handa and Tse using the van der Waals−Platteuw method.[43] A recent estimation of this enthalpy difference using the COS/G2 polarizable water force field was 301 J/mol.[36] Values of $\Delta G_{ice,clathrate}$ reported in the literature range from 699 to 1299 J/mol for sI and 366 to 1714 J/mol for sII.[40] Sloan and co-workers suggested $\Delta G_{ice,clathrate} = 937$ J/mol for sII.[44] The estimated values of $\Delta G_{ice,clathrate}$ are essential components of thermochemical cycles used for the determination of the thermodynamic stability of gas hydrate clathrates.[40] This is already commonly done in the van der Waals−Platteuw model

of clathrate hydrates and other statistical thermodynamic methods.[45] The free energy of the filled clathrate can be calculated from the stabilization of the presence of guest molecules in the cages with respect to the empty lattice.

The sign of $\Delta G_{\text{ice,clathrate}}$ indicates that the empty sI and sII clathrate lattices are less stable than ice at $p = 1$ atm (Figure 8). The negative of the slope of the free energy with respect to temperature is the entropy,

$$\left(\frac{\partial G}{\partial T}\right)_{N,P} = -S \tag{5}$$

The almost parallel $G^{\text{ex}}(T)$ for ice and clathrates indicate that the entropy is essentially the same for all these crystals. Our calculations indicate that the molar entropies of sI and sII are, respectively, 1.4 and 0.8 J/(K mol) lower than S_{ice}. These are very small differences in entropy, in agreement with the 0.61 J/(K mol) estimated from the ideal solid-solution model of van der Waals and Platteeuw by Handa and Tse.[36,43] Therefore, a change in temperature alone does not alter the relative stability of clathrates with respect to ice.

The difference in molar volume between clathrates and Ih presents the possibility that the clathrates could become the stable phase at negative pressures. This is because the molar volume of the clathrate is significantly larger than that of ice, thus the free energy of the clathrate decreases faster than that of ice under extension,

$$\left(\frac{\partial G}{\partial P}\right)_{N,T} = V \tag{6}$$

The ratio between ΔV of liquid with respect to the sII clathrate and liquid with respect to ice Ih in at room pressure is 7.49 for the mW model. Therefore, the coexistence line for liquid and empty clathrate will be steeper than that for liquid and ice (Clausius equation, $(\mathrm{d}T/\mathrm{d}p)_{\text{coexistence}} = \Delta V/\Delta S$) creating the likelihood that the melting lines of ice and clathrate will cross at some negative pressure before the liquid itself becomes unstable with respect to ice.

We determined T_{m} as a function of pressure for Ih and empty sII, the more stable clathrate. The resulting phase diagram is shown in Figure 9. As ice is denser than the clathrates, the latter become more stable than ice at negative pressures. For the mW model, the liquid−Ih and liquid−sII coexistence lines cross at $p_t \approx -1300$ atm and $T_t = 276$ K, the liquid−ice−sII triple point of the mW model.

Using the Clausius equation, we linearly extrapolated the melting lines for ice and sII clathrate to negative pressures using the ΔV and ΔS at $p = 1$ atm. The crossing of these two lines determines an approximated location of the liquid−ice−clathrate triple point. The linear extrapolation using ΔV and ΔS of the mW model results in a triple point at $p_t \approx -1400$ atm and $T_{\text{t}} = 277$ close to the $p_{\text{t}} \approx -1300$ atm and $T_{\text{t}} = 276$ K computed from the actual $T_{\text{m}}(p)$. The linear extrapolation using the experimental ΔV and ΔS yields $p_{\text{t}} = -1900$ atm and $T_{\text{t}} = 287$ K. For this extrapolation, the molar volume of the hypothetical experimental clathrate was taken as the volume of water molecules in the Ar clathrate and molar ΔS for the melting of the empty clathrate was assumed to be the same as the experimental value for melting of ice, 22 J/(K mol).

For the previous estimation of the location of the "experimental" triple point, we assumed that the experimental T_{m} for an empty sII clathrate is 252 K, the value predicted by the mW model. However, if the free energy difference between ice and sII is higher than the 415 J/mol predicted in our simulations, then the T_{m} for the empty clathrate would be lower. A lower T_{m} would result in a more negative pressure for the triple point. We constructed a thermodynamic cycle from which we can estimate the corresponding equilibrium melting temperature T'_{m} for the empty clathrate by using alternative values of $\Delta G_{\text{ice,clathrate}}$ taken from the literature

$$\begin{array}{ccc} \text{liquid}(273\ \text{K}) & \xrightarrow{\zeta} & \text{clathrate}(273\ \text{K}) \\ \int_{273\text{K}}^{T'_{\text{m}}} -S_{\text{liquid}}\,\mathrm{d}T \quad \downarrow & & \downarrow \quad \int_{273\text{K}}^{T'_{\text{m}}} -S_{\text{clathrate}}\,\mathrm{d}T \\ \text{liquid}(T'_{\text{m}}) & \xrightarrow{0} & \text{clathrate}(T'_{\text{m}}) \end{array} \tag{7}$$

where

$$\zeta = \Delta G^{\text{mW}}_{\text{ice,clath}} - \Delta G^{\text{literature}}_{\text{ice,clath}} = \int_{273}^{T_{\text{m}}} (S_{\text{clathrate}} - S_{\text{liquid}})\,\mathrm{d}T \tag{8}$$

Using the $\Delta G_{\text{ice,clathrate}}$ recommended by Sloan et al., 937 J/mol,[44] and approximating that the entropy of melting of the clathrates is the same as that of ice, would result in a T'_{m} for the sII guest-free clathrate that is ~24 K lower than the 252 K predicted by our simulations and a predicted triple point at an extremely negative pressure, $p_{\text{t}} \approx -3000$ atm. This would be inaccessible due to cavitation of liquid water.

An estimation of the ice-sII coexistence line using lattice dynamics simulations of TIP4P water resulted in a coexistence pressure of −400 atm, insensitive to temperature because $\Delta S_{\text{ice-sII}} \approx 0$.[35] As the triple point belongs to the ice−sII coexistence line, the pressure of the triple point predicted by TIP4P is $p_{\text{t}} \approx -400$ atm. No liquid-crystal equilibrium is considered in ref 35, thus the triple temperature cannot be inferred from their data. There is a striking difference in the

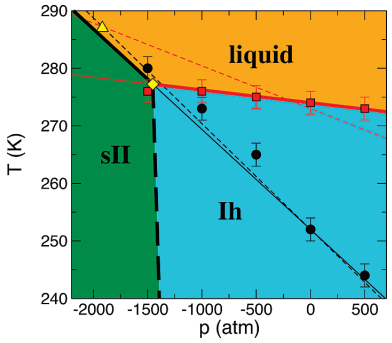

Figure 9. Phase diagram of water showing the regions of stability of hexagonal ice Ih (cyan), liquid water (orange), and guest-free water clathrate sII (green). The intersection of the melting temperatures of Ih (red squares) and sII (black circles) in the simulations predict a liquid−Ih−sII triple point at $T_{\text{t}} = 275$ K and $p_{\text{t}} \approx -1300$ atm. A linear extrapolation of the melting lines of Ih and sII using the values of $\Delta V_{\text{m}}/\Delta S_{\text{m}}$ of simulations at 1 atm yields the solid lines that, for simplicity, we use to color the phase diagram. This extrapolation leads to $T_{\text{t}} = 277$ K and $p_{\text{t}} \approx -1400$ atm (yellow diamond). An equivalent extrapolation using experimental values for $\Delta V_{\text{m}}/\Delta S_{\text{m}}$ (thin dashed lines) predicts a more negative triple pressure, $p_{\text{t}} \approx -1900$ atm.

predicted pressure regions of clathrate stability in the TIP4P atomistic model and our extrapolation of the experimental p_t based on the range of $\Delta G_{ice,clathrate}$ reported in the literature and their corresponding melting temperatures T_m^*. We doubt that the approximation of constant ΔV and ΔS is responsible for this disagreement, although both of them decrease under extension. A lower triple pressure would be obtained in our extrapolations for the experiment if the melting temperature of the clathrate were higher than the 252 K predicted by the model. That would require a smaller $\Delta G_{ice,clathrate}$, not impossible but so far not widely supported by the literature. It is also possible that the prediction of the TIP4P model is off from the extrapolation from experimental values because the thermodynamics of the phase transitions involving clathrates are not well described by that model. More atomistic studies are needed to clarify the origin of this discrepancy.

In all the scenarios presented above, the crossing of T_m of ice Ih and sII clathrate occurs in a region experimentally unexplored and probably inaccessible due to cavitation of liquid water. Experimental values for the cavitation limit of water include −260 atm at 273 K[46] and −1400 atm at 313 K.[19] Speedy predicted that the maximum extension the liquid can endure without cavitation occurs at around −2000 atm,[47] a theoretical limit that is most likely unreachable experimentally. These results suggest that empty clathrates could not be obtained from cooling of stretched liquid water in experiments.

E. Homogeneous Nucleation of Ice is Kinetically Favored over that of Clathrates. Even if the region of water clathrate stability is experimentally accessible, the question remains whether homogeneous nucleation of the clathrate occurs from supercooled stretched water. We performed quenching MD simulations of a mW liquid cell containing 32 768 water particles at $p = -2000$ atm, a region where the empty clathrate is the stable phase, applying a linear temperature ramp from 275 to 160 K at a rate of 1 K/ns. Cavitation of the liquid did not occur within the time scale of the simulations. We monitored the formation of the constitutive clathrate cages: not even a single dodecahedral cage appeared in the thousand snapshots analyzed along the cooling trajectory. Stretched supercooled liquid water spontaneously crystallized to ice, not a clathrate, at 205 K. This indicates that the barrier to nucleate any of the empty clathrates is larger than that for nucleation of ice. The reason may be sought in the structure of deeply supercooled liquid water, that bears little resemblance to the clathrate lattice and does not contain its elementary polyhedral motifs, while it is quite similar to that of Ih, as discussed in ref 13. Under extension, the structure of liquid water becomes more tetrahedral and the number of first neighbors molecules decreases from 5.1 at $p = 1$ atm to 4.8 neighbors at $p = -2000$ atm, at 275 K. The density of the liquid decreases significantly on extension: at 275 K is 0.95 g/cm^3 for −2000 atm compared to 1.00 g/cm^3 for 1 atm, and for the two pressures decreases on supercooling. The density of stretched supercooled water at −2000 atm and 205 K is 0.93 g/cm^3, 12% denser than the clathrate and only 2.1% lighter than Ih ice, all measured at the same p,T conditions. The larger gap in density between liquid and clathrate is probably commensurate with their differences in structure.

F. Comparison of the Phase Diagram of Water and Silicon under Extension. The thermodynamics of silicon and water are similar in several respects, including the existence of a density maximum, two distinct amorphous phases, and a negative slope for the melting temperature as a function of pressure.[14,16,48,49] Another commonality is that the sII lattice becomes more stable than the diamond cubic lattice at negative pressure. Using DFT calculations in the local-density approximation, Ramachandran et al. determined that Si sII clathrate will become the stable phase compared to the diamond cubic phase at −3 GPa.[50] An MD simulation using the Stillinger−Weber Si potential estimated that the diamond−liquid−sII triple pressure would be $p_t = -1.5$ GPa, and they extrapolated experimental data to predict $p_t = -2.5$ GPa.[51] A silicon pressure of −1.5 GPa corresponds to −1230 atm in mW units (the relation between the pressure in SW silicon and mW water is $p_{Si} = 12.03 p_{mW}$, where we used the definition of reduced pressure $p^* = p\sigma^3/\varepsilon$ and the σ and ε parameters of Si[20] and mW water). SW silicon corresponds to a less tetrahedral water potential, $\lambda = 21$,[20] compared to mW water, $\lambda = 23.15$. This −1230 atm water-scaled triple pressure for silicon can be compared with the $p_t \approx -1300$ atm we obtain for mW water. The comparison of the phase diagrams of these two tetrahedral substances in a common set of units reveals that, in spite of their chemical differences and the distinct nature of metallic/covalent vs hydrogen bonded interactions that bind each of the structures, water and silicon have very similar thermodynamics.[12−15,52]

G. Two Proposals to Produce Empty Water Clathrates in the Lab. Despite the low probability for the nucleation of empty clathrate hydrates from liquid water even in their region of stability, the possibility may still exist for their synthesis by other means. Guest-free Si clathrates are predicted to be the stable phase of silicon at negative pressures.[50,51] The empty silicon clathrates, however, are not produced at negative pressures but by removing the sodium guest atoms of an already formed clathrate at high temperature and vacuum.[53] We propose that the same strategy could be pursued to produce empty water clathrates from hydrogen hydrates. Hydrogen is small enough to readily diffuse in the clathrate structure.[54,55] Mao et al. have reported that at 115 K the hydrogen molecules start leaving the sII hydrogen clathrate hydrate[56] when the latter is heated from 77 K at 10 kPa. We expect that longer waiting times in this condition would lead to the total elimination of hydrogen, producing an empty water clathrate of structure sII. In the experiment of ref 56, the crystal structure collapsed at 145 K, although it is not clear whether it was already empty at lower temperatures, the collapse was induced by the desorption of the hydrogen molecules, or it is an intrinsic limit of stability of the empty lattice. If the latter were true, all existing calculations would be severely underestimating the free energy difference between ice and sII. Considering the values of $\Delta G_{ice,clathrate}$ in the literature and the thermodynamic cycle of eq 7, empty clathrates should be stable with respect to the liquid up to at least 200 K.

An alternative strategy to produce guest-free clathrates involves their growth using a filled hydrate as a template. The growth could be effected through water deposition using molecular beams[57] at temperatures lower than the glass transition temperature of water, 136 K.[58] This would deposit low-density amorphous ice (LDA) on top of the clathrate crystal.[59] Fast heating of this composite clathrate−LDA system to a temperature just below the melting temperature of the empty clathrate, ∼250 K according to our predictions, would lead to the growth of the empty clathrate structure from supercooled water. For this method to succeed, the template should be stable (or metastable) at low temperatures under high vacuum conditions and the melting temperature of the empty clathrate should be considerably higher than the temperature of homogeneous nucleation of ice, 235 K.[30] We have shown in this work that this may be the case if the free energy difference between ice and clathrate is not severely underestimated in the mW

simulations. Another assumption for the success of this strategy is that clathrates are unable to nucleate ice; this has proved to be the case in the simulations presented here and also in experiments.[60]

IV. Conclusions

Using molecular simulations, we investigated the stability and growth of empty water clathrates, a low-density crystal phase of water. We computed—for the first time, to the best of our knowledge—the equilibrium melting temperatures of empty water clathrates with crystal structure sI and sII. The mW model, that accurately represents the melting temperature of Ih ice and the relative stability of cubic and hexagonal ice, predicts that sI and sII melt at 245 ± 2 and 252 ± 2 K, respectively. In the simulations, the crystals are metastable for at least 100 ns at the melting point of ice. Shorter atomistic simulations with various atomistic models concur with this result.

Simulations with the mW model predict that empty water clathrates would be more stable than ice at pressures lower than about −1300 atm and more stable than the liquid in this negative pressure region and temperatures lower than ∼275 K. As the molar volumes of the ice and clathrate crystals predicted by the model are smaller than those found in the experiments, the predicted pressure of ice−clathrate coexistence cannot be accurately described by mW. Linear extrapolations of the melting pressures of ice and empty clathrate using the Clayperon equation indicate that guest-free clathrates may not be stable for pressures higher than −1900 atm. These results give little hope for the crystallization of empty clathrates from the liquid phase, as they lie beyond the experimental limit of cavitation of water.[19,46] Even if the liquid were stable with respect to cavitation in the region of formation of the empty clathrates, these may not crystallize spontaneously from supercooled water. Our simulations show homogeneous nucleation of ice, and not a clathrate, at $p = -2000$ atm although the latter is the most stable phase. Ice nucleation is kinetically favored—lower barrier to nucleation—because the structure of supercooled water approaches that of ice[13] and it does not resemble that of clathrates. We found no evidence of formation of dodecahedral cages in supercooled stretched water.

The mW model can grow the complex structure of clathrates, in spite of not having hydrogen atoms or electrostatics. Our results show that clathrates do not need the hydrophobic solute to grow, but to nucleate and make them stable at high temperatures. In agreement with previous MD studies of methane hydrate growth,[61] we find that the guest-free sI phase is able to nucleate the more stable sII phase. Both phases, however, seem unable to nucleate hexagonal or cubic ice, even in deeply supercooled water. This is consistent with an experimental study of homogeneous nucleation of THF hydrate clathrate, which found that clathrates are a poor template for ice nucleation.[60]

As clathrates are unable to nucleate ice, we propose that, if empty clathrates were formed, they could be kept in a metastable state up to their melting temperatures. Our results suggest that empty clathrates may play a role in the growth of gas hydrates from supercooled water and from finely divided ice in conditions in which the latter presents surface melting. The formation of structures in which a significant portion of the cages are empty, such as THF hydrate, may be influenced by the stability and growth of the empty cages.

Although gas hydrate clathrates are ubiquitous and actively studied, guest-free water clathrate structures have not been synthesized to date. We propose two strategies to make empty clathrates in the lab. The first one involves their growth using filled ones as a template. Annealing of a clathrate deposited with LDA at a temperature lower than T_m of the empty clathrate but higher than T_H of ice would lead to the growth of the empty clathrate structure from supercooled water. The success of this approach relies on the melting temperature of the clathrate being higher than T_H of ice.

In the second and most promising strategy we propose, the empty clathrate lattices would be created by allowing small guest molecules such as hydrogen to escape the cages,[54−56] leaving behind an empty water lattice. This is related to the method employed to prepare empty silicon clathrate lattices. Results published in ref 56 indicate that at low pressures H_2 starts leaving the H_2−hydrate crystal at $T \sim 115$ K. This strategy to produce guest-free water clathrates seems more robust, as it does not depend on T_m of the guest-free clathrates being higher than T_H of ice.

The experimental study of the properties of guest-free water clathrates could elucidate puzzles such as the origin of the anomalous thermal conductivity of gas-hydrates at low temperature,[62,63] provide reliable thermochemical values to evaluate the stability of yet uncharacterized gas hydrates, and shed light on the standing of this new water crystal with respect to the other known phases of water.

Acknowledgment. We are indebted to Masakazu Matsumoto for kindly sharing his ring statistics code with us. We thank Kenneth D. Jordan, Matthew Walsh, and Amadeu Sum for their comments on the manuscript. W.H. acknowledges a student fellowship from DAAD and the exchange program at TU-Braunschweig for supporting his stay at the University of Utah. We acknowledge the Center of High Performance Computing of the University of Utah for allocation of computing time.

References and Notes

(1) San-Miguel, A.; Toulemonde, P. *High Pressure Res.* **2005**, *25*, 159.
(2) McMullan, R.; Jeffrey, G. A. *J. Chem. Phys.* **1959**, *31*, 1231.
(3) Shin, K.; Kim, Y.; Strobel, T. A.; Prasad, P. S. R.; Sugahara, T.; Lee, H.; Sloan, E. D.; Sum, A. K.; Koh, C. A. *J. Phys. Chem. A* **2009**, *113*, 6415.
(4) Sloan, E. D. *Nature* **2003**, *426*, 353.
(5) Brewer, P. G.; Friederich, C.; Peltzer, E. T.; Orr, F. M. *Science* **1999**, *284*, 943.
(6) Milkov, A. V. *Earth-Sci. Rev.* **2004**, *66*, 183.
(7) Mao, W. L.; Mao, H.-k. *Proc. Natl. Acad. Sci. U. S. A.* **2004**, *101*, 708.
(8) Struzhkin, V. V.; Militzer, B.; Mao, W. L.; Mao, H.-k.; Hemley, R. J. *Chem. Rev.* **2007**, *107*, 4133.
(9) Koh, C. A. *Chem. Soc. Rev.* **2002**, *31*, 157.
(10) Guloy, A. M.; Ramlau, R.; Tang, Z. J.; Schnelle, W.; Baitinger, M.; Grin, Y. *Nature* **2006**, *443*, 320.
(11) Nolas, G. S.; Beekman, M.; Gryko, J.; Lamberton, G. A.; Tritt, T. M.; McMillan, P. F. *Appl. Phys. Lett.* **2003**, *82*, 910.
(12) Molinero, V.; Moore, E. B. *J. Phys. Chem. B* **2009**, *113*, 4008.
(13) Moore, E. B.; Molinero, V. *J. Chem. Phys.* **2009**, *130* (24), 244505.
(14) Molinero, V.; Sastry, S.; Angell, C. A. *Phys. Rev. Lett.* **2006**, *97*, 075701.
(15) Bhat, M. H.; Molinero, V.; Soignard, E.; Solomon, V. C.; Sastry, S.; Yarger, J. L.; Angell, C. A. *Nature* **2007**, *448*, 787.
(16) Debenedetti, P. G. *J. Phys.: Condens. Matter* **2003**, *15*, R1669.
(17) Mishima, O.; Stanley, H. E. *Nature* **1998**, *396*, 329.
(18) Debenedetti, P. G.; Stanley, H. E. *Phys. Today* **2003**, *56*, 40.
(19) Zheng, Q.; Durben, D. J.; Wolf, G. H.; Angell, C. A. *Science* **1991**, *91*, 254.
(20) Stillinger, F. H.; Weber, T. A. *Phys. Rev. B* **1985**, *31*, 5262.
(21) DeMille, R. C.; Molinero, V. *J. Chem. Phys.* **2009**, in press.
(22) Kastelowitz, N.; Molinero, V. manuscript in preparation.
(23) Plimpton, S. *J. Comput. Phys.* **1995**, *117*, 1.
(24) Chakoumakos, B. C.; Rawn, C. J.; Rondinone, A. J.; Stern, L. A.; Circone, S.; Kirby, S. H.; Ishii, Y.; Jones, C. Y.; Toby, B. H. *Can. J. Phys.* **2003**, *81*, 183.
(25) Fernandez, R. G.; Abascal, J. L. F.; Vega, C. *J. Chem. Phys.* **2006**, *124*, 144506.

(26) Wang, J.; Yoo, S.; Bai, J.; Morris, J. R.; Zeng, X. C. *J. Chem. Phys.* **2005**, *123*, 036101.
(27) Yoo, S.; Zeng, X. C.; Morris, J. R.*J. Chem. Phys.* **2004**, *120*, 1654.
(28) Matsumoto, M.; Baba, A.; Ohmine, I. *J. Chem. Phys.* **2007**, *127*, 134504.
(29) Davidson, D. W.; Desando, M. A.; Gough, S. R.; Handa, Y. P. *J. Inclusion Phenom. Macrocyclic Chem.* **1987**, *5*, 219.
(30) Oguni, M.; Angell, C. *J. Phys. Chem.* **1983**, *87*, 1848.
(31) Johari, G. P. *J. Chem. Phys.* **2005**, *122*, 144508.
(32) Schmeisser, M.; Iglev, H.; Laubereau, A. *Chem. Phys. Lett.* **2007**, 11271–11275.
(33) Tanaka, H. *J. Chem. Phys.* **1993**, *98*, 4098.
(34) Vega, C.; Sanz, E.; Abascal, J. L. F. *J. Chem. Phys.* **2005**, *122*, 114507.
(35) Belosludov, V.; Inerbaev, T.; Belosludov, R.; Kudoh, J.; Kawazoe, Y. *J. Supramol. Chem.* **2002**, *2*, 377.
(36) Schofield, D. P.; Jordan, K. D. *J. Phys. Chem. A* **2009**, in press.
(37) Myshakin, E. M.; Jiang, H.; Warzinski, R. P.; Jordan, K. D*J. Phys. Chem. A* **2009**, *113*, 1913.
(38) Vatamanu, J.; Kusalik, P. G. *J. Am. Chem. Soc.* **2006**, *128*, 15588.
(39) Sloan, E. D. *Clathrate Hydrates of Natural Gases*, 2nd ed.; Marcel Dekker: New York, 1998.
(40) Cao, Z. T.; Tester, J. W.; Trout, B. L. *J. Phys. Chem. B* **2002**, *106*, 7681.
(41) Koop, T.; Luo, B. P.; Tsias, A.; Peter, T. *Nature* **2000**, *406*, 611.
(42) Johari, G. P. *J. Chem. Phys.* **2000**, *112*, 8573.
(43) Handa, Y.; Tse, J. *J. Phys. Chem.* **1986**, *90*, 5917.
(44) Dharmawardhana, P.; Parrish, W.; Sloan, E. *Ind. Eng. Chem. Fundam.* **1980**, *19*, 410.
(45) Holder, G.; Malekar, S.; Sloan, E. D. *Ind. Eng. Chem. Fundam.* **1984**, *23*, 123.
(46) Herbert, E.; Balibar, S.; Caupin, F. *Phys. Rev. E* **2006**, *74*, 041603.
(47) Speedy, R. *J. Phys. Chem.* **1982**, *86*, 982.
(48) Watanabe, M.; Adachi, M.; Morishita, T.; Higuchi, K.; Kobatake, H.; Fukuyama, H. *Faraday Discuss.* **2007**, *136*, 279.
(49) Mcmillan, P. F.; Wilson, M.; Daisenberger, D.; Machon, D. *Nat. Mater.* **2005**, *4*, 680.
(50) Ramachandran, G. K.; McMillan, P. F.; Deb, S. K.; Somayazulu, M.; Gryko, J.; Dong, J. J.; Sankey, O. F. *J. Phys.: Condens. Matter* **2000**, *12*, 4013.
(51) Wilson, M.; McMillan, P. F. *Phys. Rev. Lett.* **2003**, *90*, 135703.
(52) Angell, C. A.; Bressel, R. D.; Hemmati, M.; Sare, E. J.; Tucker, J. C. *Phys. Chem. Chem. Phys.* **2000**, *2*, 1559.
(53) Gryko, J.; McMillan, P. F.; Marzke, R. F.; Ramachandran, G. K. *Phys. Rev. B* **2000**, *62*, R7707.
(54) Nagai, Y.; Yoshioka, H.; Ota, M.; Sato, Y.; Inomata, H.; Smith, R. L.; Peters, C. J. *AIChE J.* **2008**, *54*, 3007.
(55) Abbondondola, J. A.; Fleischer, E. B.; Janda, K. C.**2009**, submitted to AIChE.
(56) Mao, W. L.; Mao, H.; Goncharov, A. F.; Struzhkin, V. V.; Guo, Q. *Science* **2002**, *297*, 2247.
(57) Kimmel, G. A.; Stevenson, K. P.; Dohnalek, Z.; Smith, R. S.; Kay, B. D. *J. Chem. Phys.* **2001**, *114*, 5284.
(58) Angell, C. A. *Annu. Rev. Phys. Chem.* **2004**, *55*, 559.
(59) Dohnalek, Z.; Kimmel, G. A.; Ciolli, R. L.; Stevenson, K. P.; Smith, R. S.; Kay, B. D. *J. Chem. Phys.* **2000**, *112*, 5932.
(60) Zhang, Y. F.; Debenedetti, P. G.; Prud'homme, R. K.; Pethica, B. A. *J. Phys. Chem. B* **2004**, *108*, 16717.
(61) Vatamanu, J.; Kusalik, P. G. *J. Phys. Chem. B* **2008**, *112*, 2399.
(62) Jiang, H.; Myshakin, E. M.; Jordan, K. D.; Warzinski, R. P*J. Phys. Chem. B* **2008**, *112*, 10207.
(63) Ross, R.; Andersson, P.; Bäckström, G. *Nature* **1981**, *290*, 322.
(64) *Handbook of Chemistry and Physics*, 81st ed.; CRC: Boca Raton, 2000−2001.

JP903439A

CHAPTER 3

A METHANE-WATER MODEL FOR COARSE-GRAINED SIMULATIONS OF SOLUTIONS AND CLATHRATE HYDRATES

Reprinted with permission from the American Chemical Society

Jacobson, L. C.; Molinero, V. *J. Phys. Chem. B* **2010**, *114*, 7302

7302 *J. Phys. Chem. B* **2010,** *114,* 7302–7311

A Methane−Water Model for Coarse-Grained Simulations of Solutions and Clathrate Hydrates

Liam C. Jacobson and Valeria Molinero*

Department of Chemistry, University of Utah, 315 South 1400 East, Salt Lake City, Utah 84112-0850

Received: February 12, 2010; Revised Manuscript Received: April 19, 2010

Methane is the prototypic hydrophobic molecule; it has an extremely low solubility in liquid water that leads to phase segregation. On the other hand, at moderate pressures and room temperature, water and methane form hydrate clathrate crystals with a methane to water ratio up to a 1000 times higher than the saturated aqueous phase. This apparent dichotomy points to a subtle balance between the strong water−water hydrogen bonding, responsible for the hydrophobic effect, and water−methane attraction. Capturing these nuances with molecular models requires an appropriate balance of intermolecular interactions. Here we present such a coarse-grained molecular model of water and methane that represents each molecule by a single particle interacting through very short-range interaction potentials. The model is based on the monatomic model of water mW [Molinero, V.; Moore, E. B. *J. Phys. Chem. B* **2009**, *113*, 4008] and is between 2 and 3 orders of magnitude more computationally efficient than atomistic models with Ewald sums. The coarse-grained model of this study reproduces the solubility and hydration number of methane in liquid water, the surface tension of the water−methane interface and the equilibrium melting temperature of methane hydrate clathrates with structures sI and sII. To the best of our knowledge this is the first force-field, atomistic or coarse-grained, that reproduces these range of properties of liquid and solid phases of water and methane, making it an efficient and accurate model for the study of the mechanisms of nucleation and growth of clathrates. We expect that the results of this work will also be useful for the modeling of the hydrophobic assembly in aqueous solutions and the development of coarse-grained models of biomolecules with explicit solvation.

I. Introduction

Methane and water have extremely low mutual solubility and segregate in solution. Nevertheless, water and methane form hydrate clathrate crystals with a methane to water ratio up to a 1000 times higher than the saturated aqueous phase. Methane clathrates are nonstoichiometric crystals of water and methane, in which water forms a fully hydrogen-bonded network of polyhedral cages that contain the methane guest.[1] Natural gas hydrates normally form at high pressures and occur naturally on the ocean floor and in the permafrost.[2] Gas hydrates have gained much attention recently due to their promise as an abundant alternative energy source[3] as well as a possible vehicle for carbon sequestration.[4,5] Methane hydrates are of particular interest because, according to some estimates there is more energy contained in methane clathrate deposits than there is energy from all other conventional fossil fuel sources combined.[2] On the other hand, the occurrence of clathrate hydrates in natural gas pipelines is of great concern to the petroleum industry, because as they form in the high-pressure pipelines, they create clogs that stop the flow of gas and disrupt production, increase costs, and present a safety hazard.[2,6] Accurate modeling of the microscopic mechanisms of nucleation, growth, and decomposition of methane clathrates is important for creating clathrate inhibitors as well as devising methods to extract methane from clathrate reserves on an industrial scale.

Under pressure, methane clathrates are stable at ambient temperatures. The dissociation (also called melting) temperature of methane clathrate at 100 atm, for example, is 286.2 K, about 14 K higher than that of hexagonal ice under the same pressure. The hydrogen-bonded water network that forms the clathrate frame accounts for most of the stability of these crystals. In two independent simulation studies, using different models and simulation methodologies, Jacobson et al.[7] and Conde et al.[8] predicted that the guest-free clathrate crystal with the sII structure is a stable phase of water under extension. Our study indicates that at room temperature guest-free water clathrates are metastable with respect to ice Ih and would have a melting temperature of ∼250 K. An extrapolation of the results from ref 8 suggests an even lower value. Thus, while the water−methane attraction is weak, it is key for the formation and stabilization of methane hydrate.

Clathrate hydrates occur predominantly in two cubic structures known as sI and sII. The sI crystal is the most stable methane hydrate. Nevertheless, sI and sII crystals form together during the initial stages of growth of methane hydrate.[9,10] Using the CSM-Gem program by Sloan and co-workers,[11] which calculates multiphase equilibrium using a Gibbs free energy minimization algorithm and reproduces the experimental phase diagram of methane clathrate,[11] we find that the melting temperatures T_m of sI and sII methane hydrates differ by just 1.5 K at 100 atm. We hypothesize that the small difference in T_m (and thus in free energy) between the two crystals is responsible for the occurrence of the stable sI and metastable sII structures in the first stages of crystallization observed both in experimental[9,10] and in computational[12,13] studies. The ability of molecular simulations in reproducing and explaining the polymorphism in the growth of methane clathrates would probably depend on the accuracy of the molecular models in reproducing the closeness of the melting temperatures.

* Corresponding author. E-mail: Valeria.Molinero@utah.edu.

10.1021/jp1013576
Published on Web 05/12/2010

Atomistic simulations of methane−water systems have given valuable insight on the thermodynamic stability,[14,15] growth[16,17] and decomposition,[18,19] anomalous thermal properties,[20,21] and nucleation[12,22] of methane hydrates, as well as on hydrophobic hydration.[23−28] Atomistic models of water−methane systems are normally derived from water and methane potentials that were parametrized and validated for properties of the pure substances. The water−methane interaction parameters are then obtained using combination rules and are typically not validated with experimental thermodynamic data such as melting temperature, enthalpy of dissociation, and solubility. Docherty et al. recently demonstrated that the use of combination rules for water-methane interactions is inadequate to reproduce the solubility of methane, even when the most accurate water and methane potentials are employed.[25]

The models of water used in the simulation of clathrates predict widely different melting temperatures for ice. Of the atomistic models, only TIP4P/ice correctly predicts the experimental T_m of hexagonal ice Ih;[29] widely used models such as SPC, SPC/E, TIP3P, and TIP5P incorrectly predict that ice II and not Ih is the most stable ice crystal at room pressure.[30] It would be expected that a similar variability be observed in the melting temperatures predicted for methane hydrates. Although it is crucial to know the melting temperatures of sI and sII methane clathrate crystals for the modeling and interpretation of the mechanisms of clathrate formation, scarce thermodynamic data are available for the molecular models used for clathrate modeling. The T_m of sI methane hydrate is known for just a couple of atomistic force-fields,[31,32] and (to the best of our knowledge) the T_m of its sII polymorph has never been computed with molecular simulations.

In this work we present the parametrization and validation of a methane−water model that reproduces the experimental hydration number and solubility of methane in water and the melting temperatures of sI and sII methane hydrates. Solubility and melting temperatures are the two most important thermodynamic properties that control the crystallization of clathrates. The hydration number in solution should play a role in the magnitude of the barrier for clathrate nucleation. Different from other models available for simulations of clathrates and aqueous methane, here we present a coarse-grained molecular model. We develop a united-atom methane model and combine it with the monatomic model of water mW, which represents the water molecule by a single particle interacting through very short-ranged potentials.[33] Although mW water does not have hydrogen atoms or even electrostatic interactions, it reproduces the structure of the liquid and crystal phases of water through the use of three-body terms in the potential that encourage "hydrogen-bonded" tetrahedral configurations of the molecules. The mW model reproduces the temperature of melting, enthalpies of vaporization, melting and sublimation of water, and the liquid−vapor surface tension with precision equal or higher than the most popular atomistic water models.[33] It also reproduces the experimental radial and angular structure of liquid water and low-density amorphous ice, as well as the structure, nucleation, and growth of ice in bulk and in confinement.[7,33−36] The monatomic model correctly produces the thermodynamic and dynamic anomalies of water (increase in heat capacity on cooling, density maximum, increase of diffusivity on compression) as well as the transformation of liquid water to low-density amorphous ice and the increase in correlation length that accompanies the structural transformation of water on cooling at room pressure.[33,36] Most important for this work, mW describes the thermodynamics of guest-free clathrates, the growth of empty and filled hydrates, and the nucleation of hydrates with hydrophobic guest molecules.[7,13,37]

The main advantage of a coarse-grained model is its computational efficiency: simulations with the mW model are 180 times faster than with atomistic water models with Ewald sums.[33] An accurate and well-characterized coarse-grained model of methane and water would permit the study of the mechanisms of nucleation and growth of methane clathrates under various thermodynamic conditions with knowledge of the crystallization driving force.

Although there are benefits to using a coarse-grained water model, there are challenges associated with it as well. How well can the hydration structure around methane and the structure of the water−methane interface be reproduced using a potential that does not have atomistic resolution? Is it possible to simultaneously reproduce the solubility in liquid water and the melting temperatures of the sI and sII hydrates? Our goal in this study is to develop coarse-grained methane−methane and water−methane potentials that, in conjunction with the mW model for water, would reproduce the thermodynamics of aqueous methane and methane hydrate. We outline a strategy to parametrize the water−methane interactions and evaluate the parametrization by comparing the results of simulations with experimental values of melting temperature and enthalpy of dissociation of the hydrate, and the hydrophobic solvation of methane in water. We discuss the implications of removing degrees of freedom on the thermodynamics of dissociation of the hydrates when going from a model with atomistic resolution to a coarse-grained one.

The paper is organized as follows: In section II we describe the simulation methodology and introduce the systems modeled in this study. Section III presents the force fields: we describe the mW model, introduce the functional form of the potential for methane−methane and methane−water interactions, the parametrization of the former, and the strategy for the parametrization of the latter. The data necessary for the parametrization and validation of the water−methane interaction are presented in sections IV and V: section IV focus on the thermodynamics of clathrate formation and section V on the structure and thermodynamics of methane−water solutions. Section VI presents a summary and the most important conclusions of this work.

II. Simulation Methods

A. Simulations. Molecular dynamics (MD) simulations were performed using LAMMPS, a massively parallel MD software by Plimpton et al.[38] The absence of fast molecular rotational modes in the coarse-grained models allows for the integration of the equations of motion (velocity Verlet algorithm) with a time step of 10 fs.[33] Periodic boundary conditions were used for all systems. Except when otherwise indicated, the simulations were done in the *NpT* ensemble, with the temperature and pressure regulated by a Nose−Hoover thermostat and barostat with damping constants 5 and 25 ps, respectively. For systems with coexisting liquid and crystal phases, the three cell dimensions were allowed to dilate and contract independently.

B. Systems. ***Fluid Simulations.*** Liquid mixtures consisting of 5 methane and 507 water molecules were evolved for 800 ns at 300 K and 100 atm to gather data for the calculation of the radial distribution function between methane and water. Methane solubility and density profiles were determined from 100 ns simulations of two-phase methane−water systems containing 16 000 molecules (14 851 water molecules and 1149 methane molecules) with cell dimensions approximately 230

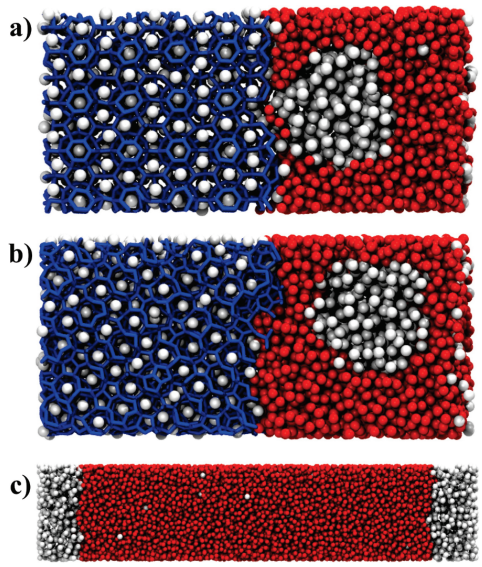

Figure 1. Simulation cells used in the phase-coexistence simulations: (a) phase coexistence of sI methane clathrate with the water-rich and methane-rich liquids; (b) phase coexistence of sII methane clathrate with the water-rich and methane-rich liquids; (c) phase coexistence of the water-rich and methane-rich liquid. Methane molecules depicted as white balls, water molecules connected by blue sticks when they are part of the clathrate cages and displayed as red balls otherwise.

× 50 × 50 Å. Fluid methane simulations were performed with systems containing 1728 coarse-grained methane particles and liquid water simulations with 9936 coarse-grained water particles. The pure liquids were equilibrated over 10 ns at the T and p conditions indicated in the text.

Crystal Simulations. Crystal structures of methane clathrate hydrates were used for the calculations of the enthalpy and the mapping of the regions of stability of each structure. The sI crystals consisted of 4 × 4 × 4 unit cells containing 2944 water molecules and 512 or 384 guest molecules. The sII crystals consisted of 3 × 3 × 3 unit cells containing 3672 water molecules and 648 or 216 guest molecules. The two methane contents for each structure correspond to all polyhedral cages occupied by methane and only the large cages occupied, respectively. The enthalpy of each crystal was averaged over 100 ps simulations for each point of the stability map as well as for the calculation of the enthalpy of dissociation of the clathrates.

Three-Phase Liquid-Crystal Coexistence Simulations. The systems used for melting point determinations were derived from a hydrate lattice (8 × 4 × 4 unit cells consisting of 5888 water molecules and 1024 guest molecules for sI and 6 × 3 × 3 unit cells consisting of 7344 water molecules and 1296 guest molecules for sII). Half of the crystal cell was melted and the liquid was first equilibrated for 10 ns to allow for the phase segregation of aqueous and methane phases. These three-phase coexistence systems are shown in the top two panels of Figure 1. The three-phase systems were evolved at various temperatures at p = 100 atm to allow the determination of the melting temperature through the direct coexistence method described in section IV. Individual simulations for temperatures close to the melting point were carried for as long as 650 ns.

III. Coarse-Grained Models and Force Fields

A. Water Model. The monatomic model of water (mW) represents a water molecule by a single particle that interacts through very short-ranged potentials.[33] The interaction in mW water has the form of the Stillinger−Weber potential:[39]

$$E = \sum_i \sum_{j>i} \phi_2(r_{ij}) + \sum_i \sum_{j\neq i} \sum_{k>j} \phi_3(r_{ij},r_{ik},\theta_{ijk})$$
$$\phi_2(r_{ij}) = A\varepsilon\left[B\left(\frac{\sigma}{r_{ij}}\right)^4 - 1\right]\exp\left(\frac{\sigma}{r_{ij} - a\sigma}\right)$$
$$\phi_3(r_{ij},r_{ik},\theta_{ijk}) = \lambda\varepsilon[\cos\theta_{ijk} - \cos\theta_0]^2 \exp\left(\frac{\gamma\sigma}{r_{ij} - a\sigma}\right)\exp\left(\frac{\gamma\sigma}{r_{ij} - a\sigma}\right) \quad (1)$$

where r_{ij} is the distance between particles i and j and θ_{ijk} is the angle subtended by the vectors between the positions of the $i-j$ and $i-k$ pairs of particles. The constants A = 7.049 556 277, B = 0.602 224 558 4, γ = 1.2, a = 1.8, and θ_o = 109.5° are the same for mW water and the original SW silicon potential.[39] The three-body terms encourage "hydrogen-bonded" configurations between mW waters by imposing a penalty to configurations with water−water−water angles that depart from the tetrahedral value, θ_o = 109.5°. The value of the parameter λ determines the strength of the tetrahedral interactions. All intermolecular forces vanish at a cutoff distance $r_c = a\sigma = 1.8\sigma$.

The interaction strength ε_w = 6.189 kcal/mol, characteristic distance σ_w = 2.3925 Å, and the tetrahedral parameter λ_w = 23.15 of the monatomic mW were optimized in ref 33 to reproduce the experimental enthalpy of vaporization and density of liquid water at 298 K and 1 atm, and the melting temperature of hexagonal ice.

B. Methane Model. The level of coarsening of the methane model of this study is the same as the OPLS united-atom (OPLS-UA) methane model:[40] a methane molecule is represented by a single particle. The OPLS-UA model uses the Lennard-Jones 12-6 potential to describe methane−methane interactions, and it reproduces the experimental heat of vaporization, density, and vapor−liquid coexistence curve of methane.[40−42] The interactions in OPLS-UA methane extend at distances considerably longer than in mW water. The combination of coarse-grained potentials with different length scales and softness produces unphysical results.[43] Here we use the two-body term of the Stillinger−Weber (SW) potential (ϕ_2 in eq 1) to describe methane−methane interactions. We set λ = 0 for methane triplets because, different from water, methane interactions are well represented by isotropic potentials. The values of A, B, and a in eq 1 are the same as listed above for mW. In what follows, we use the acronym M_{SW} to designate the coarse-grained methane model with the short-ranged SW interactions.

We adjusted the characteristic size σ_m and interaction strength ε_m between methane particles to reproduce the volume and enthalpy of vaporization, ΔH_{vap}, of methane at its boiling point at p = 1 atm and T = 111.66 K. ΔH_{vap} of the M_{SW} model was calculated as the difference in the molar enthalpy of the gas and the liquid at these conditions. The ensemble average of the enthalpy, $\langle H\rangle = \langle E + pV\rangle$ of the liquid was determined from NpT simulations of 1728 methane particles for 10 ns. The methane gas was assumed to be ideal: $H_{gas} = 1.5\,RT + pV_{gas} = 2.5\,RT$. Table 1 lists σ_m and ε_m for methane−methane interactions in M_{SW}. The model reproduces the experimental enthalpy of vaporization (1.95 ± 0.02 kcal/mol compared to 1.96 kcal/mol[40]) and density (0.424 ± 0.003 g/mL compared to 0.424 g/mL[40]).

TABLE 1: Interaction Parameters for the Coarse-Grained Model

	ε (kcal/mol)	σ (Å)	λ
water[a]	6.189	2.3925	23.15
methane	0.340	4.08	0
water−methane	0.180	4.00	0

[a] Reference 33. Interactions potential described by eq 1 with the other constants same as for mW.

TABLE 2: Density of Fluid Methane at $T = 300$ K

	ρ_{Exp}[a] (g/mL)	$\rho_{OPLS\text{-}UA}$ (g/mL)	ρ_{Msw} (g/mL)	ρ_{Msw}/ρ_{Exp}
1 atm	6.4×10^{-4}	6.6×10^{-4}	6.5×10^{-4}	1.01
50 atm	0.035	0.035	0.039	1.11
100 atm	0.075	0.075	0.10	1.33

[a] The experimental density of methane was computed using the equation of state from ref 44.

TABLE 3: Enthalpy of Fluid Methane at 300 K

	$H^{OPLS\text{-}UA}$ (kcal/mol)	H^{Msw} (kcal/mol)	$H^{Msw}/H^{OPLS\text{-}UA}$
1 atm	1.49	1.48	0.99
50 atm	1.31	1.20	0.92
100 atm	1.13	0.82	0.73

Table 2 shows the density of methane at 300 K as a function of pressure in experiments and in our simulations with the OPLS-UA and M_{SW} models. OPLS-UA methane reproduces the equation of state of methane in the range of pressures presented in Table 1.[44] The M_{SW} model reproduces the experimental density at 1 atm, but the agreement degrades at high pressures because the softer repulsive region of M_{SW} methane makes it more compressible than OPLS-UA methane. In terms of its impact on the dissociation equilibrium of methane clathrates, the density of methane is less important than its enthalpy. Table 3 shows the molar enthalpy of methane as a function of pressure for the OPLS-UA and M_{SW} models at $T = 300$ K. As observed for the density, the agreement is better at low pressures. M_{SW} underestimates the enthalpy at high pressures, probably due to the extremely short-ranged nature of the potential. A pressure of 1 atm was chosen for the parametrization of M_{SW} methane because this is the pressure for which mW water was parametrized. It is possible to parametrize M_{SW} to reproduce the experimental high-pressure behavior of methane, but we consider it unnecessary because water−water and water−methane interactions dominate the thermodynamics of clathrate formation: the error in the enthalpy of methane at 300 K and 100 atm is just 2.4% of the experimental enthalpy of dissociation of sI methane hydrate, $\Delta H_d = 13.01$ kcal/mol, under the same conditions.[45]

C. Methane−Water Interactions. Water does not form hydrogen bonds with methane; thus we set set $\lambda = 0$ for triplets that contain water and methane. The water−methane potential is described by the two-body term of eq 1 with A, B, and a identical to those of mW, as we did for the methane−methane potential. In what follows we explain the strategy we adopt in this study to determine the two remaining parameters: the characteristic distance σ_{wm} and strength of the attraction ε_{wm} of the water−methane potential.

In atomistic simulations, the cross-parameters σ_{wm} and ε_{wm} are typically derived using Lorentz−Berthelot combination rules of the parameters of the water−water and methane−methane interactions. Vega and co-workers have shown that such combination rules for the water−methane interaction in rigid water models are unable to reproduce the experimental value of the solubility of methane in water.[25] They suggest that the cause is the lack of polarizability in the rigid water models that they compensate by scaling up 7% the attraction strength ε between water and methane in a nonpolarizable model. Most of the water−water attraction in atomistic models results from electrostatic interactions and ε_{ww} is small, around 0.15 kcal/mol. In mW water, on the other hand, there are no electrostatic interactions and ε_{ww} is about 40 times larger. Use of combination rules would result in a very attractive water−methane potential, inconsistent with the known hydrophobicity of methane. Combination rules are not a good starting point to search for the optimum ε_{wm} in the coarse-grained model.

To optimize ε_{wm} and σ_{wm} of the coarse-grained model, we produce a set of candidate solute−water parameters for which we compute (i) the melting temperature T_m of the clathrates with structures sI and sII, (ii) the corresponding enthalpy of dissociation ΔH_d of the sI methane clathrate, (iii) the solubility x_m of methane in water, and (iv) the hydration number n_w of methane in water at infinite dilution. The best values of ε_{wm} and σ_{wm} are then determined by comparison of the predictions of the simulations with the experiments.

As a guide for the parametrization, we map out the regions of stability for clathrates with guest methane molecules of different structures and stoichiometry in the [σ_{wm}; ε_{wm}] parameter space. The stable crystal for each value of [σ_{wm}; ε_{wm}] is approximated as that with the lowest enthalpy of formation. A more rigorous calculation of the stabilities based on free energies is unnecessary because the map is used only as a guide for the parametrization. Using the fully occupied sII crystal as reference, we computed the difference in enthalpy for the following processes (subscripts indicate partial crystal occupancy):

$$
\begin{aligned}
&23\mathrm{sII} \leftrightarrow 68\mathrm{sI} + 8\mathrm{CH_4}\\
&\left(1\mathrm{H_2O} + \frac{3}{17}\mathrm{CH_4}\right) \leftrightarrow \left(1\mathrm{H_2O} + \frac{4}{23}\mathrm{CH_4}\right) + \frac{1}{391}\mathrm{CH_4}\\
&23\mathrm{sII} \leftrightarrow 68\mathrm{sI}_{(\text{empty dodecahedra})} + 144\mathrm{CH_4}\\
&\left(1\mathrm{H_2O} + \frac{3}{17}\mathrm{CH_4}\right) \leftrightarrow \left(1\mathrm{H_2O} + \frac{3}{23}\mathrm{CH_4}\right) + \frac{18}{391}\mathrm{CH_4}\\
&23\mathrm{sII} \leftrightarrow 23\mathrm{sII}_{(\text{empty dodecahedra})} + 368\mathrm{CH_4}\\
&\left(1\mathrm{H_2O} + \frac{3}{17}\mathrm{CH_4}\right) \leftrightarrow \left(1\mathrm{H_2O} + \frac{1}{17}\mathrm{CH_4}\right) + \frac{2}{17}\mathrm{CH_4}
\end{aligned}
\tag{2}
$$

The enthalpies of sI and sII clathrates at 100 atm and 300 K with (i) all cages occupied by methane and (ii) only the large cages filled were calculated for 3 Å < σ_{wm} < 5 Å (evaluated every 0.1 Å) and 0.1 < ε_{wm} < 0.4 kcal/mol (evaluated every 0.05 kcal/mol). The last element of the calculations, the enthalpy of methane under the same conditions, was taken from Table 3.

The resulting "stability map" as a function of σ_{wm} and ε_{wm} is shown in Figure 2. The "stability region" of each structure encompasses the values of water−methane parameters for which that crystal has the lowest enthalpy of formation. The order of the structures in terms of σ_{wm} is representative of the trend in guest size determined in experiments.[1] The smallest guest molecules favor the sII structure (also the most stable in the absence of guests[7,8]) but larger guest molecules that struggle to fit in the small dodecahedral cages stabilize the sI crystal because it has a higher ratio of large to small cages. Only the sII structure has cages large enough to accommodate the largest guest molecules. As σ_{wm} and ε_{wm} become smaller, the sII structure is favored.

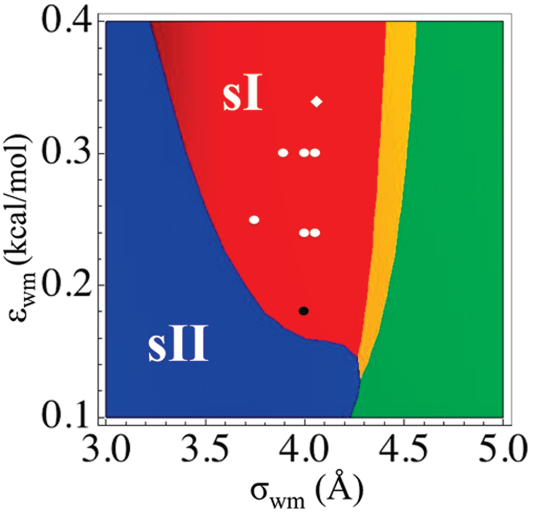

Figure 2. Regions of stability of sI and sII clathrates as a function of the water−methane interaction parameters, σ_{mw} and ε_{mw}. The colored areas indicate the regions where a clathrate structure has the lowest enthalpy of formation: blue corresponds to the sII structure with all cages occupied, red to the fully occupied sI crystal, yellow to the sI structure with occupied large cages and empty dodecahedral cages, and green to the sII structure with filled large cages and empty dodecahedral cages. The diamond indicates the parameters used for the methane−methane interactions. The circles represent the set of [σ_{wm}; ε_{wm}] parameters evaluated in this study (results listed in Table 4). The black circle indicates the parameters that best reproduce the T_m and solubility of methane, $\sigma_{wm} = 4.0$ Å and $\varepsilon_{wm} = 0.18$ kcal/mol.

Once the regions of stability were mapped, we focused our search on the region of Figure 2 where the sI methane hydrate with small and large cages occupied is the most stable crystal, as found in the experiments.[2] Sections IV and V present the analysis of the thermodynamics and structure of solutions and clathrates for which the water−guest interaction parameters lie within this region of the [σ_{wm}; ε_{wm}] space. The best methane−water parameters that result from a comparative analysis of the melting temperatures, methane solubility, and hydration number are listed in Table 1.

Molecular dynamics simulations of water corresponding to a given amount of time (e.g., 100 ns) take 180 times less computing time with mW than with atomistic water models using Ewald sums.[33] The increase in efficiency is due to the larger time steps, the decrease in the number of particles, and the extremely short-range of the interaction potentials. We refer the readers to refs 33 and 43 for details on the benchmarking of mW against the atomistic SPC/E water model and the scaling of the computing cost with the number of particles (better than for Ewald sums and slightly less favorable than for particle−particle−particle mesh Ewald). Calculations of methane−methane and methane−water interactions are faster than among water molecules, because they do not involve the more expensive calculations of the three-body forces in the potential (to this end, we modified the standard version of the Stillinger−Weber potential in LAMMPS to avoid the three-body loops when $\lambda = 0$). We benchmarked the simulation times for liquid systems composed of 6912 particles of (i) model water, (ii) M_{SW} methane, and (iii) half methane and half water, and found that pure M_{SW} simulations are about 13 times faster than the pure mW, and a 1:1 mixture of model water and M_{SW} methane is twice as fast as pure model water. On this basis, we conclude that, depending on the ratio of water and methane, this coarse-grained model speeds up the simulations by 2−3 orders of magnitude compared to the atomistic ones.

IV. Thermodynamic Stability of sI and sII Methane Clathrates

A. Melting Temperatures of sI and sII Methane Hydrates. Experiments indicate that the stable methane hydrate has the sI structure.[2] Nevertheless, several studies have shown that sII also forms in the initial stages of methane clathrate crystallization,[9,10] suggesting that the stabilities of sI and sII methane hydrates are similar. We computed the melting temperatures of these two crystals using the CSMGem program by Sloan and co-workers.[11] At $p = 100$ atm, the predicted T_m's for methane hydrate are 286.2 K for the sI structure and 284.7 K for the sII structure. The T_m for the most stable methane clathrate structure (sI) has been computed for very few force fields: TIP4P water and OPLS-AA methane predict a T_m of sI between 287 and 302 K at $p = 400$ atm[31] and the COS/G2 water model and five-site methane produce $T_m = 268 \pm 3$ K at $p = 67$ atm.[32] The melting temperature of the sII methane clathrate has not been reported for any force field.

In the melting (dissociation) of clathrates, three phases coexist in equilibrium: liquid water saturated with methane, fluid methane saturated with water, and the clathrate crystal. The melting temperatures (T_m) of the clathrates were determined using the method of direct coexistence.[46,47] The two upper panels of Figure 1 show snapshots of the three-phase systems used to determine T_m for the sI and sII clathrate crystals. This method involves performing simulations at constant pressure at a series of temperatures T for a system in which a crystal and the fluid phases are in direct coexistence. T_m was evaluated by determining at which temperature there was no net growth or decomposition of the clathrate phase. De Pablo and co-workers have used this method to determine the melting temperature of sI methane hydrate.[31] The fluid methane phase in our coexistence simulations is a cylinder (see Figure 1) because this is the shape that minimizes the area for the amount of methane in the cell. We show in section VA below that the solubility of methane in water (i.e., its chemical potential) with the cylinder and a slab of methane are indistinguishable. Thus, the melting temperatures determined in this study would be the same if measured with a slab configuration.

We determined the T_m of sI and sII structures at $p = 100$ atm for candidate water−methane parameters, [σ_{wm}; ε_{wm}], located in the region of the parameter space where the fully filled sI structure has the lowest enthalpy of formation (Figure 2). A pressure of 100 atm was selected because it is well within the hydrate-forming region of the methane hydrate phase diagram. Table 4 presents the T_m for a range of water−methane parameters. The error bar measures the temperature gap in which no net growth or dissolution could be observed. We note that within a few degrees of the melting temperature, simulations as long as 650 ns were needed to establish whether the system evolved toward the crystal or the liquid state, and in some cases there was no evolution toward crystal or liquid phase even in this time scale. The length of the simulations needed to produce a phase change close to the melting temperature grows increasingly longer as the water−methane interaction strength ε_{wm} decreases.

For all the [σ_{wm}; ε_{wm}] sets, we find that the T_m of sI is higher than, or equal within the error bar to, T_m of sII, consistent with the prediction of Figure 2. The difference between the two

TABLE 4: Thermodynamic and Structural Properties of Methane Clathrates and Aqueous Solutions as a Function of the Water−Methane Interaction Parameters

		methane−water interaction parameters [σ (Å); ε (kcal/mol)]						
property	experiment	[4.0; 0.18]	[4.05; 0.24]	[4.0; 0.24]	[4.0; 0.3]	[4.05; 0.3]	[3.90; 0.3]	[3.75; 0.25]
T_m sI	286.2[a]	285 ± 4	302.5 ± 1	308 ± 2	329 ± 1	323 ± 1	338 ± 2	333 ± 1
T_m sII	284.7[a]	286 ± 1	301 ± 1	304 ± 2	321 ± 1	318 ± 2	333 ± 2	329 ± 1
ΔH_d^{sI}	13.01 ± 0.35[b]	9.27	10.3	10.4	11.6	11.4	12.0	11.2
ΔS_d^{sI}	45	33	34	34	35	35	36	34
solubility	0.002325[c]	0.0022	0.0038	0.0049	0.015	0.013	0.018	0.012
hydration	20,[d] 19 ± 1[e]	19.3	19.7	19.7	21.8	21.7	20.9	18.9

[a] Calculated in the CSMGem software program,[11] [b] Reference 45. [c] Reference 48. [d] Reference 52. [e] Reference 51. Units: melting temperature T_m in K, solubility in methane molar fraction, enthalpy of dissociation ΔH_d in kcal/mol of methane, and entropy of dissociation ΔS_d in (cal/K)/mol of methane). ΔH_d and ΔS_d computed at $T = 300$ K and $p = 100$ atm, solubility at 313 K and 178 atm.

melting temperatures for the sI and sII crystals (ΔT_m) ranged from -1 ± 5 to 8 ± 2 K. The actual values of T_m increase with the strength of water−methane attraction ε_{wm} and decrease with increasing characteristic size σ_{wm}. The best agreement with the experiment is obtained for $\sigma_{wm} = 4.0$ Å and $\varepsilon_{wm} = 0.18$ kcal/mol, which predict $T_m = 285 \pm 4$ K for sI and 286 ± 1 for sII. The T_m for [4.0 Å; 0.18 kcal/mol] agree with the experiment within the precision of the simulations. The ΔT_m is -1 ± 5 K; thus, although it agrees with the 1.5 K predicted with the CSMGem program, the simulations cannot attain the level of precision required to distinguish two melting temperatures that are so close, even using the very long simulations of this study.

B. Enthalpy and Entropy of Dissociation of Methane Hydrate. If the methane and water liquids in equilibrium with methane hydrate were pure (a good approximation due to their very low mutual solubility), the enthalpy of dissociation of the clathrate ΔH_d could be written in terms of the enthalpy of melting of the corresponding empty clathrate frame, ΔH_m^{empty}, the enthalpy of methane with respect to a state without intermolecular interactions, $\Delta H^{\infty}_{methane}$, and the enthalpy for enclathrating the methane from a noninteracting gas state into the water clathrate frame, $\Delta H^{enclathration}_{methane-water}$:

$$\Delta H_d = 5.75\Delta H_m^{empty} - \Delta H^{\infty}_{methane} - \Delta H^{enclathration}_{methane-water} \quad (3)$$

where 5.75 is the ratio of water to methane in a fully occupied sI clathrate. The experimental enthalpy of dissociation of sI methane hydrate at 100 atm is $\Delta H_d = 13.01$ kcal per mol of gas.[45] In ref 7 we computed $\Delta H_m^{empty} = 1.05$ kcal/mol at 250 K, resulting in $5.75\Delta H_m^{empty} \approx 6.04$ kcal/mol (and expected to be larger at 300 K because the heat capacity of the liquid is larger than the heat capacity of the crystal). $\Delta H^{\infty}_{methane}$ is 0.82 kcal/mol for the M_{SW} model at 300 K and 100 atm (Table 3). This indicates that about half the enthalpy of dissociation of methane hydrate originates in the interaction between water and methane in the crystal.

As the average hydration number for methane in the fully occupied sI clathrates is 23 and the maximum water−methane interaction is ε_{wm}, to reproduce the experimental enthalpy of dissociation the value of ε_{wm} should be around 0.3 kcal/mol. We evaluated ΔH_d, of the sI clathrate at 100 atm for combinations of [σ_{wm}; ε_{wm}]. The results are listed in Table 4. ΔH_d was determined by subtracting the enthalpy of the clathrate phase from that of the separated methane and liquid water phases, each of them weighted by the stoichiometry of the reaction of formation of the sI clathrate. The enthalpies of methane and liquid water were determined from separate simulations of the coarse-grained M_{SW} and mW models at 300 K and 100 atm.

Table 4 shows that $\varepsilon_{wm} \approx 0.30$ kcal/mol overestimates the melting temperature by about 45 K. The mismatch indicates a lower entropy of dissociation of the coarse-grained model compared to that of the experiment. The enthalpy of dissociation of the clathrate ΔH_d and its corresponding phase equilibrium temperature T_m are related through $T_m = \Delta H_d/\Delta S_d$, where ΔS_d is the entropy of dissociation of the clathrate. The ΔS_d for the coarse-grained model should be lower than in the experiment because the mW water and M_{SW} methane do not have a rotational contribution to the entropy, and that should be significant for the fluids but not for the crystal phase. This limits the ability to simultaneously reproduce theT_m and the ΔH_d using a coarse-grained model. (The same should happen when atomistic models of water are combined with united atom models of methane such as the OPLS-UA model.) We note that all nonpolarizable atomistic models of water also underestimate the enthalpy of melting. For example, theT_m and ΔH_m of TIP4P/ice,[29] arguably the most accurate nonpolarizable atomistic model of water, are 272.2 K and 1.29 kcal/mol, essentially the same as for the monatomic water model mW, 274 K and 1.26 kcal/mol. For pure water, mW reproduces the experimental melting temperature of ice, while it underestimates the enthalpy of melting by 12% (1.436 kcal/mol in the experiment) and the entropy of melting by the same amount (4.61 in mW vs 5.26 cal/kmol in experiment).[33] A larger underestimation for clathrates than for ice melting is expected because of the additional contribution of the rotational entropy of methane.

Table 4 lists the enthalpy and entropy of dissociation of the sI clathrate for different water−methane potentials. The entropies of dissociation of all water−methane potentials in the coarse-grained simulations are about the same, $\Delta S_d \sim 34$ cal/kmol. This is ~75% of the experimental value, and a potential that reproduces T_m should underestimate ΔH_d by the same amount. Increasing the water−methane interaction parameter ε_{wm} leads to better agreement in ΔH_d at the expense of a worse prediction of the melting temperature. In conclusion, it is not possible to reproduce simultaneously the dissociation enthalpy and melting temperature; we privilege the latter in the parametrization of the water−methane potential because there is a physical reason for a lower entropy of melting in the coarse-grained model. In the next section we show that an increase in the water−methane attraction to produce better agreement for ΔH_d not only degrades the agreement in T_m but also leads to a high solubility of the "methane" it purportedly models.

V. Structure and Thermodynamics of Water−Methane Solutions

A. Solubility of Methane in Liquid Water. The solubility of methane in water was computed from large-scale simulations of water−methane systems in which the aqueous and organic

phases coexist in equilibrium (lower panel of Figure 1). The simulations were performed at $p = 178$ atm and $T = 313$ K to compare with the experimental solubility determined by Chapoy et al., $x_m = 0.002325$ methane molar fraction.[48] The solubility of methane in liquid water was evaluated for the same set of [σ_{wm}; ε_{wm}] used for the analysis of the thermodynamics of the clathrates.

The solubility was computed as the average molar fraction of methane in the bulk of the water phase, determined from the water and methane density profiles along the direction perpendicular to the water−methane interfaces (see Figure 1c). The solubilities for the candidate water−methane potentials decrease, as expected, with the strength of the water−methane interaction, spanning from the experimental value to an order of magnitude higher (Table 4) The water−methane parameters $\sigma_{wm} = 4.0$ Å and $\varepsilon_{wm} = 0.18$ kcal/mol reproduce the experimental solubility: 0.0022 ± 0.0001 compared to 0.002 325.[48] This is also the potential that best reproduces the T_m of the sI and sII crystals. In what follows, when we refer to results for methane and water in the simulations, we use the models with the parameters collected in Table 1.

To assess whether the curved interface present in the direct coexistence simulation cells (Figure 1) significantly affects the solubility, we evaluated x_m in an *NpT* simulation of a liquid system of 2944 water molecules and 512 methane molecules, corresponding to the same composition of the liquid half of the beginning of the direct coexistence simulations for an sI clathrate, at 313 K and 178 atm. The liquid segregated to form a cylindrical region of methane fluid, as seen in the two upper panels of Figure 1. Using a clustering algorithm to determine the number of methane molecules that did not belong to the methane cylinder phase, we computed the molar fraction of dissolved methane in equilibrium. We averaged the molar fraction of methane solute in the water phase over 145 ns simulations. The result, 0.0025 ± 0.0008, compares very well with the 0.0022 ± 0.0001 determined from simulations with a flat interface.

B. Diffusion Coefficients. Molecular diffusion is faster in the coarse-grained models, due to the lack of explicit hydrogen atoms.[33] At 298 K and 1 atm, the diffusion coefficient in mW water is 2.8 times larger than in experiments, 6.5×10^{-5} cm^2/s vs 2.3×10^{-5} cm^2/s.[33,43] We computed the self-diffusion coefficient D of methane in water under the same conditions from the mean square displacement using Einstein's relation:

$$6Dt = \lim_{t\to\infty}\langle|\mathbf{r}_i(t) - \mathbf{r}_i(0)|^2\rangle \qquad (4)$$

The coarse-grained model predicts a self-diffusion coefficient of methane in water $D = 4.8 \times 10^{-5}$ cm^2/s. This is 2.6 times the experimental result, 1.84×10^{-5} cm^2/s at 298 K.[49] This indicates that although the coarse-grained model overestimates the actual values of D, it faithfully represents the relative mobilities of the two components. This is not unexpected, as methane diffusion is probably enslaved to the mobility of the water solvent.

C. Methane Hydration in Solution. The experimental average coordination number of methane in the sI hydrate clathrates is 21 ± 1.[50] The average hydration in the crystal results from an average over the occupancy of the dodecahedral and hexakaidecahedral cages that contain 20 and 24 water molecules, respectively. In liquid water, the hydration number of methane has been determined to be 19 ± 1 by integration of the first peak of the oxygen−carbon radial distribution function (rdf or $g(r)$) obtained from neutron diffraction[51] and 20 by analysis of the chemical shifts of ^{13}C through NMR.[52] We computed the hydration number of methane in solution from the integration of the first peak of the rdf between water and methane at 100 atm and 300 K. The rdf for each of the candidate water−methane interaction potentials was averaged over 100 ns equilibrium simulation. We find that the water−methane $g(r)$ is not especially sensitive to the water−methane interaction within the parameter space we sampled: Figure 3 shows that water−methane interactions that produce a broad range of solubilities and melting temperatures yield similar water−methane $g(r)$. The experimental position of the first peak ($r_{max} = 3.5$ Å) and first minimum (r_{min} between 5.0 and 5.2 Å) are well reproduced by the simulations (e.g., 3.5 and 5.22 Å, respectively, for $\sigma_{wm} = 4.0$ Å and $\varepsilon_{wm} = 0.18$ Å. We computed the hydration number n_w by integration of the first peak of the water−methane $g(r)$,

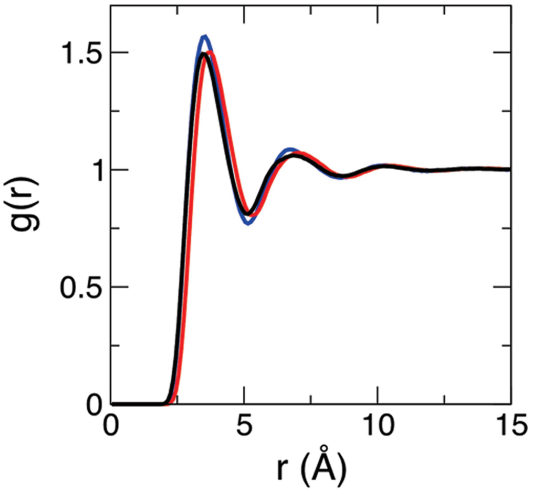

Figure 3. Water−methane radial distribution function $g(r)$ for three different sets of water−methane interaction parameters, [σ_{wm}; ε_{wm}]: [4.0 Å; 0.18 kcal/mol] in black; [4.05 Å; 0.24 kcal/mol] in red; [3.75 Å; 0.25 kcal/mol] in blue. While these parameters produce greatly different solubilities and melting temperatures (see Table 4), they all yield fairly similar water−methane distribution functions and hydration numbers.

$$n_w = 4\pi\rho_w \int_0^{r_{min}} r^2 g(r)\, dr \qquad (5)$$

where ρ_w is number density of water. n_w values for the different water−methane parameters are listed in Table 4. The hydration number ranges from 18.9 to 21.8, increasing with the size σ_{wm} and strength σ_{wm} of the water−methane potential. The parameters summarized in Table 1, which best reproduce the T_m and ΔT_m of methane clathrates and the solubility of methane in water, predict a hydration number of 19.3, in very good agreement with the 20 and 19 ± 1 deduced from the experiments.[51,52]

D. Surface Tension of the Water−Methane Interface. We calculated the surface tension of the water−methane interface from a 100 ns *NVT* simulation of the system in Figure 1c. The surface tension was determined using the relation[53]

$$\gamma = \frac{L_z}{2}[\langle p_N \rangle - \langle p_T \rangle] \quad (6)$$

where $L_z = 230$ Å is the length of the simulation cell perpendicular to the methane−water interface and $\langle p_N \rangle$ and $\langle p_T \rangle$ are the time-averaged components of the pressure tensors perpendicular and tangential to the methane−water interface, respectively. The coarse-grained model predicts a methane−water surface tension of 57 mN/m at 300 K and 100 atm compared to the experimental result of 61 mN/m under the same conditions.[54] The level of agreement is comparable to that previously reported for the surface tension of the liquid water−vacuum interface at 298 K: 66 mN/m for mW vs 71.6 mN/m in experiment.[33] The similarity in surface tension between water−vacuum and water−methane is consistent with the high hydrophobicity of methane.

E. Width of the Methane−Water Interface. The solubility of methane in liquid water is 2 orders of magnitude lower than in the hydrate crystals. Experiments indicate that nucleation of clathrates occurs close to or at the water−methane interface, where methane availability is the highest.[31] It is not clear, however, whether the nucleation occurs at the interface itself or in its immediacy, and this may be controlled by the width of the interface, which determines what is the spatial range over which the concentration of methane in water is comparable to that found in the methane hydrate.

Reed and Westacott used the SPC/E water model and the OPLS-UA methane model to determine the t_{90-10} width of the interface (the width over which the density of each component decays from 90% to 10% of the bulk density).[55] They found a t_{90-10} for water of 3.19 Å at 280 K and 120 atm. We computed the methane and water density profiles from the two-phase simulations at $T = 313$ K and $p = 178$ atm we used for the determination of the solubility. The width of the interface was rather insensitive to the change of the parameters of the water−methane potential used in this study. The methane and water density profiles for the model with the parameters of Table 1 are shown in Figure 4. The t_{90-10} length for the coarse-grained system is 4.0 Å. We note that both the atomistic and coarse-grained models predict that the width of the region for which the local concentration of methane is comparable to that in the clathrate is about the diameter of a water molecule. This is much narrower than the smallest clathrate cage, a water dodecahedron.

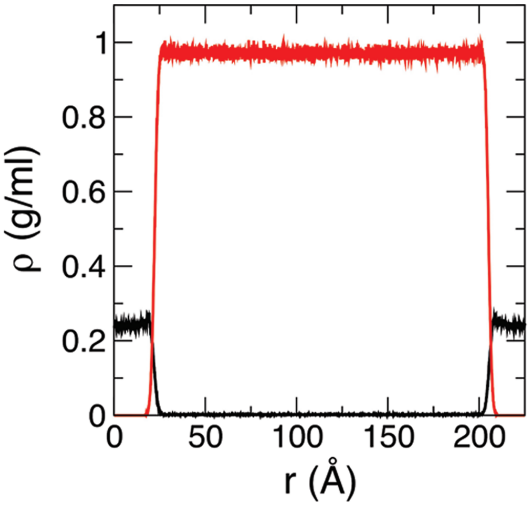

Figure 4. Density profile of water (red) and methane (black) in a two-phase liquid system (see Figure 1c) at $T = 313$ K and $p = 178$ atm. Interactions modeled with the parameters of Table 1. The width of the interface (4 Å) is narrower than a complete dodecahedral clathrate cage.

VI. Conclusion

In this work we developed a coarse-grained model for molecular simulations of water and methane. The methane and water molecules were represented as single particles interacting through short-ranged potentials. Water was modeled with the monatomic model of water mW that uses a combination of two- and three-body interactions to reproduce the anisotropic, hydrogen-bonded structures that water forms in its liquid, amorphous solid, ice, and clathrate phases.[7,33−35] Methane−methane interactions were described by short-ranged pair potentials parametrized to reproduce the enthalpy of vaporization and density of liquid methane at the experimental normal boiling point. We find that our united atom methane model is less transferable across a broad range of pressures than the OPLS-UA methane based on a Lennard-Jones potential, a difference that we attribute to the softness of the pair potential in the present study. While clathrate forming conditions usually involve high pressures, in the order of tens to hundreds of atmospheres,[2] we did not further refine the methane model because the error in the enthalpy of methane at 100 atm is about 2% of the enthalpy of formation of methane hydrate.

The parametrization of the water−methane interactions was the main focus of this study. The search for the optimum size σ_{wm} and strength ε_{wm} that define the water−methane potential was conducted in a reduced region of the parameter space where the sI hydrate with methane occupying the small and large water cages, experimentally the most stable crystal form of methane hydrate, has a lower enthalpy of formation than other clathrate structures. Properties that are key for the thermodynamics and structure of aqueous methane solutions and the formation and stability of methane clathrates were used for the parametrization and validation of the water−methane interactions: the solubility and hydration number of methane in liquid water, the surface tension and width of the water−methane interface, the enthalpy of dissociation of the sI methane hydrate crystal, and the temperature of melting of the stable (sI) and metastable (sII) methane hydrate polymorphs. The parameters that best reproduce these properties are listed in Table 1. Below we discuss the significance of each of these properties and the level of agreement between the coarse-grained model and experiment.

At a fundamental level, the solubility of methane is a measure of its excess chemical potential in water. From the point of view of the modeling of clathrate nucleation and growth, the low solubility of methane provides a barrier for the formation of clathrates that could control the determining step for the rate of crystallization.[56] Under the conditions of this study, 178 atm and 313 K, the solubilities of the coarse-grained model and experiment are identical, 0.0022 ± 0.0001 and 0.002325,[48] respectively. An analysis of the temperature and pressure dependence of the solubility exceeds the scope of this study and is left for future work. Nevertheless, we note here that there is a correlation between the ability of a water model in reproducing the temperature dependence of the solubility of small hydrophobic molecules and the temperature evolution of the density.[27] The mW model correctly predicts the density of water around room temperature and, at lower temperatures,

the existence of a density maximum followed by a sharp decrease in the density of liquid water that precedes its transformation into low-density amorphous ice.[33] This strongly suggests that this coarse-grained model would reproduce the increasing solubility on cooling that is a characteristic of hydrophobic hydration.[57−59]

The formation of clathrate crystals from aqueous solutions involves diffusion of water and methane and reorganization of the water structure around the methane to form the polyhedral water cages characteristic of each crystal phase. The coarse-grained model overestimates the mobility of water and methane in solution by a factor of about 2.7 but correctly describes the ratio between the diffusivity of water and methane. An accurate representation of the hydration shell of methane in water is a necessary (although probably not sufficient[60]) condition for the correct modeling of the nucleation of clathrates. The hydration number of methane in water predicted by the coarse-grained model, 19.3, is in very good agreement with that determined from NMR,[52] $n_w = 20$, and neutron diffraction,[51] $n_w = 19 \pm 1$. As a further characterization of the hydration shell, we compared the water−methane radial distribution functions for dilute methane in water with that obtained from the neutron diffraction experiments and found good agreement for the positions of the first maximum and minimum of the rdf.

The melting temperature of the clathrates is central for the determination of their regions of stability and the driving force for crystallization under nonequilibrium conditions. Although sI is the stable structure of methane hydrates, sII crystals also form in the initial stages of crystallization.[9,10] The melting temperatures of these two structures are close, just 1.5 K apart at 100 atm according to our calculations with the CSM-Gem program. Reproducing the melting temperatures of sI and sII and their small stability gap is crucial for the study of the origin of the mechanism of cross-nucleation in clathrates. Nevertheless, determinations of the melting temperature of methane hydrates with atomistic models have been scarce for the sI structure and nonexistent for the sII crystal. The coarse-grained model developed in this study predicts a melting temperature of 285 ± 4 K for the sI hydrate and 286 ± 1 for the sII crystal, in excellent agreement with 286.2 and 284.2, respectively, predicted by experiment and the CSM-Gem program. We have shown that the lack of rotational degrees of freedom in the monatomic water and methane leads to an underestimation of the entropy of melting by about 25%, which (combined with an accurate description of melting temperature) leads to an equivalent underestimation of the enthalpy of dissociation of the clathrate. Other models that approximate methane by a single particle (e.g., the OPLS-UA model) would face the same intrinsic limitation, although less pronounced while combined with atomistic models of water.

Finally, we have evaluated the surface tension and width of the water−methane interface, which could be a locus of crystallization of methane hydrate. The coarse-grained model reproduces the water−methane and water−vacuum surface tensions within 7% of the experiment. In the absence of experimental data on the width of the interface, we compared the coarse-grained results with those of a recent atomistic study using SPC/E water with OPLS-UA methane. The two simulations predict that the water−methane interface is sharp, its width about the diameter of a water molecule. This indicates that the region for which the average concentration of methane in the liquid is comparable to the concentration in the methane clathrate, local conditions that would favor crystallization, is narrower than the size of the smaller clathrate cage.

We are not aware of any other coarse-grained molecular model for water and methane that is parametrized to reproduce actual experimental properties of their liquid and crystal phases. We expect that this coarse-grained model will be instrumental in the study of the mechanisms of nucleation and growth of methane clathrates under various thermodynamic conditions with knowledge of the crystallization driving force. Water interaction with hydrophobic moieties plays a pivotal role in determining the structure and function of biomolecules and assembly of nanoparticles: hydrophobic forces drive the self-assembly of micelles and lipid bilayers,[61] protein structure is heavily influenced by hydrophobic interaction§[2] and the subtle influence of the hydrophobic effect limits the conditions at which the correctly folded protein structures retain their functionality before they denature at high and low temperature as well as elevated pressure,[63] and hydrophobic interactions shape the structure of DNA and the interaction of its complexes.[64] Coarse-grained modeling of these complex structures requires an accurate model of water and its interactions with hydrophobic, hydrophilic, and ionic groups. Previously, the mW model has been extended for the modeling of electrolytes in solution, without the use of electrostatics or other long-ranged interactions.[43] We expect that the methane−water model of this work will be useful for the study of hydrophobic assembly in aqueous solutions and provide a stepping-stone for the parametrization of coarse-grained models of organic and biological molecules with explicit solvation.

Acknowledgment. This work has been supported by the Beckman Foundation through a Young Investigator Award to V.M. and by the National Science Foundation through Collaborative Research grant CHE-0628257. We acknowledge the Center of High Performance Computing at the University of Utah for allocation of computing time.

References and Notes

(1) Sloan, E. D. *Nature* **2003**, *426*, 353.
(2) Sloan, E. D.; Koh, C. A. *Clathrate Hydrates of Natural Gases*, 3rd ed.; CRC Press/Taylor-Francis: Boca Raton, FL, 2007.
(3) Koh, C. A.; Sum, A. K.; Sloan, E. D. *J. Appl. Phys.* **2009**, *106*, 061101.
(4) Brewer, P. G.; Friederich, C.; Peltzer, E. T.; Orr, F. M. *Science* **1999**, *284*, 943.
(5) Park, Y.; Kim, D.-Y.; Lee, J.-W.; Huh, D.-G.; Park, K.-P.; Lee, J.; Lee, H. *Proc. Natl. Acad. Sci. U.S.A.* **2006**, *103*, 12690.
(6) Koh, C. A. *Chem. Soc. Rev.* **2002**, *31*, 157.
(7) Jacobson, L. C.; Hujo, W.; Molinero, V. *J. Phys. Chem. B* **2009**, *113*, 10298.
(8) Conde, M. M.; Vega, C.; Tribello, G. A.; Slater, B. *J. Chem. Phys.* **2009**, *131*, 034510.
(9) Schicks, J. M.; Ripmeester, J. A. *Angew. Chem., Int. Ed.* **2004**, *43*, 3310.
(10) Choukroun, M.; Morizet, Y.; Grasset, O.*J. Raman Spectrosc.* **2007**, *38*, 440.
(11) Ballard, L.; Sloan, E. D. *Fluid Phase Equilib.* **2004**, *216*, 257.
(12) Walsh, M. R.; Koh, C. A.; Sloan, E. D.; Sum, A. K.; Wu, D. T. *Science* **2009**, *326*, 1095.
(13) Jacobson, L. C.; Hujo, W.; Molinero, V. Initial Pathways in the Nucleation of Clathrate Hydrates: Effect of Guest Size and Hydrophilicity. Manuscript in preparation.
(14) Susilo, R.; Alavi, S.; Ripmeester, J.; Englezos, P. *Fluid Phase Equilib.* **2008**, *263*, 6.
(15) Alavi, S.; Ripmeester, J. A.; Klug, D. D. *J. Chem. Phys.* **2007**, *126*, 124708.
(16) Vatamanu, J.; Kusalik, P. G. *J. Phys. Chem. B* **2008**, *112*, 2399.
(17) Anderson, B. J.; Tester, J. W.; Borghi, G. P.; Trout, B. L. *J. Am. Chem. Soc.* **2005**, *127*, 17852.
(18) Ding, L. Y.; Geng, C. Y.; Zhao, Y. H.; Wen, H. *Mol. Simul.* **2007**, *33*, 1005.
(19) English, N. J.; Johnson, J. K.; Taylor, C. E. *J. Chem. Phys.* **2005**, *123*, 244503.

(20) Jiang, H.; Myshakin, E. M.; Jordan, K. D.; Warzinski, R. P*J. Phys. Chem. B* **2008**, *112*, 10207.
(21) English, N. J.; Tse, J. S.; Carey, D. J. *Phys. Rev. B* **2009**, *80*, 134306.
(22) Hawtin, R. W.; Quigley, D.; Rodger, P. M. *Phys. Chem. Chem. Phys.* **2008**, *10*, 4853.
(23) Asthagiri, D.; Merchant, S.; Pratt, L. R. *J. Chem. Phys.* **2008**, *128*, 244512.
(24) Czaplewski, C.; Rodziewicz-Motowidlo, S.; Liwo, A.; Ripoll, D. R.; Wawak, R. J.; Scheraga, H. A. *Protein Sci.* **2000**, *9*, 1235.
(25) Docherty, H.; Galindo, A.; Vega, C.; Sanz, E.*J. Chem. Phys.* **2006**, *125*, 074510.
(26) Konrad, O.; Lankau, T. *J. Phys. Chem. B* **2005**, *109*, 23596.
(27) Paschek, D. *J. Chem. Phys.* **2004**, *120*, 6674.
(28) Sobolewski, E.; Makowski, M.; Oldziej, S.; Czaplewski, C.; Liwo, A.; Scheraga, H. A. *Protein Eng. Des. Sel.* **2009**, *22*, 547.
(29) Abascal, J. L. F.; Sanz, E.; Fernandez, R. G.; Vega, C. *J. Chem. Phys.* **2005**, *122*, 234511.
(30) Vega, C.; Sanz, E.; Abascal, J. L. F. *J. Chem. Phys.* **2005**, *122*, 114507.
(31) Mastny, E. A.; Miller, C. A.; de Pablo, J. J. *J. Chem. Phys.* **2008**, *129*, 034701.
(32) Myshakin, E. M.; Jiang, H.; Warzinski, R. P.; Jordan, K. D*J. Phys. Chem. A* **2009**, *113*, 1913.
(33) Molinero, V.; Moore, E. B. *J. Phys. Chem. B* **2009**, *113*, 4008.
(34) Moore, E. B.; de la Llave, E.; Welke, K.; Scherlis, D. A.; Molinero, V. *Phys. Chem. Chem. Phys.* **2010**, *12*, 4124.
(35) Moore, E. B.; Molinero, V. Ice Crystallization in Water's "No-Man's Land". *J. Chem. Phys.*, in review.
(36) Moore, E. B.; Molinero, V. *J. Chem. Phys.* **2009**, *130*, 244505.
(37) Jacobson, L. C.; Molinero, V. Nucleation and growth of clathrate hydrates with a coarse-grained water model. In*237th ACS National Meeting & Exposition, Gas Hydrates and Clathrates Symposium*, Salt Lake City, 2009.
(38) Plimpton, S. J. *J. Comput. Phys.* **1995**, *117*, 1.
(39) Stillinger, F. H.; Weber, T. A. *Phys. Rev. B* **1985**, *31*, 5262.
(40) Jorgensen, W. L.; Madura, J. D.; Swenson, C. J. *J. Am. Chem. Soc.* **1984**, *106*, 6638.
(41) Martin, M. G.; Siepmann, J. I. *J. Phys. Chem. B* **1998**, *102*, 2569.
(42) Chen, B.; Siepmann, J. I. *J. Phys. Chem. B* **1999**, *103*, 5370.
(43) DeMille, R. C.; Molinero, V. *J. Chem. Phys.* **2009**, *131*, 034107.
(44) Setzmann, U.; Wagner, W. *J. Phys. Chem. Ref. Data* **1991**, *20*, 1061.
(45) Gupta, A.; Lachance, J.; Sloan, E. D., Jr.; Koh, C. A. *Chem. Eng. Sci.* **2008**, *63*, 5848.
(46) Yoo, S.; Zeng, X. C.; Morris, J. R.*J. Chem. Phys.* **2004**, *120*, 1654.
(47) Fernandez, R. G.; Abascal, J. L. F.; Vega, C. *J. Chem. Phys.* **2006**, *124*, 144506.
(48) Chapoy, A.; Mohammadi, A. H.; Richon, D.; Tohidi, B.*Fluid Phase Equilib.* **2004**, *220*, 111.
(49) Jähne, B.; Heinz, G.; Dietrich, W.*J. Geophys. Res.* **1987**, *92*, 10767.
(50) Koh, C. A.; Wisbey, R. P.; Wu, X. P.; Westacott, R. E.; Soper, A. K. *J. Chem. Phys.* **2000**, *113*, 6390.
(51) De Jong, P. H. K.; Wilson, J. E.; Neilson, G. W.; Buckingham, A. D. *Mol. Phys.* **1997**, *91*, 99.
(52) Dec, S. F.; Bowler, K. E.; Stadterman, L. L.; Koh, C. A.; Sloan, E. D. *J. Am. Chem. Soc.* **2005**, *128*, 414.
(53) Gloor, G. J.; Jackson, G.; Blas, F. J.; de Miguel, E. *J. Chem. Phys.* **2005**, *123*, 134703.
(54) Sachs, W.; Meyn, V. *Colloids Surf., A* **1995**, *94*, 291.
(55) Reed, S. K.; Westacott, R. E. *Phys. Chem. Chem. Phys.* **2008**, *10*, 4614.
(56) Radhakrishnan, R.; Trout, B. L. *J. Chem. Phys.* **2002**, *117*, 1786.
(57) Chandler, D. *Nature* **2005**, *437*, 640.
(58) Southall, N. T.; Dill, K. A.; Haymet, A. D. J. *J. Phys. Chem. B* **2001**, *106*, 521.
(59) Pratt, L. R.; Pohorille, A. *Chem. Rev.* **2002**, *102*, 2671.
(60) Guo, G. J.; Zhang, Y. G.; Li, M.; Wu, C. H. *J. Chem. Phys.* **2008**, *128*, 194504.
(61) Tanford, C. *Science* **1978**, *200*, 1012.
(62) Raschke, T. M. *Curr. Opin. Struct. Biol.* **2006**, *16*, 152.
(63) Pratt, L. R. *Annu. Rev. Phys. Chem.* **2003**, *53*, 409.
(64) von Hippel, P. H. *Annu. Rev. Biophys. Biomol. Struct.* **2007**, *36*, 79.

JP1013576

CHAPTER 4

AMORPHOUS PRECURSORS IN THE NUCLEATION OF CLATHRATE HYDRATES

Reprinted with permission from the American Chemical Society

Jacobson, L. C.; Hujo, W.; Molinero, V. *J. Am. Chem. Soc.* **2010**, *132*, 11806.

J|A|C|S
ARTICLES

Published on Web 07/29/2010

Amorphous Precursors in the Nucleation of Clathrate Hydrates

Liam C. Jacobson, Waldemar Hujo, and Valeria Molinero*

Department of Chemistry, University of Utah, 315 South 1400 East, Salt Lake City, Utah 84112-0850

Received June 12, 2010; E-mail: Valeria.Molinero@utah.edu

Abstract: The nucleation and growth of clathrate hydrates of a hydrophobic guest comparable to methane or carbon dioxide are studied by molecular dynamics simulations of two-phase systems. The crystallization proceeds in two steps: First, the guest molecules concentrate in "blobs", amorphous clusters involving multiple guest molecules in water-mediated configurations. These blobs are in dynamic equilibrium with the dilute solution and give birth to the clathrate cages that eventually transform it into an amorphous clathrate nucleus. In a second step, the amorphous clathrate transforms into crystalline clathrate. At low temperatures, the system can be arrested in the metastable amorphous clathrate phase for times sufficiently long for it to appear as an intermediate in the crystallization of clathrates. The "blob mechanism" unveiled in this work synthesizes elements of the labile cluster and local structuring hypotheses of clathrate nucleation and bears strong analogies to the two-step mechanisms of crystallization of proteins and colloids.

Introduction

Clathrate hydrates are crystalline inclusion compounds in which small guest molecules are contained within cages formed by a network of water molecules.[1] In clathrate hydrates, as in ice, each water molecule is hydrogen-bonded to four water neighbors. A difference, however, is the predominance of pentagonal rings in the hydrates that results in the formation of an open frame of polyhedral water cages. Although the guest-free water clathrates are metastable with respect to ice,[2] the clathrate crystal is stabilized by the interaction of water with guest molecules, even hydrophobic molecules that present very low solubility in water (e.g., methane and carbon dioxide). Methane, for example, forms clathrates with a ratio of methane to water that is about 2 orders of magnitude larger than that in the solution from which they grow. This poses the question, how do clathrates of hydrophobic guests form from aqueous solutions? Answering this question and identifying the structure of the clathrate critical nuclei are crucial for the development of strategies to inhibit and promote clathrate formation.

Different hypotheses have been proposed to explain the microscopic mechanism of nucleation of clathrate hydrates. Most of the evidence in support of and against these hypotheses arises from molecular simulations, as the crystal nuclei are usually too small for a direct experimental determination of their structure and mechanism of formation.[3] The first hypothesis for clathrate nucleation was proposed by Sloan and co-workers;[4,5] their labile cluster hypothesis (LCH) suggests that cage-like water clusters corresponding to the polyhedral cages of clathrates form around guests in solution, and these combine in the liquid to form the unit cell of the crystal. Since then, molecular simulations have shown that isolated empty or guest-filled clathrate cages in solution are rare and— when they form — have a flickering existence,of a few picoseconds.[6] Radhakrishnan and Trout computed the barrier for agglomeration of CO_2-filled cages in simulations and concluded that disintegration of the cages was more favorable than their agglomeration to grow a crystal nucleus.[7] Guo et al. searched for polyhedral cages in 60 million hydration shells of methane using molecular simulations.[8] They found that closed polyhedral shells only form in concentrated methane solutions, with probability 10^{-6}. In another study, they demonstrated that methane molecules adsorb to a dodecahedral cage and that the lifetime of the cage increases exponentially with the number of solute molecules that surround it.[9] On the basis of these results, we conjecture that, *if there is any viability for the labile cluster hypothesis, the labile clusters may not be bare cages but agglomerates that involve several guest molecules.*

The most recent mechanism proposed for clathrate nucleation is the local structuring hypothesis (LSH) of Radhakrishnan and Trout,[7] which states that the limiting step in the nucleation pathway is a concentration fluctuation that arranges a group of guest molecules in a configuration similar to that of the clathrate crystal. The water molecules, according to this hypothesis, follow the ordering of the guest molecules, building the cages that constitute the clathrate nucleus. The LSH was derived from umbrella sampling Monte Carlo simulations of aqueous solutions of CO_2, constraining the systems to sample the phase space along a series of predetermined order parameters that measure

(1) Sloan, E. D.; Koh, C. A. *Clathrate Hydrates of Natural Gases*, 3rd ed.; CRC Press/Taylor-Francis: Boca Raton, FL, 2007.
(2) Jacobson, L. C.; Hujo, W.; Molinero, V. *J. Phys. Chem. B* **2009**, *113*, 10298–10307.
(3) Koh, C. A.; Westacott, R. E.; Zhang, W.; Hirachand, K.; Creek, J. L.; Soper, A. K. *Fluid Phase Equilib.* **2002**, *194*, 143–151.
(4) Sloan, E. D.; Fleyfel, F. *AIChE J.* **1991**, *37*, 1281–1292.
(5) Christiansen, R.; Sloan, E. *Ann. N.Y. Acad. Sci.* **1994**, *715*, 283–305.
(6) Guo, G. J.; Zhang, Y. G.; Zhao, Y. J.; Refson, K.; Shan, G. H*J. Chem. Phys.* **2004**, *121*, 1542–1547.
(7) Radhakrishnan, R.; Trout, B. L. *J. Chem. Phys.* **2002**, *117*, 1786–1796.
(8) Guo, G. J.; Zhang, Y. G.; Li, M.; Wu, C. H. *J. Chem. Phys.* **2008**, *128*, 8.
(9) Guo, G. J.; Zhang, Y. G.; Liu, H. *J. Phys. Chem. C* **2007**, *111*, 2595–2606.

10.1021/ja1051445

the difference in structure between water in the liquid and in a perfect clathrate crystal.

Rodger and co-workers[10−12] and, more recently, Walsh et al.[13] were able to produce spontaneous methane hydrate nucleation in unconstrained atomistic molecular dynamics (MD) simulations of water−methane systems under conditions of high driving force. They found that a large number of methane molecules surrounded a new water cage when it formed, in agreement with the LSH. The structure of the growing nucleus in the simulations, however, was not crystalline as the LSH proposed, but an amorphous agglomerate of 5^{12} and $5^{12}6^n$ cages, with $n = 2$, 3, and 4, that were not organized nor followed the proportions found in clathrate crystals. Crystallization through an intermediate amorphous phase is not unheard of and has been demonstrated for proteins, colloids, and $CaCO_3$.[14−17] Although there is no direct experimental evidence of an amorphous phase in the pathway of methane hydrate crystallization, spectroscopic data of cage occupancy in Xe, CO_2, and CH_4 clathrates indicate that, at the beginning of the growth process, the ratio of small and large cages does not correspond to the stoichiometry of the stable sI crystal (one 5^{12} cage every three $5^{12}6^2$ cages) or to the sII crystal (two 5^{12} to one $5^{12}6^4$), but it is close to 1.[18−22] These results suggest that either an amorphous phase or a mixture of well-defined sI and sII crystals forms at initial stages of growth. The actual process has not yet been elucidated. Methane, carbon dioxide and xenon clathrates belong to the same class of hydrates: those of hydrophobic guests small enough to occupy the 5^{12} cages and for which sI is the stable polymorph. For this class, the metastable sII crystal has a free energy very close to that of sI: the melting temperature of sII is within a few degrees of that of the sI stable crystal.[23] Here we use molecular simulations to investigate the mechanism of nucleation of this class of hydrates and— in particular— elucidate the structure of the clathrate nuclei and whether there are amorphous microscopic precursors or amorphous metastable phases in the crystallization pathway of clathrate hydrates from aqueous solutions.

Amorphous precursors in the pathway to crystallization have been reported for colloids and proteins.[14−16] Crystal nucleation of these systems occurs in two steps: first, a sufficiently sized cluster of solute (protein, colloid) forms from the solution, and then that concentrated cluster reorganizes into an ordered structure. The common feature to these two quite different systems is the presence of very short-ranged attractive potentials between the crystallizing particles. In very recent work, Matsumoto computed the multibody potentials of mean force (pmf's) between four methane molecules in water.[24] He reported that although two isolated methanes in water prefer to adopt contact pair (CP) over solvent-separated pair (SSP) configurations, when four methane molecules are within distances comparable to the first methane−methane shell in clathrates, the SS configuration becomes the most stable. The stability is attained through rings of water between pairs of methane that "glue" the cluster of methanes. This results in a water-mediated methane−methane effective interaction that is attractive and very short-ranged.[24] By analogy with the phase diagram of other systems with short-ranged attractive potentials, the water-mediated interactions could stabilize relatively large clusters of water-mediated methane molecules that could assist the nucleation of the clathrate. This is the mechanism of clathrate nucleation we report in the present study.

Models and Methods

Nucleation of a new phase is a rare event, and it is computationally expensive to produce in direct atomistic simulations. We address this challenge through the use of a coarse-grained model that is 2−3 orders of magnitude more efficient than atomistic models,[23] allowing for an efficient sampling of multiple independent nucleation trajectories encompassing several microseconds of simulations. Water is described with the mW model that represents each molecule as a single particle that interacts through anisotropic short-ranged potentials that encourage "hydrogen-bonded" configurations.[25] It is important to note that although the mW model does not have explicit hydrogen atoms, it is able to reproduce the structure of liquid water, low-density amorphous ice, clathrates, and ice and has been successfully used to elucidate the nucleation and growth of ice in bulk and confinement.[2,23,25−30]

The guest M is also represented as a single particle and has properties intermediate between those of CH_4 and CO_2. The water−guest and guest−guest interactions are those of the [$\sigma_{WM} = 4.05$ Å; $\varepsilon_{WM} = 0.24$ kcal/mol] guest model developed in ref 23. At 313 and 178 K, the solubility (in molar fraction) is 0.0023 for CH_4, 0.024 for CO_2, and 0.0038 for M.[23] The melting temperatures of the polymorphs at $p = 500$ atm are, for sI and sII, respectively, 307 ± 2 and 303 ± 1 K for M, 299.2 and 293.9 K for CH_4, and 287.1 and 277.3 K for CO_2. The T_m of the model was computed following the protocols of ref 23, and the T_m values for CO_2 and CH_4 were computed using the CSM-Gem program.[31]

MD simulations were carried out using LAMMPS.[32] The velocity Verlet algorithm was used to integrate the equations of motion using a time step of 10 fs.[23] Simulations were performed in the *NpT* ensemble using a Nosé−Hoover thermostat and barostat with damping constants of 5 and 25 ps, respectively. Periodic boundary conditions were used in all directions. Twelve independent crystallization trajectories were collected at $p = 500$ atm and $T = 210$ K $= 0.7\ T_m$ from an equilibrated two-phase (aqueous solution and M fluid) system containing 8000 molecules (6847 water molecules

(10) Hawtin, R. W.; Quigley, D.; Rodger, P. M. *Phys. Chem. Chem. Phys.* **2008**, *10*, 4853–4864.
(11) Moon, C.; Taylor, P. C.; Rodger, P. M. *J. Am. Chem. Soc.* **2003**, *125*, 4706–4707.
(12) Zhang, J. F.; Hawtin, R. W.; Yang, Y.; Nakagava, E.; Rivero, M.; Choi, S. K.; Rodger, P. M. *J. Phys. Chem. B* **2008**, *112*, 10608–10618.
(13) Walsh, M.; Koh, C.; Sloan, E.; Sum, A.; Wu, D. *Science* **2009**, *326*, 1095.
(14) Savage, J. R.; Dinsmore, A. D. *Phys. Rev. Lett.* **2009**, 102.
(15) Ten Wolde, P. R.; Frenkel, D. *Science* **1997**, *277*, 1975–1978.
(16) Liu, H.; Kumar, S. K.; Douglas, J. F. *Phys. Rev. Lett.* **2009**, 103.
(17) Pouget, E. M.; Bomans, P. H. H.; Goos, J. A. C. M.; Frederik, P. M.; de With, G.; Sommerdijk, N. A. J. M. *Science* **2009**, *323*, 1555–1458.
(18) Pietrass, T.; Gaede, H. C.; Bifone, A.; Pines, A.; Ripmeester, J. A. *J. Am. Chem. Soc.* **1995**, *117*, 7520–7525.
(19) Staykova, D. K.; Hansen, T.; Salamatin, A. N.; Kuhs, W. F. *Proc. 4th Int. Conf. Gas Hydrates* **2002**, *2*, 537–542.
(20) Klapproth, A.; Goreshnik, E.; Staykova, D.; Klein, H.; Kuhs, W. F. *Can. J. Phys.* **2003**, *81*, 503–518.
(21) Staykova, D. K.; Kuhs, W. F.; Salamatin, A. N.; Hansen, T. *J. Phys. Chem. B* **2003**, *107*, 10299–10311.
(22) Moudrakovski, I. L.; Sanchez, A. A.; Ratcliffe, C. I.; Ripmeester, J. A. *J. Phys. Chem. B* **2001**, *105*, 12338–12347.
(23) Jacobson, L. C.; Molinero, V. *J. Phys. Chem. B* **2010**, *114*, 7302–7311.
(24) Matsumoto, M. *J. Phys. Chem. Lett.* **2010**, *1*, 1552–1556.
(25) Molinero, V.; Moore, E. B. *J. Phys. Chem. B* **2009**, *113*, 4008–4016.
(26) Moore, E. B.; Molinero, V. *J. Chem. Phys.* **2009**, *130*, 244505.
(27) Moore, E. B.; Molinero, V. *J. Chem. Phys.* **2010**, *132*, 244504.
(28) Moore, E. B.; Molinero, V. Is it Cubic? Ice Crystallization from Deeply Supercooled Water. To be submitted, 2010.
(29) Jacobson, L. C.; Molinero, V. Presented at the Clathrate Hydrates Symposium, 237th ACS National Meeting & Exposition, Salt Lake City, 2009.
(30) Moore, E. B.; De La Llave, E.; Welke, K.; Scherlis, D. A.; Molinero, V. *Phys. Chem. Chem. Phys.* **2010**, *12*, 4124–4134.
(31) Ballard, L.; Sloan, E. D. *Fluid Phase Equilib.* **2004**, *216*, 257–270.
(32) Plimpton, S. J. *J. Comput. Phys.* **1995**, *117*, 1–19.

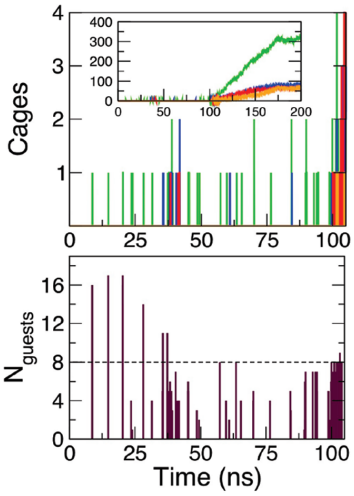

Figure 1. Upper panel: Number of cages versus time for subcritical nuclei during a typical nucleation trajectory. Green represents the 5^{12} cages, blue $5^{12}6^2$, red $5^{12}6^3$, and orange $5^{12}6^4$. The complete crystallization is shown in the inset. Lower panel: Number of guests within the first shell (8 Å) of the center of mass of the cage for frames with one cage present. The cages with more that nine surrounding guests formed at the guest−water interface.

and 1153 guest molecules). The simulations were then run for 250 ns or until nucleation and complete crystallization occurred.

Results and Discussion

The crystallization was monitored through the time evolution of the polyhedral cages that make up the clathrate lattices.[2] The cage types were identified by the number of pentagonal and hexagonal rings. All the cages in the sI and sII polymorphs, and the faults they form while growing, have 12 pentagonal rings and $n = 0$, 2, 3, or 4 hexagonal rings. These cages are commonly denoted as $5^{12}6^n$. The upper panel of Figure 1 shows the number of cages for each type versus time for a representative crystallization trajectory. All trajectories display the same characteristics: an induction period of stochastic duration during, which isolated clathrate cages form and dissolve, followed by a rapid growth in the number of cages. The final product displays small (5^{12}) and large (the sum of all $5^{12}6^n$, with $n > 0$) water cages in a ratio 1.48 ± 0.14, a ratio closer to that in sII (2) than in sI (0.33). The resulting clathrate has elements of the sI and sII structures but no long-range crystalline order. Movie 1 in the Supporting Information displays the four cage types as clathrates cages nucleate and grow to encompass all the aqueous phase. The amorphous nature of the clathrate phase obtained could be ascribed to the large driving force for the formation of both sI and sII at $0.7T_m$. We note, however, that deeply supercooled pure water can crystallize as hexagonal (Ih) and cubic (Ic) ices that have a stability gap smaller than those of the sI and sII clathrate polymorphs, in spite of which simulations of water crystallization at $0.66T_m$ yield well-defined crystallites with cubic and hexagonal stacking layers.[27,28,30] A main difference between ice and clathrates resides in the almost isotropic interaction of the clathrate cages and their versatility to fill the space, even when not forming long-ranged structures. The formation of $5^{12}6^3$ cages (Figure 1, Movie 1), not native to sI or sII but known to form at the interface between the two

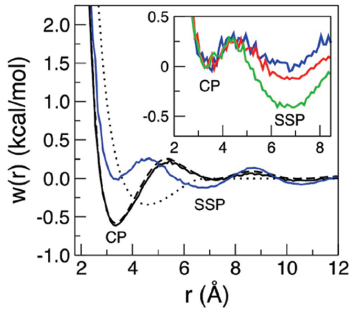

Figure 2. Potential of mean force $w(r)$ of the guest in water at 100 atm and 300 K (black dashed and solid lines) and at 500 atm and 210 K (blue line). Dashed lines indicate $w(r)$ determined from integrating constraint forces. Solid lines indicate $w(r)$ calculated from the guest−guest radial distribution function, $g(r)$, as $w(r) = -RT \ln g(r)$. The dotted line indicates the direct guest−guest interaction potential. CP indicates the contact pair configurations and SSP the solvent-separated ones. The inset shows $-RT \ln g(r)$ averaged over the induction period of the 12 crystallizing trajectories for blobs containing N guests (a cluster is defined as a group of "connected" guest molecules in the water phase, where connected means that pairs are within 8.5 Å of each other). The blue line indicates averages over clusters of $N = 2$ guests, red over clusters of 3−7 guests, and green over clusters with 8 or more guests. The curves in the inset were displaced such that the contact pair rests at 0 kcal/mol.

polymorphs,[2,33] allows for a seamless space-filling amorphous growth of clathrate cages. The lack of well-defined crystalline order and the agreement in the ratio between small and large cages in our simulations and the experiments[18,22] suggest that, under conditions of high supercooling, the amorphous solid clathrate could be an intermediate in the crystallization pathway toward crystalline clathrate hydrates.

How do clathrates nucleate? Guest M is hydrophobic, like methane: at room temperature the pmf between two M molecules in water (Figure 2) displays a clear preference for CP over SSP. Note that the direct M−M interaction is repulsive for the CP and almost null for the SSP. This shows that water−guest and, mostly, water−water interactions dominate the structure of methane in water. The cooperative multibody effect in the hydrophobic association of methane reported in ref 24 is also observed for M in water. Figure 2 shows that the SSPs are favored at low temperature: at 210 K isolated pairs of M already show a small preference for SSP over CP. Most significant for the nucleation of clathrates, we find that *the more M molecules there are in a cluster, the more the solvent-separated configurations are stabilized (inset of Figure 2)*, resulting in persistent clusters of guests separated by water (Figure 3). The multiguest clusters of M and its cementing water molecules behave like droplets of viscous liquids, i.e. *blobs*. Persistent clusters of guest molecules have been observed in other MD studies of nucleation of methane hydrate.[10,13,34] The water that separates the hydrophobic guests favors configurations of clathrate half-cages,[2] "cups" made of pentagonal and hexagonal planar rings of water molecules. These water rings were also observed between the SS methane molecules of refs 10, 13, 24, and 34.

Figure 3 displays the clathrate half-cages, the complete clathrate cages, and the guest molecules for snapshots along a

(33) Vatamanu, J.; Kusalik, P. G. *J. Am. Chem. Soc.* **2006**, *128*, 15588–15589.
(34) Vatamanu, J.; Kusalik, P. G. Observation of two-step nucleation in methane hydrates. *Phys. Chem. Chem. Phys.* **2010**, submitted.

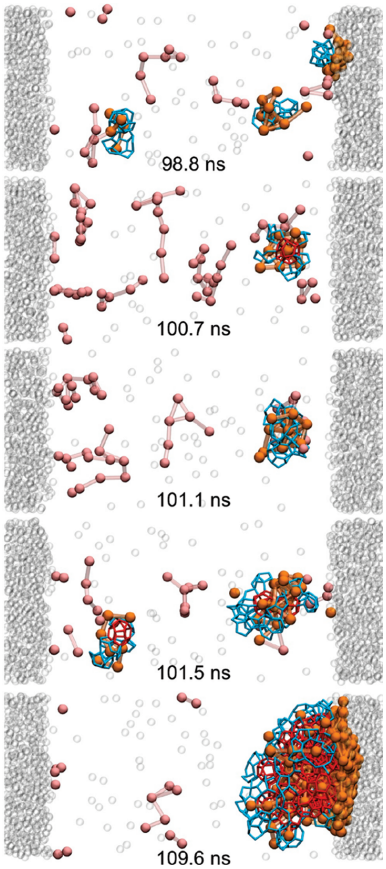

Figure 3. Time evolution of the blobs in the trajectory of Figure 1 as the system ends the nucleation period and starts forming the amorphous clathrate. Clathrate cages are colored red, and half-cages are colored cyan. Guest molecules within 5 Å of cages or half-cages are shown in orange, and guest clusters more than 5 Å away from cages or half-cages are pink. Otherwise, guest molecules are shown as translucent spheres. Images are labeled by the time elapsed from the beginning of the simulation. At 98.8 ns, multiple small clusters are present. At 100.7 ns, a transient polyhedral cage is present in the blob. At 101.1 ns, the blob remains but does not contain any polyhedral cages; it has only half-cages comprised of pentagonal and hexagonal rings. At 101.5 ns, the blob continues to grow, now with two cages. Also present is a subcritical blob to the left that dissolves. At 109.6 ns, the clathrate nucleus now has a core of polyhedral cages with half-cages on the periphery. The nucleus then continues to grow (not shown). This sequence is also shown in Movie 2 in the Supporting Information.

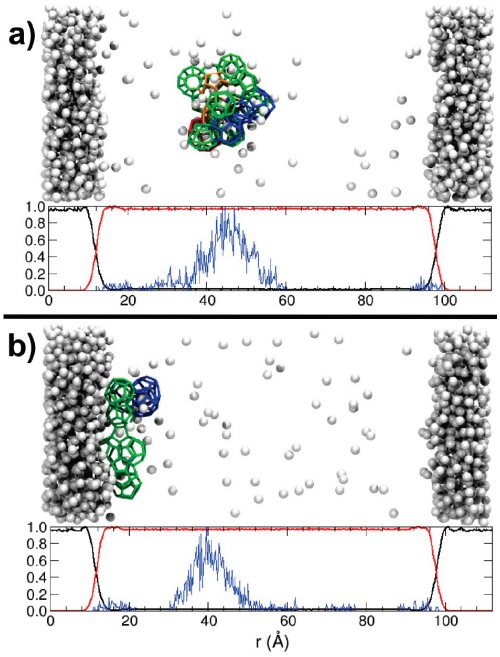

Figure 4. The locus of formation of clathrate cages is tied to the presence of blobs. Each panel shows the cages present in the nucleus immediately prior to crystallization and the density profile of the guest (black), water (red), and the polyhedral clathrate cages (blue) during the latent period that precedes it. The density profiles are scaled such that the maximum density is 1. We note that the density of cages in a region is not sufficient to predict the locus of nucleation of the clathrate. Panel (b) corresponds to a trajectory for which the higher density of cages occurred in a blob located in the bulk of the aqueous phase; nevertheless, the nucleus that successfully crystallized the system formed at the two-phase boundary.

crystallization trajectory. The time evolution is better appreciated in Movie 2 in the Supporting Information. The figure and movie show the formation and dissolution of blobs. Small blobs persist for times shorter than larger blobs (compactness of the M clusters also matters: threads of solvent-separated M molecules are much shorter lived than a compact blob). The water and guest molecules of the blob exchange slowly with the solution, producing fluctuations in blob size and structure; nevertheless "large" compact blobs (with more than about 15 guest molecules) persist at $0.7T_m$ for times longer than the characteristic diffusion time of the components. The blobs themselves are not stationary but slowly diffuse in solution. In this respect, the *blobs are large analogues of the labile clusters* proposed by Sloan and co-workers.[4,5]

Individual polyhedral clathrate cages, on the other hand, are very short-lived, and — most significant for the mechanism of clathrate nucleation — they originate within the blobs. We note that a single blob can give birth to several clathrate cages before extinguishing by dissolution or succeeding in forming a critical nucleus. The clathrate cages produced by a single blob are of different types ($5^{12}6^n$, with $n = 0$, 2, 3, and 4) and their location within the blob also changes. Multiple events of cage formation in the latent period before crystallization are shown in the trajectory of Figure 1. As these cages originate in a few persistent blobs, the spatial location of the cages is not random through the aqueous phase but on the spots where the blobs were. This is evident in Figure 4, which presents a normalized density profile for the guest molecules, all water molecules, and the water in clathrate cages along a direction perpendicular to the aqueous/guest-fluid interface, averaged over the latent period before crystallization. The cages formed in well-defined regions that correspond to the blobs. We conclude that *the blob is a guest-rich amorphous precursor in the nucleation pathway of clathrate hydrates of small hydrophobic guests.*The liquid blobs produce the clathrate cages which grow into an amorphous solid clathrate nucleus that would subsequently evolve — in a time scale exceeding those of the present simulations[18,22] — into a

crystalline clathrate. Annealing of the amorphous clathrates at 240 K ($0.8T_m$) leads to development of nanocrystalline sI *and* sII domains within 20 ns. We expect crystallinity to develop also at 210 K, although at a lower rate. The formation at low temperatures of amorphous nuclei or an amorphous metastable phase that matures to a polycrystalline state is consistent with the evolving ratio of small to large cages in the experimental studies of clathrate formation under conditions of high driving force.[18,20,22]

The LSH proposes that the number of guests around a central guest molecule is the order parameter for the advance of the clathrate crystallization. This would suggest that blobs located at the interface are more successful in leading to the formation of critical nuclei. The lower panel of Figure 1 displays the time evolution of the number of guests within the first cloaking shell of the clathrate cages (all types considered) until the onset of clathrate formation. The figure evidences that the number of guests alone is not a sufficient indicator of the success of the nucleation: the large number of guest molecules that a cage acquires by being at the fluid M/aqueous interface does not ensure the formation of a critical nucleus. The reason is probably the dense CP structure of the guest at the interface while the guest molecules in the clathrate, as in the blobs, are in SS configurations (Figure 2).

Experiments demonstrate that clathrates form close to the interface.[1,35,36] The simulations allow for a distinction between *close to* and *at* the interface: the latter would originate in a blob that rests on the fluid phase (e.g., Movie 1). We observe blobs that succeed in nucleating at the interface although they originated in the bulk, and vice versa. Of the 12 trajectories of this study, about half nucleated *at* the water−guest interface; we do not find a marked preference for nucleation at the interface.

Conclusions and Outlook

In this work we presented an analysis of a set of molecular simulations of nucleation and growth of clathrates of a hydrophobic guest with clathrate-forming properties similar to methane and carbon dioxide. The mechanism of clathrate nucleation that emerges from this study involves a first reversible step of formation of *blobs*, long-lived aggregates of guests separated by water molecules, wherein the clathrate cages repeatedly nucleate and dissolve until a cluster of cages reaches a critical size (about five cages at $0.7T_m$ supercooling) that prompts the space-filling growth of face-sharing clathrate cages. The amorphous clathrate that results from this process is a metastable intermediate toward the formation of crystalline clathrate.

The multistep process of clathrate crystallization supported by this study is *solution* ⇄ *blob* → *amorphous clathrate* → *crystalline clathrate*, where we have made a distinction between *blobs*, in which the water is not yet locked into clathrate cages, and *amorphous clathrate*, for which the positions of the guest molecules are not so distinct from the blob but the water has organized in hydrogen-bonded polyhedral cages that cement the structure. At low temperatures, the system can be arrested in the metastable amorphous clathrate state for times sufficiently long to appear as an intermediate phase. Ripening of the amorphous phase produces nanocrystals of the stable sI and metastable sII clathrates seamlessly connected through $5^{12}6^3$ cages.

The most relevant cases of clathrate crystallization involve relatively low supercooling. Is the distinction between blob and amorphous clathrate still valid when clathrates form at higher temperatures? A preliminary answer is obtained by warming amorphous clathrates to 280 K and following their dissolution. The cages in the water structure are first lost at the periphery and then at the very center of the amorphous clathrate as it dissolves. We conclude that large clusters of water-mediated guest molecules always contain a core of clathrate cages. Thus large-enough blobs are "amorphous clathrate blobs" (large clusters of guests mediated by *ordered* water). These blobs with an amorphous clathrate core, we hypothesize, are the precursors of clathrate crystallization at low driving forces.

We note that the multistep mechanism for clathrate crystallization proposed here is nonclassical, in the sense that it does not follow the tenets of classical nucleation theory which postulates that the critical nuclei form from the reactants through addition of individual "monomers" (e.g., clathrate cages) to a structure that already has the symmetry of the final phase (the clathrate crystal). The crystallization mechanism unveiled in this study evolves sequentially along three main order parameters: first, densification of the dilute solution to produce the blobs; second, ordering of the water to form the clathrate cages; and third, ordering of the guest molecules in a structure consistent with crystalline clathrates. Growth of a macroscopic crystalline clathrate phase may occur directly from amorphous nuclei or from crystalline clusters obtained through maturation of the amorphous nuclei. Studies are needed to assess the relative stability of small amorphous and crystalline clathrate clusters.

The mechanism of crystallization of clathrates bears strong analogies with the one for proteins, colloids, and nanoparticles: a first step that includes the self-assembly of denser domains from a dilute phase, followed by ordering of these domains to grow the crystal.[37,38] In these systems, nucleation is assisted by the presence in the supercooled region of their phase diagrams of a metastable fluid−fluid equilibrium involving a dilute and a concentrated liquid.[15] Our work suggests that the amorphous clathrate is the "dense fluid" and the aqueous solution of guest the "dilute fluid". It has been recently shown that the dense fluid can be an intermediate in the crystallization of proteins, even under conditions under which this dense amorphous phase is *unstable*.[16] This supports our conjecture that blobs of amorphous clathrate assist in the crystallization under conditions of low driving force. Strategies to prevent nucleation of clathrates should destabilize the formation of the blobs or their growth.

The "blob mechanism" of clathrate crystallization synthesizes elements of both the labile cluster and local structuring hypotheses. The local ordering of the guests drives the nucleation of clathrates, as suggested by LSH. The ordering, however, is not necessarily the one of the clathrate crystals. The clusters of water-mediated guests survive for times long enough to diffuse in solution, as the LCH proposes. The labile clusters, however, are not bare clathrate cages but large aggregates that may contain multiple clathrate cages. Our

(35) Koga, T.; Wong, J.; Endoh, M. K.; Mahajan, D.; Gutt, C.; Satija, S. K. *Langmuir* **2010**, *26*, 4627–30.
(36) Lehmkühler, F.; Paulus, M.; Sternemann, C.; Lietz, D.; Venturini, F.; Gutt, C.; Tolan, M. *J. Am. Chem. Soc.* **2009**, *131*, 585–589.
(37) Vekilov, P. *J. Cryst. Growth* **2005**, *275*, 65–76.
(38) Erdemir, D.; Lee, A.; Myerson, A. S. *Acc. Chem. Res.* **2009**, *40*, 621–629.

simulations indicate that the lifetime of the blobs increases with their size (probably controlled by the degree of water-mediated M−M connectivity). Large blobs of amorphous clathrates could survive in solution, without enough driving force to grow but too slow to dissolve even close to the melting point. A recent neutron and laser reflectivity study of the water−methane interface under conditions of clathrate formation close to equilibrium evidence surface roughening during the induction period, before crystallization sets it. Koga et al. propose that this is due to the presence of embryos, precursors of the crystalline clathrate phase.[35] In light of the present study, we interpret these embryos to be blobs or clathrate nuclei residing at the interface. The persistence of the roughening detected by Koga et al. during the 180 min latent period before crystallization does not imply that each of these blobs survive such a long time, nor that they remain in the amorphous state. Lehmkühler et al. used X-ray diffraction and reflectivity to study the water−carbon dioxide interface under conditions of hydrate formation.[36] They detected the formation of freely moving clathrate crystallites of size about 20 nm that nevertheless did not lead to macroscopic crystallization during the long times of the experiment. How long do blobs survive as a function of their size? What is their role in the so-called memory effect?[1] How do they develop into crystalline structures? These important questions deserve further study.

The guest M of this study has properties (solubility, hydration number, relative stability of sI and sII, T_m of sI and sII, width of the water−guest interface[23]) that make it comparable to methane and carbon dioxide. In future communications we will address the role of the size of the guest molecule (how do clathrates form if the guests cannot occupy the small cages?) and hydrophilicity (do soluble guests also form long-lived water-mediated blobs?) in the nucleation pathway of clathrate hydrates.

Acknowledgment. We gratefully acknowledge support by the Beckman Foundation through a Young Investigator Award to V.M. and the National Science Foundation through award CHE-1012651. We thank the Center of High Performance Computing at the University of Utah for allocation of computing time.

Supporting Information Available: Two movies showing the microscopic crystallization of clathrates. This material is available free of charge via the Internet at http://pubs.acs.org.

JA1051445

CHAPTER 5

NUCLEATION PATHWAYS OF CLATHRATE HYDRATES: EFFECT OF GUEST SIZE AND SOLUBILITY

Reprinted with permission from the American Chemical Society

Jacobson, L. C.; Hujo, W.; Molinero, V. *J. Phys. Chem. B* **2010**, *114*, 13796.

13796 *J. Phys. Chem. B* **2010,** *114,* 13796–13807

Nucleation Pathways of Clathrate Hydrates: Effect of Guest Size and Solubility

Liam C. Jacobson, Waldemar Hujo, and Valeria Molinero*

Department of Chemistry, University of Utah, 315 South 1400 East, Salt Lake City, Utah 84112-0850, United States

Received: August 2, 2010; Revised Manuscript Received: September 11, 2010

Understanding the microscopic mechanism of nucleation of clathrate hydrates is important for their use in hydrogen storage, CO_2 sequestration, storage and transport of natural gas, and the prevention of the formation of hydrate plugs in oil and gas pipelines. These applications involve hydrate guests of varied sizes and solubility in water that form different hydrate crystal structures. Nevertheless, molecular studies of the mechanism of nucleation of hydrates have focused on the single class of small hydrophobic guests that stabilize the sI crystal. In this work, we use molecular dynamics simulations with a very efficient coarse-grained model to elucidate the mechanisms of nucleation of clathrate hydrates of four model guests that span a 2 orders of magnitude range in solubility in water and that encompass sizes which stabilize each one a different hydrate structure (sI and sII, with and without occupancy of the dodecahedral cages). We find that the overall mechanism of clathrate nucleation is similar for all guests and involves a first step of formation of blobs, dense clusters of solvent-separated guest molecules that are the birthplace of the clathrate cages. Blobs of hydrophobic guests are rarer and longer-lived than those for soluble guests. For each guest, we find multiple competing channels to form the critical nuclei, filled dodecahedral (5^{12}) cages, empty 5^{12} cages, and a variety of filled large ($5^{12}6^n$ with $n = 2$, 3, and 4) clathrate cages. Formation of empty dodecahedra is an important nucleation channel for all but the smallest guest. The empty 5^{12} cages are stabilized by the presence of guests from the blob in their first solvation shell. Under conditions of high supercooling, the structure of the critical and subcritical nuclei is mainly determined by the size of the guest and does not reflect the cage composition or ordering of the stable or metastable clathrate crystals.

1. Introduction

Clathrate hydrates hold high promise as an energy source, for storage and transportation of natural gas and hydrogen, and for carbon dioxide sequestration.[1,2] Water forms the crystalline frame of clathrate hydrates, producing polyhedral fully hydrogen-bonded cages that can contain small, usually non-hydrogen-bonding guest molecules. By current estimates, natural gas hydrates constitute the most abundant reserve of fossil fuels on the planet.[3,4] Gas hydrate reserves are located in the permafrost and on the ocean floor, and it has been suggested that their stability may be threatened by global warming.[5,6] Exchanging the methane in natural gas hydrates with CO_2, which forms a more stable hydrate, has been proposed as a means to meet future energy needs as well as mitigate the effects of excess atmospheric carbon through CO_2 sequestration.[7,8] Using clathrate hydrates for the storage and transportation of natural gas from remote sources is also an attractive option as methane hydrate has an energy density equivalent to that of highly compressed natural gas, with fewer of the associated risks.[3,9] A prominent challenge for these applications is the slow formation kinetics of gas hydrates;[10−12] thus, strategies to increase the rate of crystallization of natural gas hydrates are urgently needed. On the other hand, the formation of gas hydrates in oil and gas pipelines is a source of economic loss for the oil industry.[2] Methods to prevent the nucleation or growth of gas hydrate crystals are much sought after. A thorough understanding of the microscopic mechanisms of hydrate formation and decomposition is therefore of paramount importance for the ability to prevent as well as promote hydrate growth.

Molecular simulations have played a prominent role in advancing the understanding of the microscopic mechanisms of clathrate nucleation from aqueous solutions.[13−24] Rodger and co-workers were first to demonstrate the spontaneous nucleation of methane clathrate hydrates in molecular simulations.[13−17] Using geometrical order parameters, they identified clathrate-like configurations of water molecules and found that the formation of these clathrate nuclei required the presence of several methane guests. The nuclei were amorphous and had a ratio of dodecahedral (5^{12}) to large tetrakaidecahedral ($5^{12}6^2$) and hexakaidecahedral ($5^{12}6^4$) cages that did not correspond to any of the known (sI and sII) crystal structures of methane hydrate. Walsh et al. studied the nucleation of methane clathrate in two microsecond-long molecular dynamics simulations.[22] In their work, nucleation of the hydrate occurred after a rare fluctuation burst a methane nanobubble, increasing the local methane supersaturation in the solution. In agreement with the results of Rodger and co-workers, they found that the clathrate nuclei lack long-range crystalline order and present cages native to the sI and sII structures, plus the $5^{12}6^3$ cages that were previously shown to form at the interface between these two crystals.[25,26]

We have recently demonstrated that the crystallization of clathrates of small hydrophobic guest molecules (e.g., methane, carbon dioxide, or noble gases) proceeds via a multistep mechanism,[24] summarized in Scheme 1. First, dense blobs of solvent-separated guests form in equilibrium with the dissolved guest in solution. These blobs persist in solution, and during their lifetime, they give birth to several clathrate cages, before

* To whom correspondence should be addressed. E-mail: Valeria.Molinero@utah.edu.

10.1021/jp107269q
Published on Web 10/08/2010

SCHEME 1: Crystallization Pathway of Hydrates of Hydrophobic Guests[a]

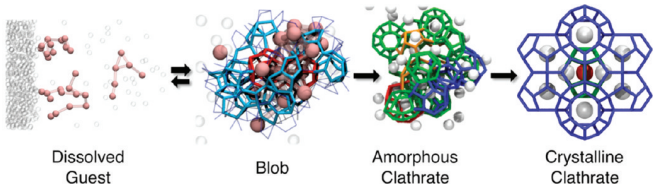

[a] The first step involves the formation of dense blobs of solvent-separated guest molecules in equilibrium with the very dilute solution (SSP guests shown as pink balls; the other guests shown in gray; the blue lines in the blob represent half-cages and the red lines full clathrate cages). In the second step, the water in the blob organizes into clathrate cages, producing an amorphous clathrate nucleus (cages colored according to type as in Figure 1). In the final step, the amorphous nucleus grows a crystalline phase. This last step may be preceded by the maturation of the amorphous nuclei to form crystalline nuclei. At conditions of high supercooling, the amorphous nuclei grow a metastable amorphous clathrate phase instead of the stable crystal.

either dissolving back into the solution or producing a sufficiently large cluster of clathrate cages and becoming a critical nucleus. Second, the critical nucleus grows, ordering the water of the blob into clathrate cages and recruiting more guest molecules from the solution. The result is an amorphous clathrate nucleus, as previously observed in atomistic simulations of methane hydrate nucleation.[13−17,22,27] In the amorphous nuclei, the water molecules are already locally ordered (i.e., they form clathrate cages), but the guests do not yet have the order of the hydrate crystals. Third, the amorphous clathrate nuclei rearrange to form a polycrystalline structure containing elements of both sI and sII. At longer time scales, we expect the clathrate to reorganize to form the thermodynamically stable crystal structure.[24] Under conditions of high driving force, the amorphous nucleus can grow into a metastable amorphous clathrate phase that develops into a crystalline clathrate after annealing.[24,27]

The "blob mechanism"[24] summarized above synthesizes elements of the local structuring[21] (LSH) and labile cluster[28,29] (LCH) hypotheses previously proposed for the mechanism of hydrate nucleation. In agreement with the LSH, the local ordering of the guest molecules drives the nucleation of the hydrates; the order is not, however, necessarily crystalline as proposed by the LSH. As predicted by the LCH, precursors of the hydrates form in solution; different from the LCH, these precursors are not individual guests surrounded by a polyhedral water cage but large aggregates of water-mediated guests.

Molecular simulations have thus far only been used to study the nucleation of methane or carbon dioxide clathrates. Although these arguably represent the two most relevant clathrate guests, they are examples of a single class, that of very low solubility guests that can occupy the large and small cages of the hydrate crystal and have sI as the most stable polymorph. In the present study, we use molecular dynamics simulations with a very efficient coarse-grained model[30] to investigate the microscopic mechanism of nucleation of hydrates of four guests that span a wide range of sizes and solubilities. These guests, which we call small (S), medium (M), large (L), and extra-large (XL), have as the stable crystal the sII, sI, psI, and psII structures, respectively (where p indicates that all dodecahedra are empty). S and M are hydrophobic; L and XL are miscible with water up to at least 0.1 molar fraction. In this work, we use these models to address three main issues:

(i) The formation of a dense blob of solvent-separated guest molecules is a slow step in the nucleation of hydrates of hydrophobic guests such as CO_2, CH_4, and the noble gases.[24] Do soluble guests also form persistent blobs? Is the formation of a blob a limiting step in the formation of hydrates of high-solubility guests?

(ii) How does the size of the guest modulate the pathways of nucleation of clathrate hydrates? The nucleation of hydrates of small guests is initiated predominantly through the formation of 5^{12} cages.[14,16,17,22,24] Large solutes, such as ethane, propane, and tetrahydrofurane (THF), are unable to occupy the dodecahedral cages, and they form hydrate crystals in which only the large cages are filled, leaving all of the dodecahedra empty. It is not known how the large solutes initiate the nucleation of clathrate hydrates. Does the preferred nucleation channel involve the formation of empty small dodecahedra or large occupied cages? We have previously demonstrated that empty 5^{12} cages do not form in the absence of guest molecules, even under thermodynamic conditions for which the guest-free sII crystal is a thermodynamically stable phase of water.[25] How do guests that cannot fill the 5^{12} build these empty cages?

(iii) What is the structure of the clathrate nuclei? Are the cage compositions of the subcritcal and critical nuclei representative of the thermodynamically more stable hydrate crystal or is the structure of the nuclei controlled by the kinetics of formation of each type of cage?

The paper is organized as follows. Section 2 presents the coarse-grained models of water and the four guests molecules and the methodology used to study the formation of clathrates. Section 3 provides a characterization of the melting temperatures of sI and sII polymorphs and the solubilities for each water−guest system. Section 4 focus on the mechanisms of nucleation of hydrates of these four guests and addresses the questions posed above. Section 5 presents the main conclusions of this work.

2. Models and Methods

Nucleation of a solid clathrate phase from a liquid solution is a rare event, and this has two main implications. First, multiple independent nucleation trajectories have to be analyzed to distinguish patterns and weigh the pathways that lead to successful formation of critical clathrate nuclei. In consideration of the stochastic nature of nucleation, we collect multiple independent trajectories for each solute. Second, the nucleation times are usually long for atomistic simulations, a problem that is aggravated by the need to produce several crystallization trajectories for a set of guests. We address this challenge through the use of a computationally very efficient coarse-grained model.

A. Coarse-Grained Models. Water is modeled with the monatomic water model mW that represents each molecule as a single particle that interacts through anisotropic short-ranged potentials that favor "hydrogen-bonded" water structures.[31] The interactions in mW have the functional form of the Stillinger−Weber potential[32]

$$E = \sum_i \sum_{j>i} \phi_2(r_{ij}) + \sum_i \sum_{j\neq i} \sum_{k>j} \phi_3(r_{ij}, r_{ik}, \theta_{ijk})$$
$$\phi_2(r_{ij}) = A\varepsilon\left[B\left(\frac{\sigma}{r_{ij}}\right)^4 - 1\right]\exp\left(\frac{\sigma}{r_{ij} - a\sigma}\right) \quad (1)$$
$$\phi_3(r_{ij}, r_{ik}, \theta_{ijk}) = \lambda\varepsilon[\cos\theta_{ijk} - \cos\theta_0]^2 \times \exp\left(\frac{\gamma\sigma}{r_{ij} - a\sigma}\right)\exp\left(\frac{\gamma\sigma}{r_{ik} - a\sigma}\right)$$

where r_{ij} is the distance between particles i and j and θ_{ijk} is the angle subtended by the vectors between the positions of the $i-j$ and $i-k$ pairs of particles. The constants are $A = 7.049556277$, $B = 0.6022245584$, $\gamma = 1.2$, $a = 1.8$, and $\theta_o = 109.5°$. The tetrahedral parameter of water is $\lambda_w = 23.15$, the characteristic size is $\sigma_{ww} = 2.3925$ Å, and the energy scale is $\varepsilon_{ww} = 6.189$ kcal/mol. The three-body term ϕ_3 encourages tetrahedral hydrogen-bonded configurations between water molecules by imposing an energy penalty on water−water−water angles that deviate from 109.5°. It is important to note that although the mW model does not have explicit hydrogen atoms, it is able to reproduce the structures and phase relations between liquid water, low-density amorphous ice, clathrates, and ice.[25,30,31,33−36]

Each guest molecule is represented by a single particle. Following the paradigm of the methane−water model that we developed in ref 30, the guest−water and guest−guest interactions of this study were modeled through the two-body term ϕ_2 of eq 1 (i.e., $\lambda = 0$). To describe the interactions of the guest molecules, only the characteristic size σ and the strength of the interactions ε were modified from the values given above for water. Table 1 lists the water−guest and guest−guest parameters for the four guest molecules of this study. Setting $\lambda = 0$ for water−guest interactions implies that the solutes, even if miscible with water, are unable to form hydrogen-bonded configurations. This is adequate for nonpolar solutes such as CO_2 or CH_4, and it could be considered a first-order approximation for weak hydrogen-bonding solutes such as THF. The water−guest and guest−guest interaction parameters were selected to stabilize a different hydrate structure for each guest molecule, sI for S, sII for M, sI with empty 5^{12} for L, and sII with empty 5^{12} for XL. Futhermore, S and M are hydrophobic, while L and XL present high solubility in water. These properties of the guests are demonstrated in section 3.

B. Simulations. Molecular dynamics (MD) simulations were carried out using LAMMPS.[37] The equations of motion were integrated using the velocity Verlet algorithm with a time step of 10 fs.[30] Simulations were performed in the *NpT* ensemble using the Nose−Hoover thermostat and barostat with damping constants of 1 and 5 ps, respectively. Periodic boundary conditions were used in all directions.

The S and M solutes have very low solubility in water (see section 3). For their crystallization, we prepared and equilibrated two-phase (guest and aqueous solution) systems containing 8000 molecules (5258 water molecules plus 2742 solute molecules for S and 6847 water molecules plus 1153 guest molecules for M). The two-phase systems were equilibrated at 250 K and 500 atm and instantaneously quenched to 210 K to study the nucleation of the hydrates. The L and XL guests are miscible with water. The crystallization of these systems was studied from one-phase solutions containing 8000 molecules in a ratio of 1 guest every 17 water molecules. The nucleation of the hydrates of L and XL was studied at 260 and 229 K, respectively, at a pressure of 500 atm.

Statistics on the pathways of clathrate formation were collected from 9, 12, 5, and 5 independent trajectories for S, M, L, and XL, respectively. Each crystallization simulation was run for up to 250 ns or until nucleation and complete transformation into a clathrate phase occurred in each system. The extent of clathrate formation was determined from the fraction of water molecules that were part of the clathrate cages, for which we used the cage identification code that we introduced in ref 25, extended to distinguish filled from empty clathrate cages. The cages identified in this study, $5^{12}6^n$ with $n = 0$, 2, 3, and 4, are the four polyhedra that constitute the vast class of Frank−Kasper phases to which the sI and sII clathrate crystals belong.

TABLE 1: Guest−Water (σ_{ws}; ε_{ws}) and Guest−Guest (σ_{ss}; ε_{ss}) Interaction Parameters

	σ_{ws}	ε_{ws}	σ_{ss}	ε_{ss}
small (S)	3.75	0.136	3.75	0.12
medium (M)	4.05	0.240	4.08	0.34
large (L)	4.20	0.360	4.20	0.34
extra-large (XL)	4.50	0.360	4.50	0.34

3. Guest Solubilities and Hydrate Melting Temperatures

The two most relevant thermodynamic properties for the nucleation of hydrate clathrates are the solubility of the guest in water (x_s), which determines the availability of the guest for the initiation of the crystallization, and the melting temperature of the hydrate crystals (T_m). The driving force for clathrate crystallization can be defined as a function of these two equilibrium values in terms of the supersaturation (x/x_s) and supercooling ($T_m - T$).[38]

The solubility of the guests in water was computed following the methods and protocols of ref 30. Guests S and M present very low solubility in water, 0.0065 and 0.0038 molar fractions, respectively, at 178 atm and 313 K.[30] For comparison, under the same conditions, x_s is 0.0023 for methane[39] and 0.024 for carbon dioxide.[40] The L and XL solutes are miscible in water up to at least a ratio of 1 in 10. The solubility of the guests in water increases, not surprisingly, with the strength of the water−guest attraction ε_{ws}.

The relative stability of the sI and sII hydrate crystals, and whether the guests can occupy their dodecahedral cages, is mainly determined by the guest−water characteristic size σ_{ws}. The unit cell of the sI lattice has 2×5^{12} cages and $6 \times 5^{12}6^2$ cages containing a total of 46 water molecules. The unit cell of the sII lattice has 16×5^{12} cages and $8 \times 5^{12}6^4$ cages with a total of 136 water molecules. The 5^{12} cages are comprised of 12 pentagonal faces made of 20 water molecules and have an approximate cavity radius of 3.95 Å.[2] The $5^{12}6^2$ cages have 12 pentagonal and 2 hexagonal faces made from 24 water molecules with an approximate cavity radius of 4.33 Å.[2] The $5^{12}6^4$ cages have 12 pentagonal and 4 hexagonal faces made from 28 water molecules with an approximate cavity radius of 4.73 Å.[2] Figure 1 shows the structure of the these cages.

In the absence of guest molecules, the empty sII water lattice is more stable than the empty sI water network.[25] The lower stability of sI can be traced to its higher fraction of water molecules in planar hexagonal rings, which strains the tetrahedrality of the water lattice.[25] As a result, solutes small enough to fit comfortably into the dodecahedral 5^{12} cages form the sII structure with small and large cages occupied. Solutes that fit into the dodecahedra but struggle to do so favor the sI structure because it has three $5^{12}6^2$ cages for every 5^{12} dodecahedral cage, while there is one $5^{12}6^4$ cage for every two 5^{12} cages in sII. Guest molecules that are slightly too large to fit into the 5^{12} cages also prefer the sI structure, but they only occupy the larger

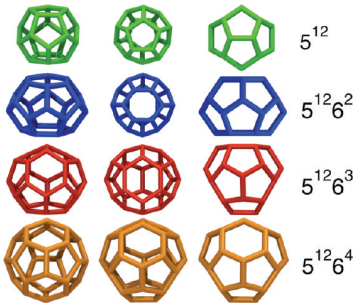

Figure 1. Polyhedral clathrate cages identified in this work. The water molecules are located at the vertices of the cages; the lines connect water molecules with its first neighbors. The sI lattice is made of 5^{12} and $5^{12}6^2$ cages. The sII lattice is made of 5^{12} and $5^{12}6^4$ cages. The $5^{12}6^3$ cages are native to neither the sI or sII structures but are found between regions of sI and sII.

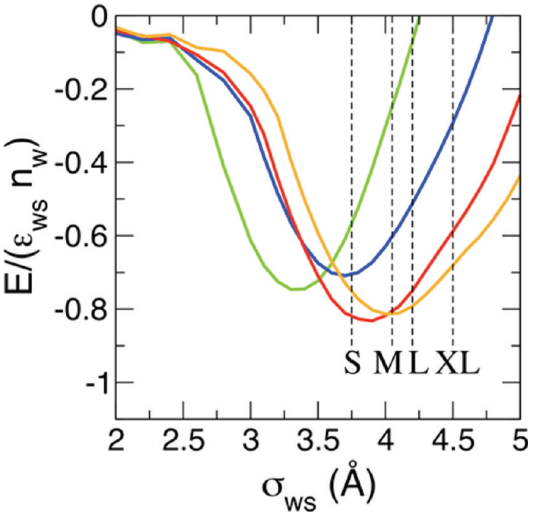

Figure 2. Cage−guest interaction energy as a function of the size of the guest. The colors correspond to the cage colors in Figure 1 (5^{12} green, $5^{12}6^2$ blue, $5^{12}6^3$ red, $5^{12}6^4$ orange). The water−solute interaction energy E for each cage type as a function of guest size was determined by running a set of 100 ps simulations for sI, sII, and tetragonal clathrate lattices with only one cage type occupied with guest molecules of varying sizes. The water−solute interaction strength ε_{ws} was maintained at 0.24 kcal/mol, and the guest−guest and guest−water interaction sizes σ_{ss} and σ_{ws} were varied from 0 to 5 Å evaluated every 0.1 Å. The total system energy at the end of the simulation was calculated, and the energy of the empty lattice was subtracted. The energy was then divided by the number of guest molecules and then again by the number of water molecules in the surrounding cage. This resulted in a representation of the stabilization energy per water−solute interaction for each cage type.

$5^{12}6^2$ cages of the sI lattice. Guest molecules that are too big to fit even in the $5^{12}6^2$ cages form the sII structure with only the $5^{12}6^4$ cages occupied. The effect of increasing the guest size on the stabilization of the molecule in each cage type is illustrated in Figure 2, which shows the interaction energy E of a guest molecule occupying each type of polyhedral cage of the hydrate crystals, normalized by the water−guest interaction strength ε_{ws} and the number of water molecules n_w in the polyhedral cage as a function of the water−guest characteristic distance σ_{ws}. The dashed vertical lines in Figure 2 indicate the sizes of the four

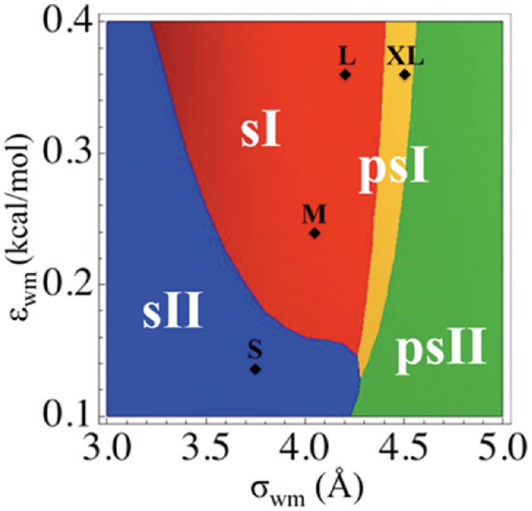

Figure 3. "Clathrate stability map" constructed in ref 30. The different colors represent the regions of the water−guest interaction potential for which each crystal has the lowest enthalpy of formation. The enthalpy of formation is, to a first approximation, an indicator of the stability of the clathrate. The actual stable structures were determined from the melting temperatures, T_m, of the clathrates and are listed in Table 2. The sII, sI, psI, and psII structures are the stable structures for the S, M, L, and XL solutes, respectively, at 500 atm.

TABLE 2: Melting Temperatures of the Clathrate Crystals of Each Guest at 500 atm

	small (S)	medium (M)		large (L)	extra-large (XL)
sI	301 ± 1 K	307 ± 2 K	psI	327 ± 2 K	295 ± 1 K
sII	307 ± 1 K	303 ± 1 K	psII	318 ± 2 K	307 ± 1 K

different guests of this study. Note that only the S and M guests have attractive interactions with the 5^{12} cages. The L and XL guests do not occupy the dodecahedral cages because their interaction with them is not attractive.

In ref 30, we computed the stability map for the sI, sII, psI, and psII crystals (where the p designates a partially filled structure with empty 5^{12} cages) as a function of the water−guest interactions using the enthalpy of formation of the hydrates as a first approximation for their free energy. This estimated clathrate stability map is presented in Figure 3, along with the location of the four guests of this study. The parameters of Table 1 were selected to produce melting temperatures at around 300 K for all guests and to stabilize for each of them a different crystal structure. The actual stabilities were determined from the equilibrium melting temperatures of the different clathrate structures at $p = 500$ atm. The melting temperatures were computed using the direct coexistence method following the protocols of ref 30, with three coexisting phases for the insoluble S and M guests and two phases for the L and XL ones; the concentrations of L and XL in the aqueous phase were set to be the same as those in the crystals.

Table 2 summarizes the melting temperatures of the sI and sII hydrates of each guest at $p = 500$ atm. The values of T_m range from 295 to 327 K. For each guest, the crystal with the highest T_m is the most stable one. The stable crystals are sII for S, sI for M, psI for L, and psII for XL (the last two are different from the predictions of the approximate stability map, which we only used as a guide for the parametrization). It should be

stressed that actual hydrates present a wide range of occupancies of the dodecahedral cages. Thus, the region indicated as sI actually encompasses a range of occupancies of the 5^{12} cages. We find that 64% of the 5^{12} cages are occupied in sI M hydrate grown from the three-phase solution at a temperature just below its melting point. The occupancy of the small cages is zero for the L and XL hydrates.

Note in Table 2 the closeness of melting temperatures (within 10 K) of the stable and metastable crystals. This implies a similarity in free energy between the sI and sII structures for all the guests of this study. The similarity in free energy of sI and sII may be a general characteristic of clathrate hydrates as most of their stabilization arises from the crystallization of water to form the empty clathrate network, for which the free energy of formation is similar (within 0.2 kJ/mol[25]) for the sI and sII polymorphs. The implication of the close melting temperatures for sI and sII is that even under conditions of moderate supercooling, the two polymorphs are stable with respect to the solution.

On the basis of the stable phase of the clathrate and solubility, we establish analogies between the four solutes of this study and actual clathrate-forming guest molecules. The S solute is similar to guest molecules such as Ar, which also forms sII clathrate hydrates for which they occupy both the large and small cages.[2] The M solute forms the sI structure and has characteristics similar to methane or carbon dioxide, as we have shown in refs 24 and 30. The L guest has similarities with trimethylene oxide, which is miscible with water and forms sI hydrate clathrates with only the large $5^{12}6^2$ cages occupied.[2] The XL solute could be considered analogous to THF, which is miscible with water and forms sII clathrates with only the large $5^{12}6^4$ cages occupied.

4. Nucleation Pathways of Clathrate Hydrates

The rate of formation of clathrates increases with the degree of supercooling of the solution. The crystallization temperature for each guest−water system was selected (by trial and error) to yield nucleation times of about 125 ns and complete clathrate formation within 250 ns. The temperatures needed to attain these time scales were between 0.7 and $0.8T_m$, 210 K for the hydrophobic S and M solutes and 260 and 229 K, respectively, for the soluble L and XL guests. The ∼125 ns window set for the induction time is appropriate to sample multiple (about 50) events of formation of subcritical nuclei before a critical nucleus is produced and clathrate growth sets in. To obtain statistically significant data, we collected several independent trajectories of clathrate formation for each solute (see Models and Methods), totaling more than 7 μs of simulations.

The simulations were analyzed for the presence of polyhedral cages that form the clathrate crystal lattices, $5^{12}6^n$ with $n = 0$, 2, 3, and 4. Figure 4 shows the time evolution of the number of the $5^{12}6^n$ cages for representative trajectories of each guest. Figure 5 displays three snapshots of the water/S system along a simulation of hydrate formation. We distinguish, for all guests, two stages. First is a nucleation or induction period during which polyhedral clathrate cages form and dissolve back into the liquid. Multiple events of cage formation occur during the induction period, mostly individual cages and rarely clusters of two cages, that survive less than the 50 ps used for the sampling of the trajectory. The induction period ends with the formation of a viable critical nucleus. Second is a growth period during which almost all of the water orders into $5^{12}6^n$ cages. The clathrates formed under the conditions of the simulations do not present long-range crystalline order; they are amorphous (as an illustration, see the lower panel of Figure 5).

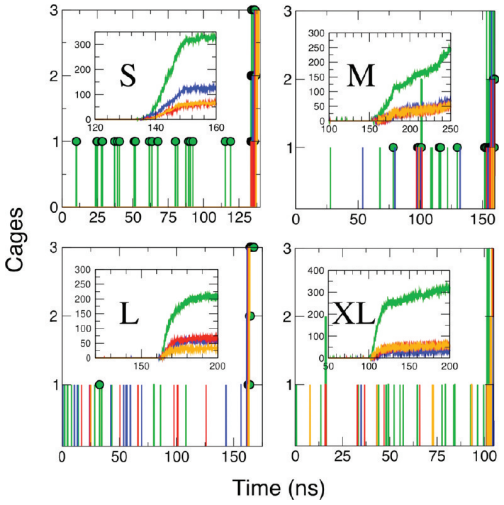

Figure 4. Number of cages versus time for representative crystallization trajectories of each guest. The induction period before growth is zoomed in the mainframe of each panel; the complete crystallization trajectories are presented in the insets. All of the simulations produce amorphous clathrate solids. Green represents the 5^{12} cages, blue the $5^{12}6^2$, red the $5^{12}6^3$, and orange the $5^{12}6^4$. Green lines topped by circles indicate that the corresponding dodecahedral 5^{12} cages are occupied with a guest molecule; the other dodecahedra are empty.

A. Do Soluble Guests Form Persistent Blobs? The first step in the nucleation of hydrates of hydrophobic guests is the formation of dense clusters of solutes consolidated by water molecules.[24] The formation of these blobs from a very dilute solution is represented by the first step in the mechanism of Scheme 1. The blobs of hydrophobic solutes are stabilized by the water-mediated attraction between guests.[24,41] An important result of ref 24 is that the stabilization of the solvent-separated guest configurations that cement the blob increases with the number of guests involved in the cluster. The upper left panel of Figure 6 shows that the work needed to dissociate solvent-separated pairs (SSP) of M molecules, or to collapse them to form contact pairs (CPs), is larger in blobs containing multiple guests than that for a single pair of M solutes in water.

The L and XL solutes are more soluble than the hydrophobic S and M guests. Their higher solubility is accompanied by the formation of stable CPs in solution. The right panel of Figure 6 presents the potential of mean force between a pair of XL solutes in water; the results are qualitatively the same for L. CPs between guests are favored for L and XL at temperatures for which the SSP is already stable for the more hydrophobic M solute.[24] Clustering of several XL molecules increases the stability of the SSP configurations (Figure 6), but the effect is considerably less pronounced than that for the M guest. Note that for both M and XL, the positions of the first and second SSP coincide with the first and second peaks of the guest−guest radial distribution function (rdf) in the hydrate (Figure 6); these distances are already favored for a pair of guests molecules in solution, although the water ordering around and between the pair of guests in solution is quite different from the one found in the hydrates (compare the ordering of water in the crystalline and amorphous hydrates presented in Schemes 1 and 2 with the snapshots of the SSP configurations in Figure 6).

The dense clusters of XL contain guests in both CP and SSP configurations. A picture of such an XL blob with mixed CP

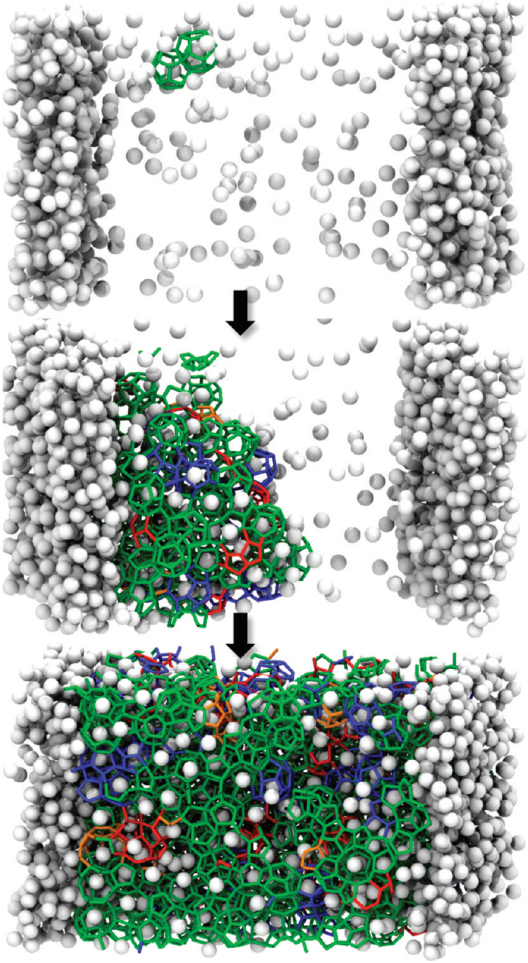

Figure 5. Nucleation and growth of a hydrate of the S guest from a two-phase system at $p = 500$ atm and $T = 0.7T_m$. Guest molecules are shown as balls, and water molecules are only shown when they are part of a cage: 5^{12} (green), $5^{12}6^2$(blue), $5^{12}6^3$ (red), and $5^{12}6^4$ (orange). The nucleation starts with two filled dodecahedra solvated by several guests (upper panel). The nucleus grows (middle panel), converting all of the water phase to an amorphous clathrate (lower panel).

and SSP configurations is shown in Scheme 2. The scheme represents the pathway of nucleation of the XL hydrate. The formation of dense blobs that are the birthplace of the clathrate cages is the first step in the mechanism. Formation of dense clusters of guests is a limiting step for the nucleation of hydrates of the hydrophobic guests S and M (Scheme 1) but not for the highly soluble L and XL guests. The higher concentration of guest molecules in solution does not, by itself, promote the nucleation of clathrates. Only when the CPs separate into the solvent-separated clusters can the water order and the nucleation of the clathrate proceed. Thus, we conjecture that the separation of these compact CP guests into solvent-separated configurations represents a significant contribution to the barrier of nucleation of guests L and XL.

Under the conditions of the simulations, the blobs of the M solute persist about 10 times longer than those of the XL solute before the guests dissociate into the solution. This is consistent with the higher stabilization of solvent-separated clusters for the M solute compared to that for the XL solute. The shorter lifetime of the blobs for the XL guest, coupled with the 20 times higher concentration of XL in solution compared to M, results in the formation of a higher number of short-lived subcritical blobs for XL. The more uniform distribution of blobs in the simulation box is reflected in the location of the clathrate cages that originate within them. Figure 7 shows the distribution along the direction perpendicular to the water−methane interfaces of clathrate cages that formed during the nucleation period for representative trajectories of the four guests. Cages appear in well-defined regions of space (where the persistent blobs are) for simulations with the S and M guest, while they are spread all along the simulation box for L and XL, consistent with the fast formation and short lifetime of the blobs of soluble guests.

B. Subcritical Nuclei: Statistics of Clathrate Cages during the Induction Period. We now turn our attention to the statistics of clathrate cages that precede the formation of the critical nuclei that grow the clathrates. Figure 4 shows that the frequency of each cage type in the nucleation period depends largely on the size of the guest molecule. This is summarized in Table 3, which presents the percent contribution of each cage type averaged over the nucleation period (before the formation of the critical nuclei) of all of the trajectories for each of the four guest molecules of this study. While 78% of the cages formed by the S guest in the nucleation period are filled dodecahedra, their participation sharply drops with increasing guest size, to 18% for M, 6% for L, and 0% for XL. The inability of the L and XL guests to stabilize filled dodecahedra is consistent with the guest−cage energies displayed in Figure 2; the L guest has no net stabilization energy when it is in the 5^{12} cage, and the interaction of XL with 5^{12} is repulsive. The guest−cage energies suggest, however, that S would form a considerable fraction of the large cages as the size of S is optimum for the $5^{12}6^2$ cage. Nevertheless, only 3% of the water cages formed by S in the nucleation period are $5^{12}6^2$. We conjecture that the bias toward smaller cages may be related to a kinetic barrier associated with the reorganization of the water around the guests; in the aqueous phase, S is solvated by an average of 16.5 water molecules, far from the 24 that it needs to form a $5^{12}6^2$ cage. The hydration numbers of the guests in solution and in the cages are presented in Table 3. The filled cages that form the most for each guest during the induction period are the ones for which the numbers of water molecules in the hydration shell in solution and in the cage are similar. These results suggest kinetic, rather than thermodynamic, control of the formation of the individual filled clathrate cages, with the water reorganization in the first shell of the guest having an important role in their rate of formation.

The argument based on hydration numbers would suggest that the primary channel of nucleation of the XL guest is through the formation of large cages. Table 3, however, shows that the percent of large cages ($5^{12}6^n$ with $n > 0$) increases from 5% for S, to 39% for M, to 61% for L and then *drops* to 40% for XL. The nonmonotonous contribution of nucleation channels based on large cages is due to the competition of an alternative nucleation pathway, the formation of *empty* dodecahedra. The empty 5^{12} constitute 60% of the cages formed by XL during the induction period.

Empty 5^{12} cages are a major component of the nuclei of all but the S guest. Empty large cages, on the other hand, are extremely rare (we found a single empty $5^{12}6^2$ cage in one trajectory for S) and do not contribute to the nucleation pathway of any of the studied guests. In a previous study, we determined

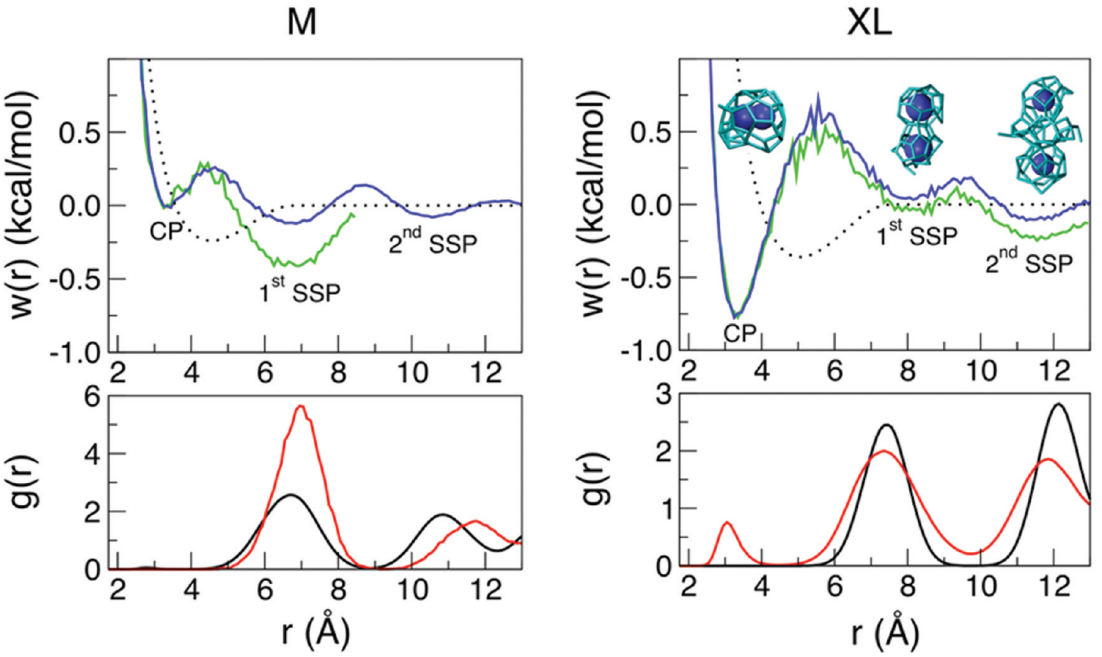

Figure 6. Potential of mean force and radial distribution functions (rdf) for the M (left) and XL (right) guests in solution and in the clathrates. Upper panels: The blue curves show the potential of mean force $w(r)$ for a pair of solute molecules in solution computed from the rdf, $g(r)$, as $w(r) = -RT \ln[g(r)]$ at 210 K and 500 atm. The green curves show $-RT \ln[g(r)]$ for clusters of eight or more solutes, where a cluster is defined as guest molecules within 8.5 Å of each other for the M solute and 13 Å for the XL solute. The clusters for the M solute were obtained from the induction period of the crystallization trajectories described in section 2. The clusters for the XL solute were identified in a simulation with an XL molar fraction of 0.0039, similar to the equilibrium concentration of M in solution. The dotted lines indicate the guest−guest interaction potentials. Representative configurations of a pair of guests and its surrounding water molecules in the CP, first SSP, and second SSP configurations are shown for the XL guest. Lower panels: Black lines correspond to the guest−guest rdf $g(r)$ for the sI M clathrate (left) and the sII XL clathrate (right). The red lines indicate the guest−guest $g(r)$ for the amorphous clathrates resulting from the crystallization trajectories described in section 2.

SCHEME 2: Crystallization Pathway for Hydrates of the Soluble L and XL Guests[a]

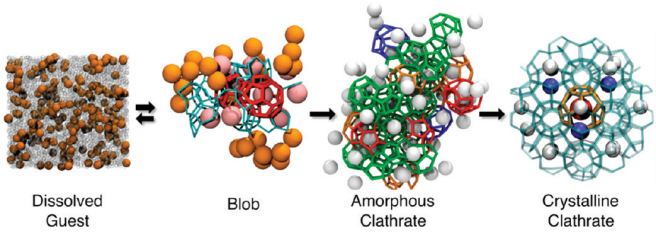

[a] The steps are equivalent to those for the S and M hydrophobic guests of Scheme 1, except for the existence of guests in CP configurations in the blob that have to dissociate to grow the amorphous clathrates. The XL guests in the blob are colored according to their closeness to the clathrate cages, pink if they are within 6 Å, orange if they are farther. Note that most of the orange-colored guests are in CP configurations.

that supercooled liquid water does not nucleate empty cages in the absence of guest molecules, even in the region of the phase diagram where the empty sII clathrate is the stable phase of water.[25] The stabilization of the empty cages arises from the presence of guest molecules "solvating" the water cage. A typical configuration of a guest-cloaked empty 5^{12} cage is displayed in the lower b panel of Figure 8; the empty dodecahedron appears in conjunction with surrounding guest molecules positioned over the planes of the pentagonal rings that comprise the cage. Pentagonal rings that make up partial polyhedral cages envelop the surrounding guest molecules themselves. The formation of pentagons is a natural consequence of the lack of water−guest hydrogen-bonding interactions as planar pentagons optimize the water−water hydrogen-bonding interactions while allowing for effective van der Waals interactions between the water in the five-member ring and the guest on top of it. This suggests that the effect of increasing the hydrophilicity of a solute (increasing the water−solute interaction strength) will not substantially alter the nucleation pathways if the guest molecule does not make hydrogen bonds with water. Effectively, we find the same type of configurations for the soluble L and XL guests.

To better understand the ordering of the guest molecules in the proximity of the empty dodecahedra, we computed the rdf between the centers of mass of the empty 5^{12} cages formed during the induction period and the surrounding guest molecules. We sampled over all configurations that contained a single empty dodecahedra in the induction period of the 12 crystal-

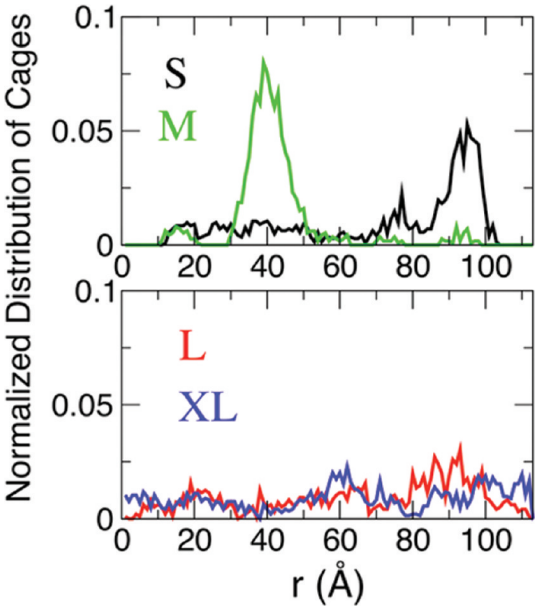

Figure 7. Normalized distribution of clathrate cages formed during the induction period along the length of the simulation box. The distribution is obtained from a histogram of the position of the water molecules that belong to clathrate cages along the longer dimension of the cell. A representative crystallization trajectory was considered for each solute. The probability was averaged over the nucleation period minus its last 5 ns to avoid including the critical nuclei in the sampling. The S and M solutes (upper panel) show a preference for localized formation of cages due to the presence of few and persistent blobs. The cages for the L and XL solutes (lower panel) are distributed across the system as they originate in shorter-lived and more numerous blobs. The number of cages that appeared in the induction period of each of these trajectories was 54 for S, 43 for M, 37 for L, and 60 for XL.

TABLE 3: Percent Contribution of Each Cage Type to the Subcritical Hydrate Nuclei of the Guests[a]

	small (16.5)	medium (21.5)	large (26)	extra-large (27)
Empty 5^{12}	17	**43**	**33**	**60**
Filled 5^{12} (20)	**78**	18	6	0
Filled $5^{12}6^2$ (24)	3	24	32	4
Filled $5^{12}6^3$ (26)	2	14	25	25
Filled $5^{12}6^4$ (28)	0	1	5	10

[a] The major contributor is indicated in bold. Hydration numbers of the guests in solution and within each cage type are indicated in parentheses in the top row and left column, respectively.

lization trajectories for the M guest. The resulting rdf is shown in the upper panel of Figure 8, along with the corresponding rdf between the guests and the center of mass of the 5^{12} cages the sI and sII M hydrates. The guest molecules "solvate" the empty cages that appear in subcrititcal nuclei at distances corresponding to those observed in the sI M hydrate and different from the sII hydrate, also shown in the figure. Although sI proto-ordering is consistent with the near-absence of $5^{12}6^4$ cages for M during the induction period (Table 3), the $5^{12}6^4$ cages effectively form during the growth period (inset of Figure 4 and subsection C below). The same analysis of the rdf for empty cages in simulations with the XL solute shows that the 5^{12} cage−guest distances are consistent with the rdf of the sII

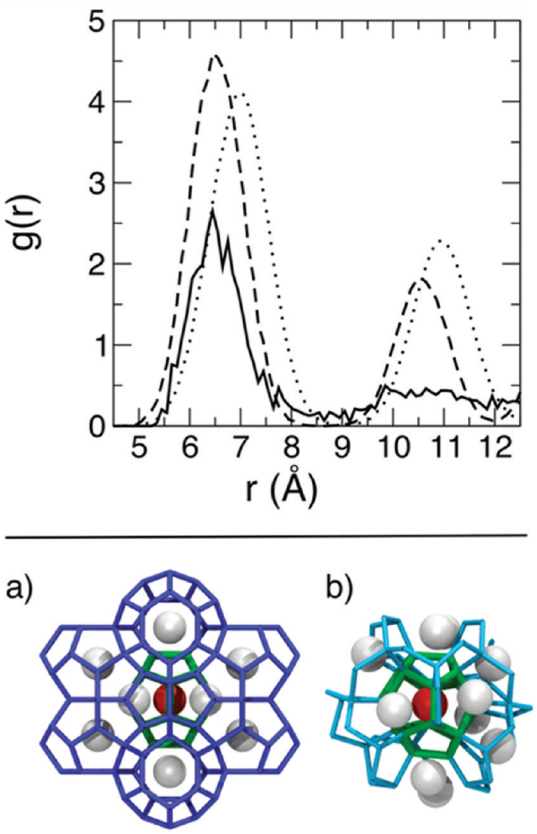

Figure 8. Distribution of guest molecules around empty dodecahedral cages. Upper panel: The solid line represents the rdf between the center of mass of empty dodecahedra and their surrounding M guest molecules, averaged over the nucleation period of the 12 trajectories of the M guest. The dashed line represents the rdf of M guest molecules in the dodecahedral cage with those in the $5^{12}6^2$ cages of the sI lattice. The dotted line is the rdf of M guest molecules in the dodecahedral cage with those in the $5^{12}6^4$ cages of the sII lattice. Lower panel: (a) twelve $5^{12}6^2$ cages (blue) surround a central 5^{12} cage (green, with a red ball indicating its center of mass) in the crystalline sI lattice; (b) an empty 5^{12} cage (green, filled with a red ball) that formed during the nucleation of M hydrate. The cage formed surrounded by M guests (white balls) and water molecules forming pentagonal rings (cyan). The pentagonal rings form partial cages that are the precursors to full polyhedral cages around the empty 5^{12}.

lattice, its most stable polymorph. We note, nevertheless, that the same analysis for S indicates that the guests around the empty 5^{12} occur at distances consistent with sI and not its stable sII crystal. Thus, we conclude that the preference for sI or sII-type distances around the empty 5^{12} does not mirror the relative stabilities of the two crystal phases, but it reflects the guest size as the S and M guests favor the shorter distances typical of sI and the XL the larger ones typical of sII.

The average number of M guests surrounding the empty dodecahedra formed during the induction period is 7.3. This suggests that the presence of multiple guest molecules is necessary for the appearance of empty dodecahedra. Gou et al. determined that the lifetime of dodecahedral cages in solution increases exponentially with the number of methane guest molecules surrounding them.[19] In order to determine the minimum number of surrounding guest molecules needed for

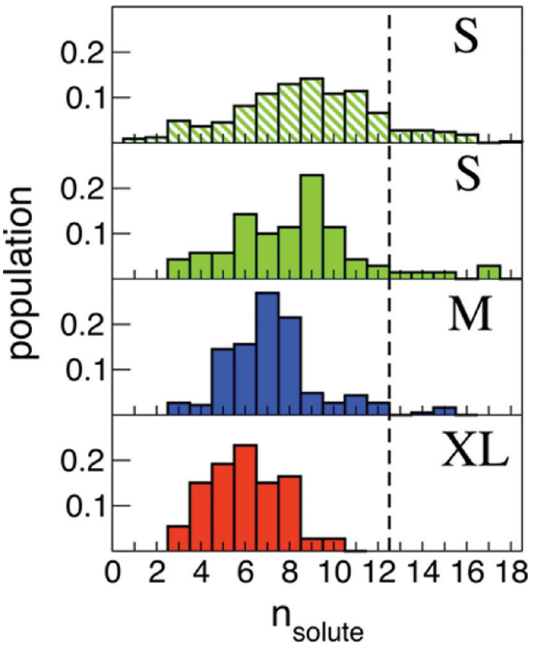

Figure 9. Histograms showing the distribution in the number n of guests within 8 Å of the center of mass of 5^{12} cages formed in the nucleation period. The green histograms represent the S guest around filled (striped green) and empty (solid green) 5^{12} cages. The blue and red histograms represent the distribution of M and XL guests, respectively, around empty 5^{12} cages. The minimum number of neighbor solutes needed for the formation of the empty 5^{12} cage is 3. The filled 5^{12} cage of the S solute was able to form in one instance with zero neighbors within 8 Å. The dashed line indicates the point at which the number of surrounding guests exceeds the number of faces on the 5^{12} cages. More than 12 neighbors occur only at the guest fluid−water interface. The filled S and empty S, M, and XL histograms were constructed from 332, 70, 186, and 73 configurations, respectively.

the appearance of an empty cage, we counted the surrounding guest molecules within 8 Å of the center of mass of the empty 5^{12} for each empty cage in the nucleation period. Figure 9 shows the resulting histograms for the S, M, and XL solutes. We find that empty 5^{12} cages do not form with less than three guest molecules around them, irrespective of the guest size and its concentration in solution. To investigate the difference in nearest neighbors for filled and empty cages, we also computed the number of surrounding guest molecules required for the appearance of filled 5^{12} cages for the S solute. The distribution, also shown in Figure 9, shows that the filled 5^{12} cages are less sensitive to the presence of surrounding guest molecules. A small fraction of filled 5^{12} cages formed with as few as zero or one neighbor solutes, stabilized by the central guest. Some dodecahedra are surrounded by more than 12 guests (the number of faces of the cage). A close look at these configurations reveals that these "over-solvated" cages form at the interface between the guest fluid and aqueous solution (note their absence in the one-phase XL/water system). We have shown in ref 24 that these extra guests located at the interface are not particularly effective in promoting crystallization as the guests at the interface are in CP configurations and not in the solvent-separated configurations that are the hallmark of clathrate hydrates.

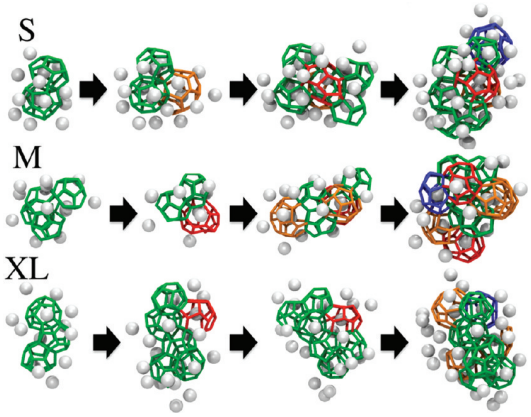

Figure 10. Clathrate nuclei representative of different nucleation pathways for the S guest (top), M guest (middle), and XL guest (bottom). The S solute fills all of the cages, the M fills primarily the large cages, and the XL fills only the large cages. Note that the nuclei do not possess the proportion of cage types nor the long-range order of either the sI or sII clathrate lattices. Face-sharing 5^{12} cages (a characteristic of the sII structure) are a common occurrence for all solutes, irrespective of their thermodynamic preference for sI or sII.

C. Structure of the Critical Hydrate Nuclei and Their Growth. A single polyhedral cage is insufficient to produce the growth of the clathrate phase, and there is an absence of clusters with more than two polyhedral cages in the precrystallization stage (as an exception, we found a subcritical nucleus with seven cages in an additional short simulation for the solution of XL at 229 K). On the basis of the maximum number of cages in subcritical nuclei observed in the induction periods, we estimate that the critical nuclei under the conditions of this study contain three to five clathrate cages. A more precise determination of the critical nucleus size would require the analysis of more trajectories and the calculation of the survival probabilities of nuclei comprised of different numbers and types of cages. A complete characterization of the critical nucleus should take the blob guests into account. In previous simulations, the critical nucleus size was estimated to have about 30 cages (r_c = 14.5 Å) for CO_2 hydrate[21] and about 200 water molecules in clathrate-like configurations (but very few complete cages) for CH_4 hydrate.[15] The conditions of supersaturation and supercooling of refs 15 and 21 are different from the present simulations, hindering a quantitative comparison. A critical radius of 32 Å at 5 K supercooling has been estimated using classical nucleation theory.[42] In general, the number of cages in the critical nucleus and the barrier for its formation increase as the driving force is reduced.[43]

In order to better understand the nature of the critical nuclei, we identified the clusters of cages present at the onset of crystallization and their surrounding guest molecules. Figure 10 shows nuclei representative of the various pathways to nucleation, clusters comprised of filled dodecahedra, empty dodecahedra, and filled $5^{12}6^n$ cages, as well as the guest molecules in and around them. When multiple 5^{12} cages form in the clathrate nuclei, they preferentially occur in face-sharing configurations. The same result has been previously reported for the nucleation of methane hydrate.[13−17,22] Face-sharing dodecahedra are characteristic of the sII structure; they are nevertheless common in the critical nuclei of all guests, irrespective of their thermodynamic preference for sI or sII.

We computed the frequency of each cage type for the clusters comprised of three cages in the same way that we did for the subcritical nuclei. The average contribution of each cage type to the critical nuclei is almost identical to that reported in Table 3 for the subcritical nuclei. We find a preponderance of 5^2 cages during the initial growth of the critical nuclei, in agreement with previous atomistic simulations of nucleation of methane hydrate.[16,22] Different from previous studies that focused on small solutes and used algorithms that only searched for filled cages, we observe a dominance of empty 5^{12} cages in the nucleation of clathrates with large solutes. Even for the M solute that fills 64% of the 5^{12} cages in the sI hydrate grown from solution around T_m (see section 3), 70% of the 5^{12} cages in the subcritical and critical nuclei produced at $0.7T_m$ are empty. We conclude that the cage composition of the critical nuclei does not reflect the cage ratios of the stable hydrate crystal. The similarity in cage populations in the subcritical and critical nuclei suggests that the structure of the critical nuclei is also controlled by the reorganization of the first hydration shell of the guests.

The critical nucleus comprises not only the clathrate cages but also the surrounding solvent-separated guest molecules in the blob. In the initial stages of growth, the water network in the blob reorganizes several times, producing equivalently sized clusters with different cage types or involving different water molecules (while the guests remain essentially in the same positions) until they settle and start the fast growth. This is illustrated in Figure 10. The transformation between different $5^{12}6^n$ cages usually involves very little change in the positions and identity of most of the molecules that form the cages, suggesting that other topological related polyhedral cages may also be involved. The role of this apparently easy interconversion between polyhedral cages on the barriers for clathrate nucleation deserves further study.

We find that about 10 cages are needed to settle the structure of the core of the nucleus under the conditions of supercooling of the present simulations. As new cages form around this core, the time scales necessary to produce reorganization of the cages of the amorphous nucleus into a crystalline clathrate become too long compared with the growth rate of new cages from the supercooled solution. At higher temperatures, the nuclei would grow slower and, at some stage, could reorganize to develop crystalline order; alternatively, the crystalline clathrate may grow from amorphous embryos. The assessment of these two scenarios in the development of clathrate crystallinity will be the topic of a future communication.

The clathrate nuclei start with a cage composition that depends on the size of the guest and reach the cage composition of the final amorphous product (which is not very sensitive to the guest size; see below) when the nuclei contain about 50 cages. By the end of the simulations, most of the space that was occupied by water is seamlessly filled by $5^{12}6^n$ cages with $n = 0$, 2, 3, and 4 (see, for example, Figure 5). The relatively fast transformation of the water into clathrate cages for the low-solubility S and M guests is possible because their simulations are performed at 210 K, about 30 K below the temperature of melting of the empty sI and sII clathrates at 500 atm;[25] thus, the growth of clathrate cages is not ultimately limited by the low availability of guests. At the temperatures of this study, the sI and sII hydrates of the four guests are stable with respect to the solution and could grow from the amorphous nuclei. Nevertheless, the clathrates produced are not crystalline but amorphous with occasional sI or sII domains interconnected through $5^{12}6^3$ cages. We note that under conditions of even larger supercooling and using the same coarse-grained model, pure water crystallizes to produce well-defined crystallites of ice I with cubic and hexagonal stacking faults.[33,35,36] An important difference between ice and clathrates is the almost isotropic interaction of the clathrate cages and their ability to fill the space, even when they do not form structures with long-range order.

The formation of the amorphous clathrates is mostly driven by the fast reorganization of water to produce the cages. The enthalpy of formation of the empty water network in the amorphous clathrate is ~75% of the enthalpy of formation of the empty clathrate crystals. The enthalpy of melting of the amorphous clathrates, computed for the L hydrate with 1 guest every 17 water molecules, is 65% of that for the sII crystal. As the entropy of melting of the amorphous hydrates must be lower than that for the crystalline clathrates and $T_m = \Delta H_m/\Delta S_m$, the melting temperature of the amorphous clathrates is at least 65% of the T_m of the crystals. The growth of the amorphous clathrates, which are metastable with respect to their crystalline counterparts, indicates that they are stable with respect to the liquid at the temperatures of this study.

The resulting amorphous clathrates contain about 55−60% of the 5^{12} cages and 10−15% of each of the $5^{12}6^n$ large cages. We do not observe a systematic difference in the cage composition of the amorphous clathrate as a function of the guest size. The ratio of small to large cages observed in the amorphous clathrates is similar to that computed in the initial stages of the experimental crystallization at very low temperatures in ref 44, and it may reflect the relative kinetics of growth of the $5^{12}6^n$ cages.

Polymorphism of clathrates in the initial stages of nucleation and growth has been reported in experimental studies.[45−47] Warming up of the amorphous clathrates of this study yields polycrystalline clathrates with regions of the sI and sII polymorphs.[24] Development of crystallinity upon warming of amorphous clathrates has also been observed in atomistic simulations of methane hydrates.[27] As in previous simulations of hydrate nucleation and growth, we observe that regions of sI and sII character are connected through $5^{12}6^3$ cages.[22,25,27] We expect that nucleation of the clathrates at conditions closer to equilibrium will produce structures that are more crystalline and that better reflect the thermodynamic preferences of each guest, especially for those that present a significant gap in melting temperatures for sI and sII. The transformation of amorphous to crystalline clathrates and the crystallization pathways at low driving force will be analyzed in future work.

5. Conclusions

Using molecular dynamics simulations with a very efficient coarse-grained model, we investigated the mechanisms of nucleation of clathrate hydrates of four model guests that span a 2 orders of magnitude range of solubility in water and that encompass sizes which stabilize each one in a different hydrate structure (sI and sII, with and without occupancy of the dodecahedral cages). This work is the first to report nucleation of clathrate hydrates of large guests or high-solubility guests using molecular simulations.

The mechanism of crystallization of clathrates unraveled in ref 24 for a small hydrophobic guest and verified here for the large and soluble ones is summarized in Schemes 1 and 2 and involve a first step of formation of dense clusters of solvent-separated guests, which we name blobs, followed by organization of the water to acquire the structure of clathrate cages, and finally, development of crystallinity.

We find some significant differences in the stabilities and lifetimes of the blobs of the hydrophobic (S and M) and soluble

(L and XL) guests. First, the formation of blobs of the hydrophobic guests is a rare event that limits the nucleation of their hydrates, while the formation of dense agglomerates of guest molecules is common in the high-concentration L and XL solutions. Second, the blobs of hydrophobic guests are longer-lived, each producing a larger number of clathrate cages during the nucleation period. Their longer lifetime seems to be associated with a higher stability of solvent-separated configurations. Third, the L and XL guests favor the formation of contact pair configurations that permit high concentrations of guests in solution; the system has to surmount a free-energy barrier to separate the CPs and successfully transform the blobs into amorphous clathrate nuclei. The formation of CPs may not be a general characteristic of soluble guests; more research is needed to establish the structure and lifetime of blobs of soluble guests that do not form CPs in solution.

The blobs are the birthplace of the clathrate cages. Individual polyhedral water cages are created through the reorganization of the water network of the blobs. Multiple cages form and dissolve until a critical nucleus forms and initiates the growth of the clathrate. Under the high supercooling conditions of this study, blobs containing as little as three clathrate cages seem to be already critical. We note that a proper set of reaction coordinates to describe the nucleation and growth of clathrates should include not only the cages formed by the water but also a measure of the number of guest molecules involved in the blob and their connectivity as this study demonstrates that guest molecules outside of the cages play a fundamental role in enabling the nucleation of hydrates.

The size of the guest is the main factor that modulates the nucleation pathways of clathrate hydrates. For each guest, we find multiple competing channels to form the critical nuclei, filled dodecahedral cages, empty dodecahedral cages, and a variety of filled large cages. The initial stages of methane clathrate nucleation in atomistic simulations were dominated by the appearance of filled 5^{12} cages.[16,22] Our study shows that the formation of empty 5^{12} cages represents an alternative pathway to start the nucleation of clathrates. The nucleation of hydrates of guests that are too large to fit in the 5^{12} cages occurs through competing channels that involve filled large $5^{12}6^n$ ($n > 0$) cages and empty 5^{12}. The empty 5^{12} cages are stabilized by the presence of guest molecules from the blob in their first solvation shell. A minimum of three solvating guest molecules is required for the formation of empty 5^{12}, while filled 5^{12} can form solvated by as little as zero or one guest.

The population of the guest-filled $5^{12}6^n$ cages in the subcritical and critical nuclei does not seem to correlate with their stability but with the closeness in hydration number for the guest in the cage and in the aqueous solution. This suggests that the free-energy barrier for the reorganization of water in the first hydration shell of the guest has an important role in controlling the pathways for clathrate nucleation. We conclude that, under conditions of high supercooling, the structure of the critical nuclei bears no relation to the structure of the most stable, or even metastable, clathrate crystal.

This mechanism displays strong similarities to two-step mechanisms of crystallization of colloids, proteins, and nanoparticles.[48−54] In these two-step mechanisms, the densification and ordering needed to produce the final crystalline phase do not occur concurrently but in sequence. A common feature of these systems is the existence of a fluid−fluid equilibrium between a dilute and a dense disordered phase in the supercooled region of the phase diagram. In the case of the clathrates, we ascribe the dilute phase to the solution and the dense disordered phase to the amorphous clathrate. On the basis of the enthalpy of melting of the amorphous hydrates and the spontaneous formation of amorphous clathrate phases from the liquid solutions, we tentatively estimate that their melting temperature (analogous to the fluid−fluid equilibrium that controls the two-step mechanism of other systems) is at least 65% and most probably around 80% of the T_m of the stable crystal. Recent work shows that the dense fluid can be an intermediate in the crystallization of colloids or proteins even at temperatures above the fluid−fluid equilibrium line, where the dense disordered phase is unstable.[50] This suggests that the formation of amorphous precursors would also be relevant for the crystallization of clathrates at conditions of low driving force. Additional studies are needed to determine whether the mechanisms elucidated here for the formation of hydrates at low temperatures hold for crystallization closer to the thermodynamic equilibrium, in particular, whether the nuclei that grow the clathrate crystal are themselves crystalline or amorphous. If they are amorphous, an important question is how does the amorphous structure grow a crystal phase; if the nuclei are crystalline, the main questions are at which stage and how does the amorphous nuclei develop crystallinity and does their structure reflect the stable hydrate crystal of the guest.

Acknowledgment. This work has been supported by the Arnold and Mabel Beckman Foundation through a Young Investigator Award to V.M. and by the National Science Foundation through award CHE-1012651. We thank the Center of High Performance Computing of the University of Utah for allocation of computing time.

References and Notes

(1) Boswell, R. *Science* **2009**, *325*, 957.
(2) Sloan, E. D.; Koh, C. A. *Clathrate Hydrates of Natural Gases*, 3rd ed.; CRC Press/Taylor-Francis: Boca Raton, FL, 2007.
(3) Sloan, E. D. *Nature* **2003**, *426*, 353.
(4) Sum, A. K.; Koh, C. A.; Sloan, E. D. *Ind. Eng. Chem. Res.* **2009**, *48*, 7457.
(5) Brewer, P. G. *Ann. N.Y. Acad. Sci.* **2000**, 195.
(6) Krey, V.; Canadell, J. G.; Nakicenovic, N.; Abe, Y.; Andruleit, H.; Archer, D.; Grubler, A.; Hamilton, N. T. M.; Johnson, A.; Kostov, V.; Lamarque, J.-F.; Langhorne, N.; Nisbet, E. G.; O'Neill, B.; Riahi, K.; Riedel, M.; Wang, W.; Yakushev, V. *Environ. Res. Lett.* **2009**, *4*, 034007.
(7) Warzinski, R. P.; Holder, G. D. *Energy Fuels* **1998**, *12*, 189.
(8) Seo, Y. T.; Lee, H.; Yoon, J. H. *J. Chem. Eng. Data* **2001**, *46*, 381.
(9) Susilo, R.; Alavi, S.; Ripmeester, J.; Englezos, P. *Fluid Phase Equilib.* **2008**, *263*, 6.
(10) Abbondondola, J. A.; Fleischer, E. B.; Janda, K. C. *J. Phys. Chem. C* **2009**, *113*, 4717.
(11) Gulluru, D. B.; Devlin, J. P. *J. Phys. Chem. A* **2006**, *110*, 1901.
(12) Wang, X.; Schultz, A. J.; Halpern, Y. *J. Phys. Chem. A* **2002**, *106*, 7304.
(13) Moon, C.; Taylor, P. C.; Rodger, P. M. *Can. J. Phys.* **2003**, *81*, 451.
(14) Moon, C.; Taylor, P. C.; Rodger, P. M. *J. Am. Chem. Soc.* **2003**, *125*, 4706.
(15) Moon, C.; Hawtin, R. W.; Rodger, P. M. *Faraday Discuss.* **2007**, *136*, 367.
(16) Hawtin, R. W.; Quigley, D.; Rodger, P. M. *Phys. Chem. Chem. Phys.* **2008**, *10*, 4853.
(17) Zhang, J.; Hawtin, R. W.; Yang, Y.; Nakagava, E.; Rivero, M.; Choi, S. K.; Rodger, P. M. *J. Phys. Chem. B* **2008**, *112*, 10608.
(18) Guo, G. J.; Zhang, Y. G.; Li, M.; Wu, C. H. *J. Chem. Phys.* **2008**, *128*, 8.
(19) Guo, G. J.; Zhang, Y. G.; Liu, H. *J. Phys. Chem. C* **2007**, *111*, 2595.
(20) Guo, G. J.; Zhang, Y. G.; Zhao, Y. J.; Refson, K.; Shan, G. H. *J. Chem. Phys.* **2004**, *121*, 1542.
(21) Radhakrishnan, R.; Trout, B. L. *J. Chem. Phys.* **2002**, *117*, 1786.
(22) Walsh, M.; Koh, C.; Sloan, E.; Sum, A.; Wu, D. *Science* **2009**, *326*, 1095.
(23) Ripmeester, J. A.; Alavi, S. *ChemPhysChem* **2010**, *11*, 978.

(24) Jacobson, L. C.; Hujo, W.; Molinero, V. *J. Am. Chem. Soc.* **2010**, *132*, 11806.
(25) Jacobson, L. C.; Hujo, W.; Molinero, V. *J. Phys. Chem. B* **2009**, *113*, 10298.
(26) Vatamanu, J.; Kusalik, P. G. *J. Am. Chem. Soc.* **2006**, *128*, 15588.
(27) Vatamanu, J.; Kusalik, P. G. *Phys. Chem. Chem. Phys.* **2010**, DOI: 10.1039/C0CP00551G.
(28) Sloan, E. D.; Fleyfel, F. *AIChE* **1991**, *37*, 1281.
(29) Christiansen, R.; Sloan, E. *Ann. N.Y. Acad. Sci.* **1994**, *715*, 283.
(30) Jacobson, L. C.; Molinero, V. *J. Phys. Chem. B* **2010**, *114*, 7302.
(31) Molinero, V.; Moore, E. B. *J. Phys. Chem. B* **2009**, *113*, 4008.
(32) Stillinger, F. H.; Weber, T. A. *Phys. Rev. B* **1985**, *31*, 5262.
(33) Moore, E. B.; de la Llave, E.; Welke, K.; Scherlis, D. A.; Molinero, V. *Phys. Chem. Chem. Phys.* **2010**, *12*, 4124.
(34) Moore, E. B.; Molinero, V. *J. Chem. Phys.* **2009**, *130*, 244505.
(35) Moore, E. B.; Molinero, V. *J. Chem. Phys.* **2010**, *132*, 244504.
(36) Moore, E. B.; Molinero, V. Is It Cubic? Ice Crystallization from Deeply Supercooled Water. To be submitted.
(37) Plimpton, S. J. *J. Comput. Phys.* **1995**, *117*, 1.
(38) Kashchiev, D.; Firoozabadi, A. *J. Cryst. Growth* **2002**, *241*, 220.
(39) Chapoy, A.; Mohammadi, A. H.; Richon, D.; Tohidi, B.*Fluid Phase Equilib.* **2004**, *220*, 111.
(40) Wiebe, R. *Chem. Rev.* **1941**, *29*, 475.
(41) Matsumoto, M. *J. Phys. Chem. Lett.* **2010**, *1*, 1552.
(42) Larson, M. A.; Garside, J. *Chem. Eng. Sci.* **1986**, *41*, 1285.
(43) Kashchiev, D.; Firoozabadi, A. *J. Cryst. Growth* **2002**, *243*, 476.
(44) Moudrakovski, I. L.; Sanchez, A. A.; Ratcliffe, C. I.; Ripmeester, J. A. *J. Phys. Chem. B* **2001**, *105*, 12338.
(45) Choukroun, M.; Morizet, Y.; Grasset, O.*J. Raman Spectrosc.* **2007**, *38*, 440.
(46) Schicks, J. M.; Ripmeester, J. A. *Angew. Chem., Int. Ed.* **2004**, *43*, 3310.
(47) Staykova, D. K.; Kuhs, W. F.; Salamatin, A. N.; Hansen, T. *J. Phys. Chem. B* **2003**, *107*, 10299.
(48) Savage, J. R.; Dinsmore, A. D. *Phys. Rev. Lett.* **2009**, *102*, 198302.
(49) Ten Wolde, P. R.; Frenkel, D. *Science* **1997**, *277*, 1975.
(50) Liu, H.; Kumar, S. K.; Douglas, J. F. *Phys. Rev. Lett.* **2009**, *103*, 018101.
(51) Vekilov, P. *J. Cryst. Growth* **2005**, *275*, 65.
(52) Erdemir, D.; Lee, A.; Myerson, A. S. *Acc. Chem. Res.* **2009**, *40*, 621.
(53) Duff, N.; Peters, B. *J. Chem. Phys.* **2009**, *131*, 184101.
(54) Whitelam, S. *J. Chem. Phys.* **2010**, *132*, 194901.

JP107269Q

CHAPTER 6

CAN AMORPHOUS NUCLEI GROW CRYSTALLINE CLATHRATES? THE SIZE AND CRYSTALLINITY OF CRITICAL CLATHRATE NUCLEI

Reprinted with permission from the American Chemical Society

Jacobson, L.; Molinero, V. *J. Am. Chem. Soc.* **2011**, *133*, 6458

JACS
JOURNAL OF THE AMERICAN CHEMICAL SOCIETY

ARTICLE

pubs.acs.org/JACS

Can Amorphous Nuclei Grow Crystalline Clathrates? The Size and Crystallinity of Critical Clathrate Nuclei

Liam C. Jacobson and Valeria Molinero*

Department of Chemistry, University of Utah, 315 South 1400 East, Salt Lake City, Utah 84112-0850, United States

ABSTRACT: Recent studies reveal that amorphous intermediates are involved in the formation of clathrate hydrates under conditions of high driving force, raising two questions: first, how could amorphous nuclei grow into crystalline clathrates and, second, whether amorphous nuclei are intermediates in the formation of clathrate crystals for temperatures close to equilibrium. In this work, we address these two questions through large-scale molecular simulations. We investigate the stability and growth of amorphous and crystalline clathrate nuclei and assess the thermodynamics and kinetic factors that affect the crystallization pathway of clathrates. Our calculations show that the dissociation temperature of amorphous clathrates is just 10% lower than for the crystals, facilitating the formation of metastable amorphous intermediates. We find that, at any temperatures, the critical crystalline nuclei are smaller than critical amorphous nuclei. The temperature dependence of the critical nucleus size is well described by the Gibbs−Thomson relation, from which we extract a liquid-crystal surface tension in excellent agreement with experiments. Our analysis suggests that at high driving force the amorphous nuclei may be kinetically favored over crystalline nuclei because of lower free energy barriers of formation. We investigated the role of the initial structure and size of the nucleus on the subsequent growth of the clathrates, and found that both amorphous and sI crystalline nuclei yield crystalline clathrates. Interestingly, growth of the metastable sII crystal polymorph is always favored over the most stable sI crystal, revealing kinetic control of the growth and indicating that a further step of ripening from sII to sI is needed to reach the stable crystal phase. The latter results are in agreement with the observed metastable formation of sII CO_2 and CH_4 clathrate hydrates and their slow conversion to sI under experimental conditions.

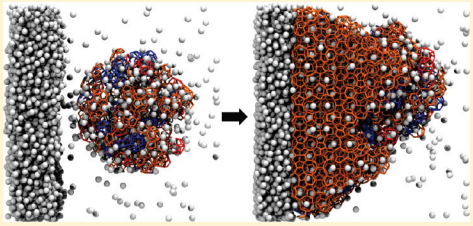

INTRODUCTION

Clathrate hydrates are crystals in which hydrogen-bonded water networks form polyhedral cages that enclose nonpolar molecules such as methane and carbon dioxide. Clathrates occur naturally and in great abundance on the sea floor, and are the most abundant source of fossil fuels on our planet.[1] The crystallization of clathrate hydrates is of utmost importance in a wide range of applications, from the prevention of clogging in oil and gas pipelines to the safe transportation of natural gas from remote resources.[2] Methods to promote and prevent the formation of clathrate hydrates are of significant importance to scientists and engineers. Therefore, there is great interest in understanding the mechanism of hydrate nucleation, and the nature of the nascent clathrate nuclei.

State of the art experimental techniques are not yet able to resolve and characterize the structure of clathrate nuclei.[3] Some insights on the structure of clathrate nuclei, however, have been obtained from molecular simulations.[4−7] These are typically carried out under conditions of high driving force such as supercooling the system with respect to the clathrate phase or supersaturating the solution with guest molecules. Such simulations at high driving force result in the formation of amorphous clathrate structures.[4−7] These amorphous clathrates are made of the same polyhedral cage building blocks of the crystalline clathrates, but lack their long-range order. In a previous simulation study, we have shown that the nucleation of clathrate hydrates in supercooled conditions takes place through a multistep mechanism involving amorphous precursors.[6] The same mechanism has been observed by Vatamanu et al. using different model and simulation methodology.[7] These results are in contrast to classical nucleation theory that states that the nucleation of the crystalline phase takes place through a building up of monomers already arranged with the symmetry of the crystal phase.

The "blob mechanism" of clathrate crystallization proposed in ref 6 involves first the creation from the dilute solution of a blob: an amorphous cluster of solvent-separated guest molecules with interstitial water that continually rearranges to form *transient* clathrate cages. If the blob intermediate is sufficiently large and long-lived, the water molecules surrounding the solvent-separated guests form *persistent* polyhedral cages resulting in an amorphous clathrate intermediate that is able to nucleate the growth of the crystalline clathrate phase. Similar multistep mechanisms have been proposed for the crystallization of proteins and colloids: a sequence of steps that include first the densification from a dilute phase into a dense amorphous intermediate and subsequent ordering of the dense intermediate into a more stable

Received: February 14, 2011
Published: April 05, 2011

   dx.doi.org/10.1021/ja201403q | *J. Am. Chem. Soc.* 2011, 133, 6458–6463

crystal.[8,9] Ten Wolde and Frenkel modeled globular proteins using Lennard-Jones particles with attractive, short-ranged interactions and discovered that the dilute fluid phase has a fluid−fluid coexistence curve with the dense amorphous phase that is metastable to the dilute fluid-crystal coexistence curve.[10] Below the fluid−fluid coexistence line, the free energy of the dense, disordered intermediate phase is lower than for the solution. Above this coexistence line, the intermediate is metastable to both the dense disordered and ordered phases.[11] Recent work involving simulations of protein crystallization indicates that the dense disordered phase might still be an intermediate above the fluid−fluid coexistence line where the dense amorphous phase is unstable.[9,12] These results suggest that amorphous intermediates might form in the nucleation pathway, even under conditions of low driving force. Therefore, it is important to understand the properties that such amorphous nuclei might have as well as whether and how the amorphous clathrates might be able to grow the crystal phase.

The formation of amorphous clathrates in simulations at high supercooling indicates that they are stable with respect to the solution under these conditions. A first question addressed in this study is whether there are temperatures for which the amorphous clathrate is more stable than the crystal. We compute the dissolution (i.e., melting) temperatures of amorphous and crystalline clathrates and determine the size of their respective critical nuclei as a function of temperature. We further investigate whether there could be conditions for which the amorphous clathrate nuclei are favored not by thermodynamics but by a lower free energy of formation from the solution. A second question we address is whether amorphous clathrate nuclei can grow into crystalline clathrates by either reorganization of the amorphous network or by growth of a crystalline phase around an amorphous seed. Answering this question is key to determine the feasibility of a multistep mechanism of clathrate crystallization involving amorphous clathrate nuclei.

The nucleation of clathrates in simulations is a rare event, and the time scales and computational resources needed to observe nucleation at low driving force are immense. Thus in this work we focus on the stability and growth of premade amorphous and crystalline nuclei, and not on their initial formation from the solution. A second challenge arises from the growing size of the critical nuclei on decreasing the driving force, requiring large-scale simulation cells that would make this study computationally very expensive with the use of atomistic models. We surpass this challenge through the use of a coarse-grained model of water and a methane-like guest that accurately describes the thermodynamics of clathrate formation and the mechanisms of nucleation and growth from solution, and it is 2−3 orders of magnitude computationally more efficient than fully atomistic atomistic models.[6,13−15]

METHODS

Force Fields. Water was modeled using the monatomic water model mW.[16] The guest, that we call M here and in refs 6 and 14, is also represented by a single particle with properties intermediate between methane and carbon dioxide.[13] The melting temperatures of sI and sII clathrate hydrates of the M guest, along with structural and thermodynamic properties of these crystals and the M-water solutions were presented and validated in refs 6, 13, and 14.

Simulations. Molecular dynamics simulations were carried out with LAMMPS.[17] The equations of motion were integrated with the velocity Verlet algorithm using 10 fs time steps.[16] Simulations were performed in the isothermal−isobaric (NpT) ensemble using the Nose−Hoover thermostat and barostat with damping constants 1 and 5 ps, respectively. All simulations were performed at pressure of 50 MPa. Periodic boundary conditions were used in the three dimensions.

Systems. A 128 Å × 128 Å × 128 Å simulation cell (54,000 molecules) of bulk sI clathrate crystal with all cages occupied by single M guests was equilibrated at T = 270 K and p = 50 MPa. Approximately spherical crystalline clathrate clusters were constructed by freezing the positions of the water and guest molecules within 10, 15, 20, 25, and 30 Å of the center of the equilibrated lattice and melting the rest of the molecules, after transforming them all to water. A slab of water particles of the liquid was converted to M particles, and equilibrated at 300 K and 50 MPa for 10 ns, resulting in a three phase system: a slab of M liquid in contact with a water solution saturated with M containing a solid clathrate nucleus. The solubility of M in water is 0.0038 mol fraction at 178 atm and 313 K, intermediate between the one of methane, 0.0023, and carbon dioxide, 0.024, under the same conditions.[13] Amorphous clathrate nuclei of initial radii 10, 20, and 30 Å were obtained in a similar fashion, selecting spherical regions from the last configuration of a deeply supercooled simulation[14] in which a water-guest solution produced an amorphous clathrate solid. Guest molecules were placed in the center of mass of all clathrate cages.

We considered a single amorphous nucleus for each radius R. While the amorphous clathrates do not have a unique structure, we previously demonstrated that the percentage of each cage type ($5^{12}6^n$ with n = 0, 2, 3 and 4) in the amorphous clathrates is constant across different simulations.[14] Thus, we expect that due to self-averaging of different local structures, amorphous nuclei of radius R prepared from distinct simulation runs would result in the same thermodynamic properties. The excellent fit of the amorphous dissociation temperature data to the Gibbs−Thomson (GT) equation, and the agreement between the bulk value of melting temperature obtained from the GT equation and the direct determination from the bulk simulations, both presented in the Results and Discussion section below, strongly suggests that the self-averaging of the amorphous structures is valid down to the smallest nucleus size considered in this study.

Thermodynamic Data. The melting temperatures (T_m) for bulk crystalline sI and sII clathrates with the M guest at p = 50 MPa were determined in a previous study.[6] The T_m for the spherical nuclei of the crystalline sI and amorphous clathrates as well as the bulk amorphous clathrate were determined using the method of direct coexistence with the protocols detailed in ref 13. Phase coexistence simulations were repeated in steps of 5 K. Simulation times of up to 100 ns were needed to observe the advance of crystallization or dissolution of the system.

As the nuclei can be modified during their initial pre-equilibration with the solution, the sizes of nuclei used for the melting point determinations were measured in terms of the number of guest molecules N_g that belonged to each clathrate cluster after the equilibration process indicated above. N_g was determined by identifying the solvent-separated guest molecules that belonged to the same cluster. The effective radius of the cluster R is obtained by using the average number density of guests in the clathrate lattice $\rho = N_g/V$, where $V = (4/3)\times\pi R^3$ is the volume of a sphere, resulting in R = 0.365 nm × $(N_g)^{1/3}$ for the crystalline nuclei and R = 0.43 nm × $(N_g)^{1/3}$ for the amorphous nuclei.

The enthalpy of dissociation or melting ΔH_m per mole of water was calculated by subtracting the enthalpy of liquid water and the enthalpy of the guest from the enthalpy of the clathrate using the appropriate stoichiometry. The entropy of dissociation was determined as $\Delta S_m = \Delta H_m/T_m$. The enthalpy for the amorphous phase was determined by calculating the enthalpy $\langle H\rangle = \langle E + pV\rangle$, normalized per mole of water, of a system of amorphous clathrate. Since not all the water was converted to amorphous clathrates during their formation,[14] the enthalpy of the

Table 1. Thermodynamic Properties of Bulk Amorphous and sI Crystalline Clathrates

property	amorphous	crystalline	amorphous/crystalline
T_m (K)[a]	276 ± 6	307 ± 2	0.90
T_m (K)[b]	281	300	0.94
ΔH_m (kJ/mol)[c]	5.40	6.53	0.83
ΔS_m (J/K mol)[c]	19.8	21.3	0.93
K_{GT} (K nm)	34.8	36.6	0.95
γ (mJ/m^2)	<32	36	--

[a] Computed from phase coexistence method of bulk slabs. [b] Determined from Gibbs−Thomson relation (eq 1). [c] Normalized per mole of water.

N_w "non-clathrate" water molecules present in the amorphous clathrate simulation cell but that did not belong to any clathrate cages was subtracted as that of liquid water: $\langle H\rangle_{amorphous} = \langle H\rangle_{system} - \langle H\rangle_{non\text{-}clathrate\ water}$, where $\langle H\rangle_{non\text{-}clathrate\ water}$ is determined from simulations of liquid water under the same conditions $\langle H\rangle_{non\text{-}clahtrate\ water} = N_w \langle H\rangle_{water}$, $\langle H\rangle_{water}$ is the enthalpy of liquid water.

RESULTS AND DISCUSSION

The stable phase of the M clathrate hydrate is, same as for CH_4 and CO_2 clathrates, the sI crystal, with a melting temperature $T_m^X = 307 \pm 2$ K.[14] The sII crystal is metastable to sI but close in free energy, with a melting temperature 303 ± 1 K.[14] We find that the melting temperature of the amorphous clathrate is about 90% of the melting temperature of the crystal, $T_m^A = 276 \pm 6$ K. Interestingly, the ratio between T_m^A and T_m^X is almost the same as found for the stable liquid-crystal and metastable liquid−liquid equilibrium in the crystallization of lysozyme, a protein that −as the clathrates− presents a multistep mechanism of crystallization assisted by a dense but disordered amorphous phase.[11]

Table 1 shows the interplay between entropy and enthalpy on the relatively high stability of the amorphous clathrate. The amorphous clathrate has higher entropy than the crystal, favoring its formation from the liquid. The enthalpies of melting for the amorphous and crystalline clathrates are close (5.4 and 6.5 kJ/mol; Table1), with values comparable tothe those for the melting for ice (5.3 kJ/mol[16]) and the empty clathrate (4.4 kJ/mol[15]). These results indicate that the enthalpies of all these phase transitions are dominated by the ordering of liquid water to form a fully hydrogen-bonded network.

In the nucleation of a new phase, nuclei that are smaller than the critical size dissolve and those that are larger grow. We determined the size of the critical clathrate nuclei through the computation of the dissolution temperature of premade spherical nuclei: for a given temperature T the critical radius R is the one for which its melting point $T_m(R)$ equals T. Figure 1 presents the melting temperatures for the crystalline and amorphous nuclei as a function of their radii R and their respective fits to the Gibbs−Thomson equation for spherical particles,

$$T_m(R) = T_m^{bulk} - \frac{2K_{GT}}{R} \qquad (1)$$

The Gibbs−Thomson constant is $K_{GT} = T_m^{bulk}\gamma v/\Delta H_m$, where γ is the liquid−solid surface tension, v is the molar volume and ΔH_m is the bulk enthalpy of melting. Equation 1 gives a very good description of the data (correlation coefficient above 0.998) and predicts values for T_m of the bulk phases, $T_m^A = 281$ K and $T_m^X = 300$ K, in excellent agreement with those determined from

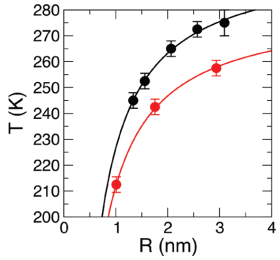

Figure 1. Melting or dissociation temperature of crystalline (black) and amorphous (red) nuclei as a function of their radius. The lines are the fits with the Gibbs−Thomson relation (eq 1) with the parameters of Table 1, and indicate the critical nucleus size R for each temperature T. According to classical nucleation theory, the radius of the critical nucleus is $R^*(T) = -2\gamma/(\Delta\mu(T)\rho_l) \approx 2\gamma/(\rho\Delta S_m(T_m^{bulk} - T))$. The coarse-grained model predicts correctly γ but underestimates the experimental ΔS_m by about 20%, because the monatomic it cannot account for the increase in rotational entropy of the water and guest on melting.[13] Thus, for a given supercooling $T_m^{bulk} - T$ the radii of the critical nuclei would be about 20% smaller than predicted by the simulations.

the direct phase coexistence method. For any temperature, we find that the critical size for crystalline nuclei is smaller than for amorphous nuclei, with the two becoming essentially indistinguishable in terms of stability for nuclei with less than 15 guest molecules, a size comparable to the unit cell of the clathrate.

The Gibbs−Thomson constants we obtained for the amorphous and crystalline clathrates are $K_{GT}^A = 34.8$ K nm and $K_{GT}^X = 36.6$ K nm. These are comparable to the value for ice, 26 K nm as determined from experimental thermodynamic data.[18] When comparing to results from the literature, it is important to note that some authors include the factor of 2 from eq 1 in the definition of K_{GT}. The mW water model used in this study accurately predicts[19] the freezing point depression of water confined in cylindrical nanopores measured in cryoporometry[20] and calorimetry[21] experiments.

Using K_{GT}, bulk T_m, ΔH_m, and molar volume of the hydrate, we determined the surface tensions between liquid and sI crystal, $\gamma_x = 36 \pm 2$ mJ/m^2. The surface tension determined from the simulations is in excellent agreement with those determined from the experimental melting temperatures of CH_4 and CO_2 clathrates in cylindrical pores of various radii. Anderson et al. determined the experimental water-sI CH_4 and CO_2 clathrates interfacial energies by measuring hydrate equilibria in mesoporous silica.[22] They obtained surface tensions γ equal to 32 ± 3 and 30 ± 3 mJ/m^2 for CH_4 and CO_2 clathrate−water interfaces, respectively. Using the same methods, they determined γ for the ice−water interface to be 32 ± 2 mJ/m^2. Uchida et al. obtained clathrate−water surface tension values of 17± 3 and 14 ± 3 mJ/m^2 for CH_4 and CO_2 clathrate-water interfaces, respectively.[23] Anderson et al. recalculated the values using the experimental results of Uchida et al., but accounting for the correct hysteresis conditions and obtained values of 34± 6 mJ/m^2 and 28 ± 6 mJ/m^2 for CH_4 and CO_2 clathrate-water interfaces, respectively.[22]

The same analysis employed for the crystal could be used to estimate the surface tension of the amorphous nuclei. We note, however, that the amorphous nuclei used in this study are porous and not fully filled with clathrate cages, thus they effectively have a considerable larger exposed liquid−solid area than expected for a perfect sphere. This implies that the surface tension predicted

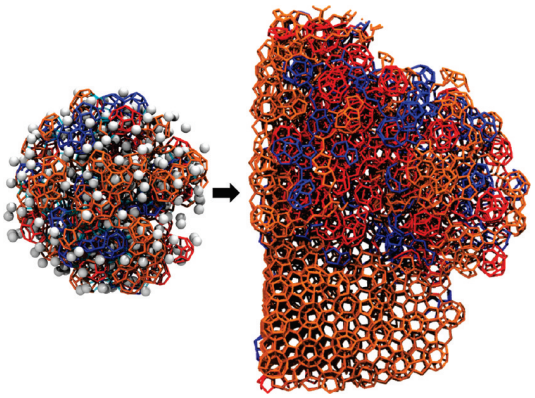

Figure 2. Amorphous nucleus with R = 30 Å at the beginning of the simulation (left) and after 100 ns of growth (right) at T = 250 K. The nucleus at the beginning of the simulation had 2128 water molecules that belonged to a polyhedral clathrate cage. Of those, 20% were identified as being sI (shown in blue) and 50% were identified as being sII (shown in orange). Cages shown in red correspond neither to the sI or sII structure. Although initially there were no large crystalline domains of any of the two crystals, the amorphous nucleus grew a crystalline clathrate. After 100 ns of growth, there were 10438 water molecules in polyhedral cages. Of those, 12% were identified as sI and 64% were identified as sII. Guest molecules (white balls) have been omitted from the final structure so that the sII crystalline lattice is clearly appreciated. The flat edge of the final structure rests on the guest-water interface, as also shown in the Abstract graphic.

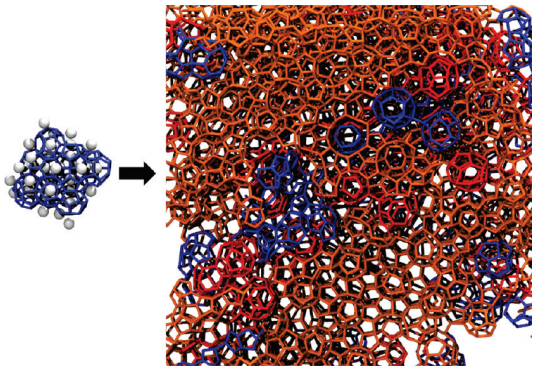

Figure 3. Crystalline sI nucleus with R = 10 Å at the beginning of the simulation (left) and after 100 ns of growth (right) at T = 240 K. The domains of sI clathrate are identified in blue and the domains of sII clathrate are colored orange. Guest molecules (white balls) have been omitted from the final structure for clarity.

from the Gibbs−Thomson constant by assumption of spherical geometry, γ_a = 32 mJ/m^2, is an upper limit to the real value for the amorphous clathrate. From the porosity of the amorphous nuclei, we estimate that the surface tension of compact amorphous clathrates could be as small as half that value. A more accurate knowledge of that surface tension would permit the estimation of the relative barriers of formation of the amorphous and crystalline nuclei from solution. According to classical nucleation theory, the free energy barrier to nucleation is

$$\Delta G^* = \frac{16\pi\gamma^3 v^2}{\Delta\mu^2} \quad (2)$$

where $\Delta\mu = \Delta T \Delta S_m$, and $\Delta T = T_m^{bulk} - T$.[24] The ratio ζ of the free energy barriers for nucleation of the amorphous and crystalline structures would then only depend on the ratio between their solid−liquid surface tensions and the driving force

$$\zeta = \frac{\Delta G_A^*}{\Delta G_X^*} = \frac{{\gamma_A}^3 {\Delta S_X}^2 (T_m^X - T)^2}{{\gamma_X}^3 {\Delta S_A}^2 (T_m^A - T)^2} \quad (3)$$

Nucleation of clathrates in simulations at temperatures up to as high as ∼20% supercooling start with amorphous nuclei.[1−6,14,25−28] This suggests that although the amorphous critical nuclei are larger than the crystalline nuclei for any temperature, their formation may be kinetically favored by lower free energy barriers. Equation 2, along with the data of Table 1, indicates that formation of amorphous nuclei could be kinetically favored up to 255 K (17% supercooling) if γ_a/γ_x were 0.5 and up to 230 K (25% supercooling) if the ratio of the surface tensions were 0.66). For these estimations, we used the melting temperatures of sI and amorphous clathrates obtained by the phase-coexistence method; the ${T_m}^x$ and ${T_m}^A$ predicted by the extrapolation of the Gibbs−Thomson equation are closer, predicting an even larger temperature range for which nucleation through amorphous clusters would be kinetically favored. Further work is needed to more accurately assess the interfacial energies of compact amorphous nuclei.

Finally, we investigated the growth of the clathrate nuclei and the degree of crystallinity in the structures grown from amorphous and crystalline seeds. To identify the clathrate cages that belong to sI and sII domains we used order parameters developed in a separate study.[29] Each water molecule in the sI and sII lattice is the vertex of four polyhedral cages; we distinguish water molecules that belong to the sI and sII crystals by identifying the unique vertices of polyhedra present in the clathrate lattices where the polyhedral cages meet. Water molecules in the sI vertices belong to only $5^{12}6^2$ cages, or to both $5^{12}6^2$ cages and 5^{12} cages. Water in the sII vertices belong only to 5^{12} cages, or to 5^{12} and $5^{12}6^4$ cages, or to only $5^{12}6^4$ cages. These order parameters give us the ability to determine whether the amorphous nuclei lead to the formation of additional amorphous clathrate or grew crystalline clathrates. This analysis also allowed us to investigate whether the sI clathrate lattice could cross nucleate the sII clathrate, a phenomenon previously observed in the growth of methane and guest-free clathrates.[15,30]

A notable finding from this study is that crystalline clathrates can grow from amorphous nuclei. This is illustrated in Figures 2–4 that show initial amorphous and crystalline clathrate and the structures they grow from the solution at temperatures just below their respective melting points. All nuclei, whether crystalline or amorphous, eventually lead to the growth of crystalline and polycrystalline domains. The growth of clathrate cages around the nucleus was faster than the reorganization of the initial core of amorphous nuclei to form crystalline clathrates, thus an amorphous core remained encased within a crystalline (or polycrystalline) shell. Figure 3 shows that the smallest crystalline nucleus ($R \approx$ 10 Å) leads to the growth of polycrystalline domains, perhaps because the increased supercooling of the system (held at 240 K) with respect to both the bulk sI and sII phases. We note that the conditions of this study favor relatively fast growth of post critical nuclei, because there is no mass-transport

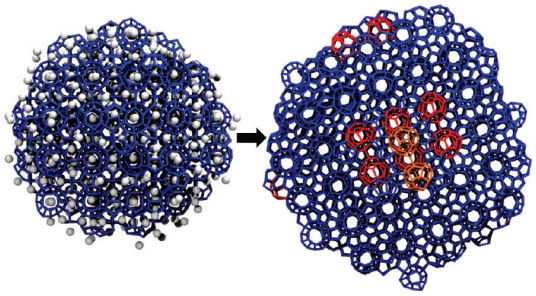

Figure 4. R = 30 Å sI nucleus at the beginning of the simulation (left) and after 52 ns of growth (right) at T = 270 K. The sI lattice (blue) is able to template the growth of sII (orange) through the $5^{12}6^3$ cages (red). The nucleus started out with 3406 water molecules belonging to cages in the sI structure. The final structure shown above has 7629 water molecules as part of a polyhedral cage, 90% of which were identified as being sI. For clarity, guest molecules (white balls) are not shown in the final structure.

limitation (the guest molecules have to cross a short path from the guest liquid slab to reach the nucleus; see the Abstract graphic). We expect that even if amorphous nuclei formfirst, favored by a lower free energy barrier at high supercooling, slow growth of these critical nuclei under conditions where the accessibility of guests to the growing surface is a limiting factor should lead to an increase in nuclei crystallinity already for small sizes, before they grow a macroscopic crystal phase.

Large sI crystalline nuclei grow sI clathrates, nevertheless we also observe cross-nucleation of the sII crystal from the sI core facilitated by the formation of $5^{12}6^3$ cages, as shown in Figure 4. Despite the sI or amorphous nature of the initial nuclei, all the systems eventually grow predominantly the sII structure, and not the most stable sI crystal. In this regard, this is different from the cross-nucleation from sI to sII in guest-free clathrates, where the sII structure is the most stable phase.[15] The relative stabilities of sI and sII in the methane-water model used in ref 30 are not known; nevertheless the results presented here demonstrate that cross-nucleation toward the least stable crystal is possible under conditions where the two crystals are more stable than the solution.

The cross nucleation of sII from sI, even though the sI crystal is thermodynamically more stable, attests to the important role of kinetic factors not only for the nucleation but also for the subsequent growth of the clathrates. Our finding is in agreement with experimental observations of methane hydrate formation in which the metastable sII structure preferentially forms at the onset, but later transforms into the stable sI polymorph.[31,32] The transformation of the kinetically favored metastable sII crystal into the stable sI lattice can take hours to days,[31,32] and is not observed in the time scale of the simulations. The very slow kinetics of the sII to sI ripening suggests that advanced sampling methods are necessary for its study through molecular simulations.

■ CONCLUSIONS AND OUTLOOK

We used molecular dynamics simulations with a very efficient force-field to investigate the thermodynamics, size and crystallinity of clathrate hydrate clusters of a small hydrophobic guest with properties intermediate between those of CH_4 and CO_2, and evaluate their potential as nuclei for the crystallization of clathrates. A main finding of this study is the relatively high stability of the amorphous solid clathrate phase, more stable than the water-guest solution for supercooling larger than 10%. The stability of the amorphous clathrate is key in favoring nucleation pathways that proceed, as previously reported for the crystallization of proteins, colloids and nanoparticles,[8−12,33,34] through amorphous intermediates.[6,7,14]

We determined the critical nucleus size for amorphous and crystalline clathrates as a function of temperature and found that it is well-described by the Gibbs−Thomson equation, from which we extract a liquid-crystal surface tension in excellent agreement to that determined from the experimental study of melting of CH_4 and CO_2 clathrates in nanopores. While for each temperature the size of the critical amorphous nuclei is predicted to be larger than the critical crystalline nuclei, our analysis based on tentative values of the liquid-amorphous clathrate surface tension suggest that, at high supercooling, the nucleation through amorphous clathrates could be kinetically favored by lower free energy barriers, thus explaining the results obtained in simulations at high driving force, where amorphous nuclei initiate the formation of clathrates.[4−6,14,25−28]

This study demonstrates that amorphous nuclei can grow crystalline clathrates, even under conditions where they do not ripen to crystalline nuclei before growing. This implies that the observation of macroscopic crystalline clathrates should not be used to rule out a mechanism of formation that proceeds through an amorphous clathrate intermediate. Most important, the cross-nucleation from the stable sI to the least stable sII crystal under conditions where the two are more stable than the solution reveals the importance of kinetic factors in the growth of clathrates. Recent work by Peters stresses the role of the diffusion tensor anisotropy on polymorph selection for the crystallization of a mixture of oppositely charged colloids.[35] It would be of interest to investigate whether the formation of sII is favored over the growth of sI by lower free energy barriers in the nucleation pathway or by purely dynamical effects.

An important and still not fully answered question is what is the highest temperature for which nucleation through amorphous clathrate nuclei is competitive with respect to the formation of smaller crystalline nuclei. The infrared spectra of clathrates formed from aqueous nanodroplets at 200 K show signatures that are not consistent with sI, sII or a combination of the two crystals,[36] suggesting that amorphous clathrates may have formed under those conditions. At low driving forces, outside of the region of stability for the amorphous clathrate, only crystalline nuclei could be stable. The critical radius of crystalline nuclei at the temperature of melting of bulk (i.e., infinite) amorphous clathrate is about 4 nm, thus large clathrate nuclei must be crystalline. Consistent with this prediction, Lehmkühler et al. identified CO_2 clathrate crystal clusters of about 20 nm diameter close to the water-CO_2 interface for conditions of relatively low driving force, that nevertheless do not grow macroscopic clathrates within the time scale of their experiments.[37] It is possible, however, that even at low driving force, density fluctuations of the guest molecules in solution that form a transient amorphous intermediate could facilitate the growth of crystalline clathrates. Enhanced sampling techniques are needed to determine in an unbiased way the actual pathways, free energy barriers and dynamical factors involved in the crystallization of clathrates at low driving force.

AUTHOR INFORMATION

Corresponding Author
Valeria.Molinero@utah.edu

ACKNOWLEDGMENT

We gratefully acknowledge support by the National Science Foundation through award CHE-1012651 and thank the Center of High Performance Computing of the University of Utah for allocation of computing time.

REFERENCES

(1) Sloan, E. D.; Koh, C. A. *Clathrate Hydrates of Natural Gases*; 3rd ed.; CRC Press/Taylor-Francis: Boca Raton, FL, 2007.
(2) Koh, C. A.; Sum, A. K.; Sloan, E. D. *J. Appl. Phys.* **2009**, *106*, 061101–14.
(3) Sum, A. K.; Koh, C. A.; Sloan, E. D. *Ind. Eng. Chem. Res.* **2009**, *48*, 7457–7465.
(4) Hawtin, R. W.; Quigley, D.; Rodger, P. M. *Phys. Chem. Chem. Phys.* **2008**, *10*, 4853–4864.
(5) Walsh, M.; Koh, C.; Sloan, E.; Sum, A.; Wu, D. *Science* **2009**, *326*, 1095.
(6) Jacobson, L. C.; Hujo, W.; Molinero, V. *J. Am. Chem. Soc.* **2010**, *132*, 11806–11811.
(7) Vatamanu, J.; Kusalik, P. G. *Phys. Chem. Chem. Phys.* **2010**, *12*, 15065–15072.
(8) Erdemir, D.; Lee, A. Y.; Myerson, A. S. *Acc. Chem. Res.* **2009**, *42*, 621–629.
(9) Whitelam, S. *J. Chem. Phys.* **2010**, *132*, 194901–5.
(10) Wolde, P. R. t.; Frenkel, D. *Science* **1997**, *277*, 1975–1978.
(11) Vekilov, P. G. *J. Cryst. Growth* **2005**, *275*, 65–76.
(12) Liu, H.; Kumar, S. K.; Douglas, J. F. *Phys. Rev. Lett.* **2009**, *103*, 018101.
(13) Jacobson, L. C.; Molinero, V. *J. Phys. Chem. B* **2010**, *114*, 7302–7311.
(14) Jacobson, L. C.; Hujo, W.; Molinero, V. *J. Phys. Chem. B* **2010**, *114*, 13796–13807.
(15) Jacobson, L. C.; Hujo, W.; Molinero, V. *J. Phys. Chem. B* **2009**, *113*, 10298–10307.
(16) Molinero, V.; Moore, E. B. *J. Phys. Chem. B* **2009**, *113*, 4008–4016.
(17) Plimpton, S. J. *J. Comput. Phys.* **1995**, *117*, 1–19.
(18) *Handbook of Chemistry and Physics*; CRC: Boca Raton, FL, 2000−2001; Vol. 81.
(19) Moore, E. B.; de la Llave, E.; Welke, K.; Scherlis, D. A.; Molinero, V. *Phys. Chem. Chem. Phys.* **2010**, *12*, 4127–4134.
(20) Petrov, O. V.; Furó, I. *Prog. Nucl. Magn. Reson. Spectrosc.* **2009**, *54*, 97–122.
(21) Jaehnert, S.; Vaca Chavez, F.; Schaumann, G. E.; Schreiber, A.; Schoenhoff, M.; Findenegg, G. H. *Phys. Chem. Chem. Phys.* **2008**, *10*, 6039–6051.
(22) Anderson, R.; Llamedo, M.; Tohidi, B.; Burgass, R. W. *J. Phys. Chem. B* **2003**, *107*, 3507–3514.
(23) Uchida, T.; Ebinuma, T.; Takeya, S.; Nagao, J.; Narita, H. *J. Phys. Chem. B* **2002**, *106*, 820–826.
(24) Kashchiev, D.; Firoozabadi, A. *J. Cryst. Growth* **2002**, *243*, 476–489.
(25) Liang, S.; Kusalik, P. G. *Chemical Science* **2011**, under review.
(26) Moon, C.; Taylor, P. C.; Rodger, P. M. *J. Am. Chem. Soc.* **2003**, *125*, 4706–4707.
(27) Zhang, J.; Hawtin, R. W.; Yang, Y.; Nakagava, E.; Rivero, M.; Choi, S. K.; Rodger, P. M. *J. Phys. Chem. B* **2008**, *112*, 10608–10618.
(28) Moon, C.; Hawtin, R. W.; Rodger, P. M. *Faraday Discuss.* **2007**, *136*, 367–382.
(29) Jacobson, L. C.; Molinero, V. "Order parameters for the multistep crystallization of clathrate hydrates", in preparation.
(30) Vatamanu, J.; Kusalik, P. G. *J. Am. Chem. Soc.* **2006**, *128*, 15588–15589.
(31) Staykova, D. K.; Kuhs, W. F.; Salamatin, A. N.; Hansen, T. *J. Phys. Chem. B* **2003**, *107*, 10299–10311.
(32) Murshed, M. M.; Kuhs, W. F. *J. Phys. Chem. B* **2009**, *113*, 5172–5180.
(33) Savage, J. R.; Dinsmore, A. D. *Phys. Rev. Lett.* **2009**, 102.
(34) Duff, N.; Peters, B. *J. Chem. Phys.* **2009**, *131*, 184101.
(35) Peters, B. *J. Chem. Phys.* **2009**, *131*, 244103.
(36) Devlin, J. P.; Monreal, I. A. *Chem. Phys. Lett.* **2010**, *492*, 1–8.
(37) Lehmkühler, F.; Paulus, M.; Sternemann, C.; Lietz, D.; Venturini, F.; Gutt, C.; Tolan, M. *J. Am. Chem. Soc.* **2009**, *131*, 585–589.

CHAPTER 7

ORDER PARAMETERS FOR THE MULTISTEP CRYSTALLIZATION OF CLATHRATE HYDRATES

This chapter has been submitted to the Journal of Chemical Physics

Abstract

Recent reports indicate that the crystallization of clathrate hydrates occurs in multiple steps that involve amorphous intermediates and metastable clathrate crystals. The elucidation of the reaction coordinate for clathrate crystallization requires the use of order parameters able to identify the reactants, products and intermediates in the crystallization pathway. Nevertheless, existing order parameters cannot distinguish between amorphous and crystalline clathrates or between different clathrate crystals. In this work, we present the first set of order parameters that discern between the sI and sII clathrate crystals, the amorphous clathrates the blob of solvent-separated guests and the liquid solution. These order parameters can be used to monitor the advance of the crystallization and for the efficient implementation of methods to sample the rare clathrate nucleation events in molecular simulations. We illustrate the use of these order parameters in the analysis of the growth and the dissolution of clathrate crystals and the spontaneous nucleation and growth of clathrates under conditions of high supercooling.

Introduction

Clathrate hydrates are crystalline inclusion compounds in which water molecules form a hydrogen-bonded network of polyhedral cages that can host small non-hydrogen bonding molecules such as methane and carbon dioxide. Clathrates occur predominantly in two cubic crystalline structures, sI and sII. These crystals are tiled by a combination of small dodecahedral cages (noted as 5^{12}), and larger polyhedral cages ($5^{12}6^2$ cages in sI and $5^{12}6^4$ cages in sII). Depending on the size of the guest molecules, a significant fraction – even all – of the dodecahedral cages can be unoccupied.[1]

Clathrate hydrates hold great promise in the fields of energy, carbon sequestration, industrial separations, and natural gas transportation.[2] Methane hydrate is an important

energy resource, estimated to be the most abundant reserve of hydrocarbon energy in the planet.[3,4] Clathrates also form, unwanted, in high-pressure pipelines and deep-water wells, presenting a significant challenge to the oil and gas industry.[3] Therefore, methods to promote and prevent clathrate formation are highly sought after. A barrier to fully harnessing the promise of clathrates is the insufficient fundamental understanding of the mechanism of clathrate nucleation. Current experimental techniques are still limited in their ability to resolve the nanoscopic structure of clathrate nuclei and their mechanisms of formation, therefore computer simulations have proven an indispensable tool in the study of clathrate crystallization.[5-15]

Three different hypotheses have been proposed to explain the mechanism of nucleation of clathrate hydrates. The Labile Cluster Hypothesis proposed by Sloan and coworkers in 1991 states that the nucleation takes place through the formation and subsequent aggregation of individual clathrate cages in solution.[1,16] Since then, molecular simulations have shown that individual polyhedral cages form rarely in solution[11] and when they form, do not survive for times long enough to agglomerate.[7] The Local Structuring Hypothesis put forward by Radhakrishnan and Trout in 2002 proposes that a rare fluctuation of the guest molecules in solution gives rise to guest-guest ordering similar to that found in the clathrate crystal, leading to the reorganization of water molecules to build the clathrate lattice.[11] Recent simulations of nucleation at high driving force reveal that the initial clathrates formed are amorphous structures made of the same polyhedral building blocks of the clathrate crystals, but the ordering and the ratio in the number of the different polyhedral cages does not correspond to any of the crystalline clathrates.[9,10,15,17]

The most recent mechanism for clathrate crystallization, the Blob Hypothesis by Jacobson, Hujo and Molinero, was developed from the analysis of trajectories of nucleation

and growth of clathrates in molecular dynamics simulations.[17,18] The Blob Hypothesis states that the crystallization of clathrates proceeds in multiple steps that involve amorphous intermediates.[17] Using different models and simulation methodology than Jacobson et al., Vatamanu and Kusalik also observed a multistep mechanism of crystallization involving amorphous clathrate intermediates.[15,19] The blob mechanism, schematized in Figure 1, involves a first step of densification of the dilute guests to form *blobs*, clusters of solvent-separated guests (SSG). The water between the guests mediates and cements the interactions between the guest molecules.[17,20] The stability and lifetime of the blobs increases with the number of guest molecules that are part of the cluster.[17,20] The next step in the nucleation pathway involves the rearrangement of the water molecules that surround the guest molecules into polyhedral cage structures.[17,18] Simulations under conditions of high supercooling produce amorphous clathrates, that are metastable with respect to the crystalline clathrates, but stable with respect to the liquid at temperatures up to ~90% of the melting point of the crystalline clathrates.[21] The reorganization of the amorphous clathrates to render crystalline clathrates in deeply supercooled solution is slow compared with the hundreds of nanoseconds reached by molecular simulations, but can be attained on warming of the system.[17-19] Alternatively, crystalline clathrates can grow from amorphous clathrate nuclei.[21]

Nucleation of clathrates at high driving force occurs spontaneously within time scales accessible to molecular simulations.[8-10,13,15,17,19] There has been, however, no report of clathrate nucleation in simulations at low driving force, the usual conditions for clathrate formation in the laboratory and in nature. The elucidation of reaction coordinates and rates of crystallization of clathrates at conditions close to equilibrium requires the use of advanced methods to sample the rare nucleation events, such as transition path sampling,[22-25] aimless

shooting,[26,27] transition interface sampling,[28,29] forward flux sampling[30-32] or metadynamics.[33,34] In principle, these methods do not require a priori knowledge of the reaction coordinate and use order parameters as a guidance to measure the advance of the reaction (nucleation). In practice, the efficiency of these methods is quite sensitive to the choice of order parameters.[35-38] While the order parameters used to monitor the advance of the reaction do not need to be the actual reaction coordinates, appropriate order parameters are necessary to identify the basins of configurational space that correspond to the reactants, products and intermediates (e.g., dilute solution, crystalline clathrate and blob and intermediate clathrate, respectively) and assist in the interpretation of the pathway of nucleation.

Some order parameters (OP) have been proposed in the literature to characterize the advance of the crystallization of clathrates from aqueous solutions. Rodger and coworkers defined a torsional order parameter F_4 between neighboring water molecules to identify hydrate-like water molecules and distinguish the clathrate phase from ice and liquid water.[8,9,39] While the combined use of these order parameters allows for the identification of regions of solid clathrate, these OP cannot distinguish amorphous from crystalline clathrates or distinguish regions with different clathrate crystal structures. Radhakrishnan and Trout evaluated Steinhardt bond-orientational order parameters[40] with $l = 4$ and 6 for the ordering of the guests and the water molecules in crystalline clathrate and aqueous solution of CO_2 and found that none of these OP were appropriate to distinguish between these two phases: the only guest-guest bond-order parameter that was not zero in liquid and the perfect sI crystal, W_4^{gg}, was rendered ineffective in the thermalized clathrate because the symmetry of the guest-guest ordering is broken by the translational freedom of the guest in the cages.[11] Instead, they used as leading OP for their analysis of clathrate nucleation with Umbrella Sampling methods the tetrahedral order parameter for water,[41] that measures the deviation

of the water-water-water angles from 109.5°, and a guest-guest order parameter ζ_{gg1} that is the ratio of the area under the first peak of the guest-guest radial distribution function in the solution and in the crystal. The tetrahedral OP, however, cannot distinguish ice from clathrate, or amorphous from crystalline clathrate, less indeed differentiate among clathrate polymorphs. Similarly, ζ_{gg1} measures the loss of translational symmetry of the guests, but it cannot distinguish whether the increase in the number of guest neighbors is due to the formation of a blob, an amorphous or a crystalline clathrate.

The aim of this work is to develop a set of order parameters that can distinguish between amorphous, sI and sII clathrates and quantify the advance of each of the steps in the mechanism of formation of clathrates shown in Figure 7.1. The paper presents the simulation methods, introduces the order parameters, illustrates the evolution these order parameters during the growth and nucleation of clathrate hydrates from solution.

Simulation Model and Methods

The simulations analyzed in this work were performed with a coarse-grained molecular model of water and guest molecules. The order parameters presented in this work, however, are equally applicable to configurations produced with atomistic models, as only the position of the oxygen of the water molecules and the center of mass of the guest molecules are used to construct the order parameters of this work.

Water was modeled with the monatomic water model mW.[42] The guest molecules were modeled using the M potential parameterized and validated in Ref. [17] for its use in the modeling of clathrate hydrates and aqueous solutions. The M solute is a single particle with solubility in water, hydration number, and melting temperature of the sI and sII clathrates intermediate between those of methane and carbon dioxide.[17] For details on the force fields

and their validation for the thermodynamics, nucleation and growth of clathrates and ice we refer the readers to Refs. 17,18,21,42-44.

We analyze molecular dynamics simulation trajectories of dissolution, growth and nucleation of clathrates. The simulations were performed with LAMMPS,[45] using the velocity Verlet algorithm to integrate the equations of motion with a 10 fs time step.[42] The simulations were performed in the NpT ensemble, the temperature and pressure controlled with the Nose-Hoover thermostat and barostat with damping constants of 1 and 5 ps, respectively. The *clathrate nucleation* trajectories, from Reference 17, started from periodic simulation cells with two-phases (a fluid of guest molecules and the saturated aqueous solution of the guest) in contact. The periodic cells contained 8000 molecules (6847 water molecules and 1153 guest molecules) and were evolved at 210 K and 500 atm, well below the equilibrium three-phase (fluid-fluid-clathrate) coexistence temperature T_m = 307 K at 500 atm.[17] The *growth and dissolution of the clathrates* was investigated for a system with 5888 water molecules and 1024 guest molecules that initially consisted of 4×4×4 unit cells of sI clathrate in contact with a liquid slab containing the same number of molecules, prepared as in Ref [46]. The dissolution and growth simulations were performed at p = 500 atm and temperatures 5 K above and 5 K below, respectively, the melting temperature of the sI M clathrate hydrate at that pressure.[46]

Order Parameters

In this section we propose order parameters to quantify the advance of clathrate formation through each of the steps of Figure 7.1: A) densification of guest molecules in solution, B) appearance of polyhedral water cages, and C) development of sI and sII crystallites.

Densification of guest molecules

The blob is a cluster of solvent-separated guests (SSG). We use the number of guests in the largest blob as order parameter for the advance of the densification of guest molecules from solution; we call this the LCSSG OP. In order to distinguish the blobs from the bulk guest phase and guest-only clusters, the contact-pair configurations between guest molecules must be excluded. We first identify pairs of solvent-separated guest (SSG) molecules based on the guest-guest distance, then use a clustering algorithm to connect the SSG pairs and identify the largest SSG cluster. For the M guest, SSG configurations occur at distances between 5 Å and 9 Å.[17] This range of separations for the SSG can be gleaned either from the potential of mean force (PMF) to bring the guests together in water or, as a good approximation, from the radial distribution function (RDF) of the clathrate crystals in which neighbor guests are separated by pentagonal or hexagonal rings of water molecules.[17] The LCSSG OP can be used to follow the advance from solution to blob; we note however that LCSSG OP is insensitive to the ordering of the SSG and the water molecules, and cannot distinguish blob from guest-filled amorphous or crystalline clathrates.

In addition to the number of guests in the largest blob, we define the guest-coordination (GC) OP as the average guest-guest coordination in the largest blob. The coordination of each guest is determined by counting the number of guest neighbors within 9 Å. The average coordination in bulk amorphous or crystalline clathrates with all cages occupied should be between 12 (the coordination in a 5^{12} cage) and 16 (the coordination in a $5^{12}6^4$ cage). The GC OP has similarities to the ζ_{gg1} OP of Ref. [11] which was used in that work as the leading reaction coordinate for driving the crystallization of CO_2 hydrate. A significant difference, however, is that ζ_{gg1} is a global OP, while GC is a local OP, defined for the largest

blob. The pitfalls of using global order parameters for the study of the mechanisms and rates of nucleation of crystals has been stressed by ten Wolde et al.[47] The guest-coordination OP is as a measure of the compactness of the blob and it should be relevant to the nucleation coordinate, as is has been shown that the nascent clathrate cages are stabilized by guest molecules in its first neighbor shell.[6,9,18]

Appearance of polyhedral water cages

The building blocks of the clathrates are the hydrogen-bonded water polyhedra $5^{12}6^{n}$ with n = 0, 2, 3 and 4. The $5^{12}6^{3}$ cages are not native to sI or sII but occur in amorphous clathrates[17,21] and at the interface between sI and sII phases.[43,48] The $5^{12}6^{n}$ cages were identified with the algorithm of Reference 43, which first finds the five- and six-membered rings[49] of water molecules within 3.5 Å, and then searches for five-membered (six-membered) rings that have five (six) other five-membered rings connected on each edge. We refer to this structures, that are half a clathrate cage, as a "cup". The $5^{12}6^{n}$ cages are built by merging cups. The number of clathrate cages (the cage OP) distinguishes the solution and the blob, which in principle are devoid of cages, from the amorphous and crystalline clathrates. The cage OP, however, does not indicate whether the growing nucleus is amorphous or crystalline.[21]

Development of crystallinity

Each water molecule in the clathrate crystals is hydrogen-bonded to four other water molecules and constitutes a vertex shared by four polyhedral cages. We denote the water vertices by v_{jklm}, where the indexes j, k, l and m are the number of 5^{12}, $5^{12}6^{2}$, $5^{12}6^{3}$, and $5^{12}6^{4}$ cages, respectively that converge in that vertex. The sI lattice is comprised of 5^{12} and $5^{12}6^{2}$ cages and contains two types of vertices: the v_{0400} shared by four $5^{12}6^{2}$ cages and the v_{1300} that

involves one 5^{12} and three $5^{12}6^2$ cages. The sII lattice is tiled by 5^{12} and $5^{12}6^4$ cages and contains three distinct vertices: the v_{4000} vertex, that involves four 5^{12} cages and the v_{3001} and v_{2002} vertices that belong to 5^{12} and $5^{12}6^4$ cages. Figures 7.2 and 7.3 show the spatial distribution of these vertices in the sI and sII crystals, respectively.

We quantify the crystallinity of the clathrates by determining the number of vertices of sI-type and sII-type. A further requirement that the four neighbors of the sI-type (sII-type) vertices are also of sI-type (sII-type) would ensure that these vertices belong to the bulk of an sI (sII) crystallite. This latter requirement of a vertex to be bonded (i.e. at 3.5 Å) of a vertex of the same type would be analogously to ten Wolde et al.'s definition of crystalline bonds for local bond-order parameters.[47] The vertex order parameter accounts for all the water molecules in the sI and sII crystals and differentiates the two crystal polymorphs. The approach used to identify sI and sII could be generalized for the identification of other crystals of the Frank-Kasper family to which the clathrates belong, as all Frank-Kasper structures result from the packing of the four polyhedra considered in this work.[50-52] For example, bromine hydrate crystallizes in the tetragonal structure tsI,[53] also known as the Frank-Kasper s phase, that contains nine distinct vertices (v_{1300}, v_{3010}, v_{2110}, v_{1120}, v_{0310}, v_{0220}, v_{2200}, v_{1210} and v_{0400}) two of which (v_{1300} and v_{0400}) occur in sI and none in sII. Although the sI and tsI phases share two vertex types, the two phases can be differentiated by using the fact that complete $5^{12}6^2$ cages that do not share vertices with $5^{12}6^3$ cages only occur in the sI clathrate lattice.

The number of sI-type and sII-type vertices is an appropriate OP to monitor the development of crystallinity from solution or from amorphous clathrates. This vertex OP can be used as global or local order parameters. The global order parameter identifies the total number of vertex types in a configuration. As a local OP, the water molecules can be

classified in terms of the number and identity of the polyhedral cages they belong to. A water that is a v_{0400} or v_{1300} vertex is a sI-water, v_{4000}, v_{3001} or v_{2002} vertex is a sII-water, water molecules with four indexes different from those above are assumed to be amorphous clathrate (crystalline structures different from sI and sII are rare in clathrates); sI (sII) crystallites are found by clustering of sI-water (sII-water) molecules within first neighbor distances (3.5 Å). Vertices of a specific clathrate crystal structure that are not four-coordinated to others of the same crystal type identify the interfaces between crystalline domains in a polycrystalline structure. Water molecules at the clathrate-liquid interface belong to just one to three polyhedral cages, while the water in the solution phase or in ice belongs to no polyhedral cage. If ice were present or presumed to form in the simulations, the CHILL algorithm, based on Steinhardt bond-order parameters, can be used to identify water molecules that belong to the ice phase.[54]

The OPs for clathrate crystallinity developed in this work are exclusively based on the ordering of the water molecules. Alternative OPs based on the ordering of the guests could be constructed, as the network formed by the guests of the fully filled clathrates is the topological dual of the network formed by the water molecules. For example, the guest inside a dodecahedron plus the guests in its twelve neighbor cages form an icosahedron, the dual of the dodecahedron. While in principle no more difficult to implement than the water-based OPs, guest-based OPs for crystalline order in clathrates are less convenient because i) the dual cages formed by the guests are inherently larger than the water cages (the water cages encapsulate the guests) therefore a guest-based OP may not identify small or nascent crystallites, and ii) not all the cages in the clathrates are filled with guests; a sizeable fraction of 5^{12} cages are usually empty, decreasing the symmetry of the guest ordering in the clathrate.

The latter is a more fundamental limitation for the use of guest-based OP to detect and quantify crystallinity in clathrate hydrates.

Order Parameter Analysis of Clathrate Formation

In what follows we illustrate the use of the order parameters for the processes of melting and growth of clathrate crystals, and the nucleation and growth of hydrate from a two-phase solution.

Growth and melting of clathrate crystals

We analyzed two simulation trajectories that started from identical three-phase configuration in which about half the simulation cell is occupied by an M-filled sI hydrate and the other half contained a saturated aqueous solution of M and a separate M fluid phase.[18] One of the simulations was evolved at temperature 5 K above the melting point of the crystal, leading to its melting. The other was run at 5 K below the melting temperature and resulted in growth of the hydrate. The upper panel of Figure 7.4 displays the size of the largest clusters of SSG along these trajectories. The LCSSG OP monitors the change of the size of the guest-rich phase(s) with time, but cannot tell whether the sII crystal grew from the sI crystal. The lower panel of Figure 7.4, that shows the number of sI-type and sII-type water vertices as a function of time, demonstrates that all the growth was due to sI.

In cases where there is formation of both sI and sII, mapping of the water molecules according to their individual vertex indexes permits the identification of sI and sII crystalline domains. Figure 7.5 presents the time evolution of the fraction of vertices (i.e. water molecules) that belong to clathrate cages and their assignment to sI-type, sII-type and amorphous- or interfacial-types for the growth of guest-free clathrate from supercooled water. The simulation started from a slab of sI crystal in contact with liquid water;[43] after a

feeble attempt to grow the sI crystal, the system developed a layer of $5^{12}6^3$ cages (identified as amorphous/interfacial) at the surface of sI, from which it nucleated the sII crystal (final configuration shown in the lower panel of Figure 7.5). The vertex OPs correctly identify the sI and sII domains and the interfacial amorphous layer between them.

Nucleation of clathrate hydrates at high supercooling

We analyzed the time evolution of the size of the largest cluster of solvent-separated guests (LCSSG OP), the average coordination of the guests in that cluster (GC OP), the total number of polyhedral clathrate cages (cage OP) and the number of sI-type and sII-type vertices (vertex OPs) in eleven independent simulations that nucleated and grew clathrate hydrates from a saturated aqueous solution in contact with a fluid of M guest molecules at 500 atm and 210 K.[17] The temperature of the simulations is ~30% lower than the equilibrium coexistence temperature for the crystalline clathrates: sI is the most stable M hydrate crystal (T_m^{sI} = 307±2 K) and sII is slightly less stable (T_m^{sII} = 303±1K).[18] It is also important to note that the amorphous clathrate hydrate of the M guest (T_m^{A} = 276±6 K[21]) and the crystalline guest-free clathrates ($T_m^{sII\text{-}empty} \approx 250$ K[43]) are metastable with respect to the M clathrate crystals but more stable than the liquid solution at the temperature of the simulations.

The eleven trajectories share similar traits: there is an induction period that involves the creation of clusters of solvent-separated guests followed by the creation of clathrate cages within the blob, until a critical blob is formed, initiating a fast growth of clathrate cages. This fast growth results in a region of amorphous clathrate solid that subsequently nucleates and grows guest-free sII crystal. The OP analysis of Figures 7.6 and 7.7

demonstrates the time separation between these steps for a representative simulation trajectory.

The formation of blobs from the dilute aqueous solution is the first step in the pathway of formation of clathrates. Subcritical clusters of SSG form and dissolve back into solution. Clathrate cages appear within the blobs[17] once the SSG cluster has reached a critical size and connectivity. In the trajectory of Figure 7.6 the first cages appear at ~30 ns, coinciding with a sudden increase in the average guest coordination and blob size. The reorganization of the water molecules in the SSG clusters to yield clathrate cages stabilizes the blobs. Nevertheless, not all the blobs that generate cages survive and grow.[17] The critical number of clathrate cages in a blob that leads to its growth is about 3 for the deeply supercooled conditions of these simulations.[17] The size of the blobs that contain these few cages, however, is considerably larger, with about 20 guest molecules. The larger number of guests compared to the number of cages is consistent with previous results showing that the cages are stabilized by the presence of guests in their first solvation shell.[6,17]

The sII-type vertices dominate in the initial clathrate nuclei due to the preponderance of face-sharing dodecahedra (Figure 7.7), as also observed in previous studies.[9,10,18] While this may suggest that the initial nucleus is crystalline, a more strict assignment of crystallinity based not only on the vertex indexes but also on their connectivity to other vertices of the same type, demonstrates that there is no long-range crystalline order in the initial nucleus. After the nucleus of SSG guests and polyhedral cages reaches a critical size, new polyhedral water cages form at a rate that outstrips the rate of mass transfer of guest molecules, therefore the cages form empty: note in Figure 7.6 the plateau in the size of the LCSSG after 70 ns, while the number of cages continues to increase. The guest-free regions have a high degree of crystallinity (Figure 7.7) that may be

due to their formation at relatively low driving force. The crystallization of the metastable guest-free sII clathrate is favored by the low temperatures and the scarce solubility of the guest, and it is always preceded by the creation of guest-filled clathrate cages: the cages can grow empty at $T < 250$ K, but guest molecules are necessary to nucleate the first polyhedral cages. This is consistent with previous work that demonstrated that in the absence of guest molecules, the guest-free clathrates do not nucleate spontaneously from supercooled liquid water even under conditions of negative pressure for which the empty sII phase is the most stable phase of water.[43]

Conclusions

We developed order parameters to distinguish between dilute solution, blob, amorphous clathrates and crystalline clathrates. These order parameters are appropriate for monitoring the advance of the multistep crystallization of clathrate hydrates, making them valuable for the efficient implementation of methods to sample the rare nucleation events.

The vertex order parameters of this work are, to the best of our knowledge, the first that distinguish amorphous from crystalline clathrates and molecules in the sI crystal from molecules in the sII crystal. The vertex OPs can be implemented as global or local OP and can be used to investigate the growth over time of different crystalline domains and their consolidation into larger crystallites. Simulations[21] and experiments[55-57] of formation of methane clathrate show that the metastable sII clathrate is the first crystal to form. The vertex order parameters should be useful for monitoring the formation of distinct crystallites and the transformations between polymorphs.

Analysis of the evolution along crystallization trajectories of the order parameters proposed in this work should help assess what elements of the three major mechanistic hypotheses of clathrate crystallization are valid, and under which conditions. The Labile

Cluster Hypothesis proposes the existence of individual clathrate cages in solution that live enough to agglomerate with each other. The identification of polyhedral cages in solution indicates that individual cages are short-lived and do not last long enough to agglomerate. The Local Structuring Hypothesis indicates that the clathrate nucleates through an ordering of the guest molecules in the positions they would have in the crystal lattice, immediately followed by the reorganization of the water molecules to form the polyhedral clathrate cages. The simulations of spontaneous clathrate nucleation indicate that clathrate cages already form with the guests are at solvent-separated distances but not not necessarily ordered as they would be in a clathrate crystal. The Blob Hypothesis proposes that the nucleation of the clathrate crystal takes place through the formation of an amorphous intermediate. The OP analysis for simulations at high supercooling evidences a separation of time scales between the formation of the blob, the appearance of the cages within the blob and the development of crystal domains. Recent determination of the critical radius of spherical amorphous and crystalline clathrate nuclei demonstrate that, for each temperature, the amorphous critical nucleus is always larger than the crystalline critical nucleus.[21] Whether the blob produces amorphous nuclei, or only crystalline nuclei, at low supercooling is still an open question that could be monitored with the order parameters proposed in this work.

Acknowledgements

We gratefully acknowledge support by the National Science Foundation through award CHE-1012651 to VM. We thank the Center of High Performance Computing of the University of Utah for allocation of computing time.

References

(1) Sloan, E. D.; Koh, C. A. *Clathrate Hydrates of Natural Gases*, 3rd ed.; CRC Press/Taylor-Francis: Boca Raton, 2007.

(2) Sum, A. K.; Koh, C. A.; Sloan, E. D. *Ind. Eng. Chem. Res.* **2009**, *48*, 7457.

(3) Sloan, E. D. *Nature* **2003**, *426*, 353.

(4) Zhang, X.; Hester, K. C.; Ussler, W.; Walz, P. M.; Peltzer, E. T.; Brewer, P. G. *Geophys. Res. Lett.* **2011**, *38*, L08605.

(5) Ripmeester, J. A.; Alavi, S. *ChemPhysChem* **2010**, *11*, 978.

(6) Guo, G. J.; Zhang, Y. G.; Liu, H. *J. Phys. Chem. C* **2007**, *111*, 2595.

(7) Guo, G. J.; Zhang, Y. G.; Li, M.; Wu, C. H. *J. Chem. Phys.* **2008**, *128*, 8.

(8) Moon, C.; Taylor, P. C.; Rodger, P. M. *J. Am. Chem. Soc.* **2003**, *125*, 4706.

(9) Hawtin, R. W.; Quigley, D.; Rodger, P. M. *Phys Chem Chem Phys* **2008**, *10*, 4853.

(10) Walsh, M. R.; Koh, C. A.; Sloan, E. D.; Sum, A. K.; Wu, D. T. *Science* **2009**, *326*, 1095.

(11) Radhakrishnan, R.; Trout, B. L. *Journal of Chemical Physics* **2002**, *117*, 1786.

(12) Moon, C.; Taylor, P. C.; Rodger, P. M. *Can J Phys* **2003**, *81*, 451.

(13) Moon, C.; Hawtin, R. W.; Rodger, P. M. *Faraday Discuss.* **2007**, *136*, 367.

(14) Zhang, J.; Hawtin, R. W.; Yang, Y.; Nakagava, E.; Rivero, M.; Choi, S. K.; Rodger, P. M. *J. Phys. Chem. B* **2008**, *112*, 10608.

(15) Vatamanu, J.; Kusalik, P. G. *Phys. Chem. Chem. Phys* **2010**, *12*, 15065.

(16) Sloan, E. D.; Fleyfel, F. *AIChE* **1991**, *37*, 1281.

(17) Jacobson, L. C.; Hujo, W.; Molinero, V. *J. Phys. Chem. B* **2010**, *114*, 13796.

(18) Jacobson, L. C.; Hujo, W.; Molinero, V. *J. Am. Chem. Soc.* **2010**, *132*, 11806.

(19) Liang, S.; Kusalik, P. G. *Chemical Science* **2011**, *In Press*.

(20) Matsumoto, M. *Journal of Physical Chemistry Letters* **2010**, *1*, 1552.

(21) Jacobson, L.; Molinero, V. *J. Am. Chem. Soc.* **2011**, *DOI: 10.1021/ja201403q*

(22) Dellago, C. *Advanced Computer Simulation Approaches for Soft Matter Sciences III*, 2008.

(23) Dellago, C. *Atomistic Approaches in Modern Biology: from Quantum Chemistry to Molecular Simulations*, 2007.

(24) Bolhuis, P. G.; Chandler, D.; Dellago, C.; Geissler, P. L. *Annu. Rev. Phys. Chem.* **2002**, *53*, 291.

(25) Dellago, C.; Bolhuis, P. G.; Geissler, P. L. *Adv. Chem. Phys.* **2003**, *123*, 1.

(26) Peters, B.; Trout, B. L. *J. Chem. Phys.* **2006**, *125*, 054108.

(27) Peters, B.; Beckham, G. T.; Trout, B. L. *J. Chem. Phys.* **2007**, *127*, 034109.

(28) van Erp, T. S.; Moroni, D.; Bolhuis, P. G. *J. Chem. Phys.* **2003**, *118*, 7762.

(29) van Erp, T. S.; Bolhuis, P. G. *J. Comput. Phys.* **2005**, *205*, 157.

(30) Allen, R. J.; Frenkel, D.; ten Wolde, P. R. *J. Chem. Phys.* **2006**, *124*, 024102.

(31) Allen, R. J.; Warren, P. B.; ten Wolde, P. R. *Phys. Rev. Lett.* **2005**, *94*, 018104.

(32) Valeriani, C.; Allen, R. J.; Morelli, M. J.; Frenkel, D.; ten Wolde, P. R. *J. Chem. Phys.* **2007**, *127*, 114109.

(33) Laio, A.; Rodriguez-Fortea, A.; Gervasio, F.; Ceccarelli, M.; Parrinello, M. *J. Phys. Chem. B* **2005**, *109*, 6714.

(34) Laio, A.; Gervasio, F. L. *Rep. Prog. Phys.* **2008**, *71*, 126601.

(35) Dickson, B. M.; Makarov, D. E.; Henkelman, G. *J. Chem. Phys.* **2009**, *131*, 074108.

(36) Escobedo, F. A.; Borrero, E. E.; Araque, J. C. *J. Phys.: Condens. Matter* **2009**, *21*, 333101.

(37) Allen, R. J.; Frenkel, D.; ten Wolde, P. R. *J. Chem. Phys.* **2006**, *124*, 194111.

(38) Allen, R. J.; Valeriani, C.; Wolde, P. R. t. *J. Phys.: Condens. Matter* **2009**, *21*, 463102.

(39) Rodger, P. M. *Ann. N. Y. Acad. Sci.* **2000**, *912*, 474.

(40) Steinhardt, P. J.; Nelson, D. R.; Ronchetti, M. *Phys. Rev. B* **1983**, *28*, 784.

(41) Errington, J. R.; Debenedetti, P. G. *Nature* **2001**, *409*, 318.

(42) Molinero, V.; Moore, E. B. *J. Phys. Chem. B* **2009**, *113*, 4008.

(43) Jacobson, L. C.; Hujo, W.; Molinero, V. *J. Phys. Chem. B* **2009**, *113*, 10298.

(44) Moore, E. B.; Molinero, V. *J. Chem. Phys.* **2010**, *132*, 244504.

(45) Plimpton, S. J. *J. Comput. Phys.* **1995**, *117*, 1.

(46) Jacobson, L. C.; Molinero, V. *J. Phys. Chem. B* **2010**, *114*, 7302.

(47) ten Wolde, P.-R.; Ruiz-Montero, M. J.; Frenkel, D. *Faraday Discuss.* **1996**, *104*, 93.

(48) Vatamanu, J.; Kusalik, P. G. *J. Am. Chem. Soc.* **2006**, *128*, 15588.

(49) Matsumoto, M.; Baba, A.; Ohmine, I. *J. Chem. Phys.* **2007**, *127*, 134504.

(50) Frank, F. C.; Kasper, J. S. *Acta Crystallographica* **1958**, *11*, 184.

(51) Dutour Sikiric, M.; Delgado-Friedrichs, O.; Deza, M. *Acta Crystallographica Section A*, *66*, 602.

(52) Matsumoto, M.; Tanaka, H. *Submitted* **2011**.

(53) Goldschleger, I. U.; Kerenskaya, G.; Janda, K. C.; Apkarian, V. A. *J. Phys. Chem. A* **2008**, *112*, 787.

(54) Moore, E. B.; de la Llave, E.; Welke, K.; Scherlis, D. A.; Molinero, V. *Phys. Chem. Chem. Phys.* **2010**, *133*, 034513.

(55) Staykova, D. K.; Kuhs, W. F.; Salamatin, A. N.; Hansen, T. *J. Phys. Chem. B* **2003**, *107*, 10299.

(56) Murshed, M. M.; Kuhs, W. F. *J. Phys. Chem. B* **2009**, *113*, 5172.

(57) Schicks, J. M.; Ripmeester, J. A. *Angew. Chem., Int. Ed.* **2004**, *43*, 3310.

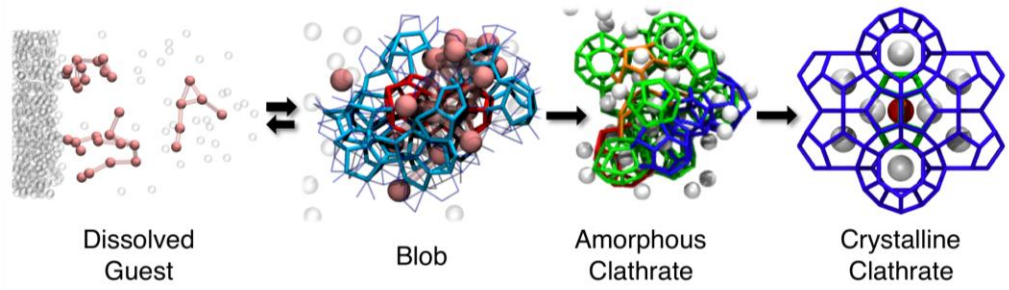

Figure 7.1. Multistep blob mechanism of crystallization clathrate hydrates. The dissolved guests form blobs -clusters of solvent-separated guests- within which the water molecules reorganize to produce polyhedral clathrate cages, resulting in an amorphous clathrate nucleus. The amorphous nucleus then reorganizes into a crystalline nucleus and grows a crystalline clathrate or grows a crystal around the amorphous seed. Nucleation of clathrates under conditions of high supercooling, at temperatures well below the melting temperature of the amorphous clathrate, can result in the formation of a metastable amorphous clathrate phase. Colors in the scheme: dissolved guest: clusters of solvent-separated guests shown as connected pink balls, other guests as gray empty balls, water not shown; blob: guests shown as pink balls, half clathrate cages (cups) in cyan, and full clathrate cages in red; amorphous clathrate nucleus: guest shown as white balls and cages with lines colored by type (green is 5^{12}, blue is $5^{12}6^{2}$, red is $5^{12}6^{3}$ and orange is $5^{12}6^{4}$); crystalline clathrate: balls are guests, lines represent connections between water molecules. (Figure reproduced from Ref. [18], with permission from the American Chemical Society).

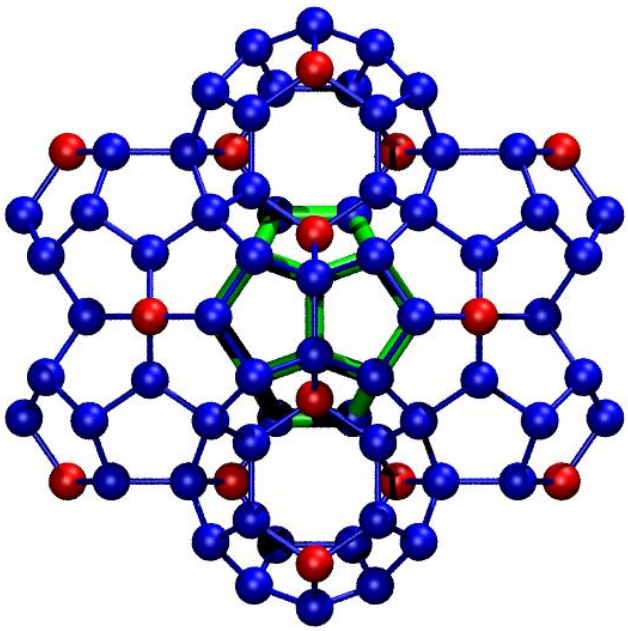

Figure 7.2. Vertex types of the sI clathrate crystal. Only the water network is shown; the water molecules are located in the vertices (balls). The motif of the sI lattice consists of a central dodecahedral cage (green lines) surrounded by twelve $5^{12}6^2$ cages (blue lines). There are two vertex types: v_{1300} (blue balls) identify water molecules shared by one 5^{12} and three $5^{12}6^2$ cages, and v_{0400} (red balls) are water molecules shared by four $5^{12}6^2$ cages.

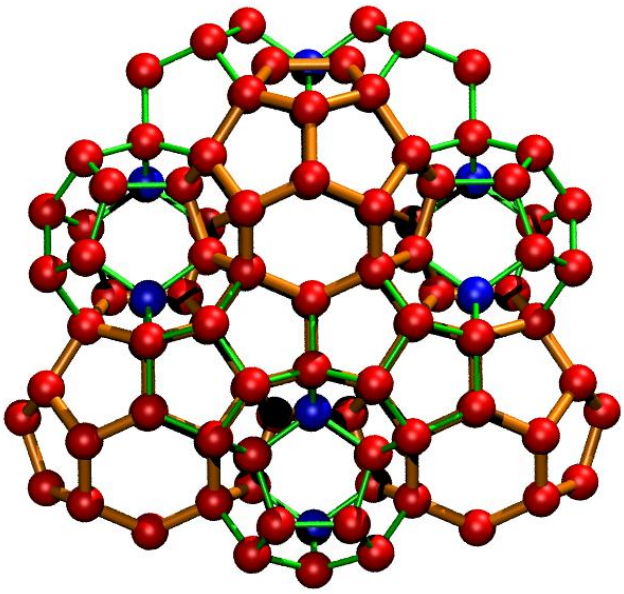

Figure 7.3. Vertex types of the sII clathrate crystal. Only the water network is shown; the water molecules are located in the vertices (balls). The motif of the sII lattice encompasses five $5^{12}6^4$ cages (orange lines) in a tetrahedral arrangement with twelve 5^{12} cages (green lines) attached to the pentagonal faces of the central $5^{12}6^4$ cage plus $5^{12}6^4$ cages attached to the hexagonal faces. There are two vertex types: v_{3001} and v_{2002} (both shown as red balls) are water molecules that belong to both 5^{12} and $5^{12}6^4$ cages, and v_{4000} (blue balls) are water molecules shared by four 5^{12} cages.

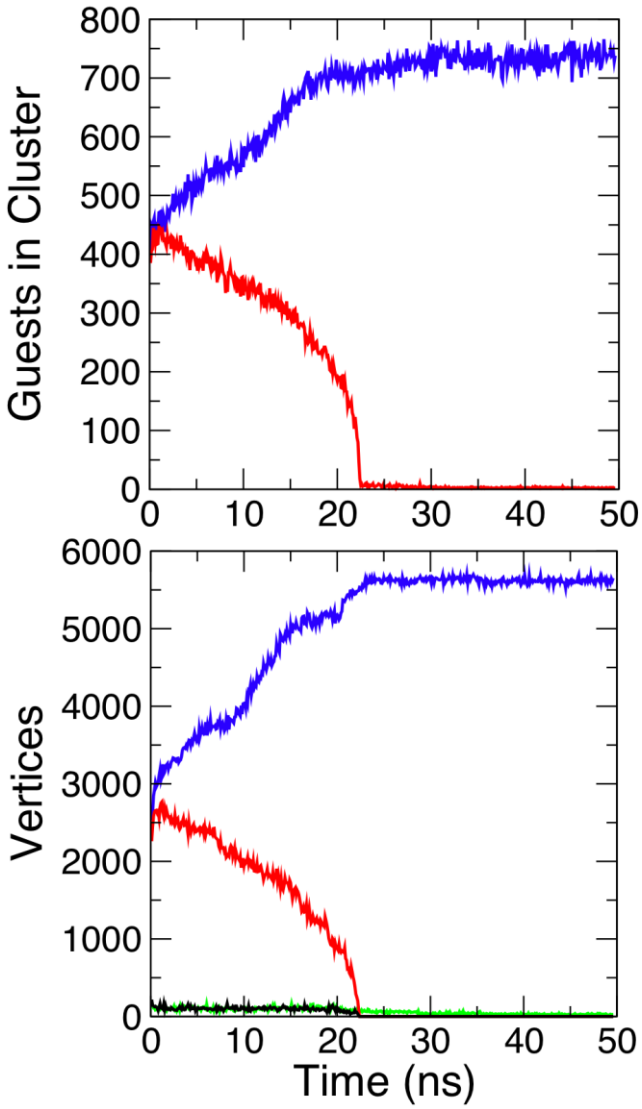

Figure 7.4. Evolution of the size of largest cluster of solvent-separated guests and vertex-crystallinity order parameters during the dissolution and growth of sI clathrate hydrate of the M guest. Upper panel: Number of guest molecules in the largest cluster of solvent-separated guests (that in this case corresponds to the guests in the crystal) for the growth (blue) and dissolution (red) of the crystal. Lower panel: Number sI-type water molecules during the growth (blue) and dissolution (red) of the sI M clathrate hydrate. The number of sII-type vertices for the growth (green) and dissolution (black) are insignificant.

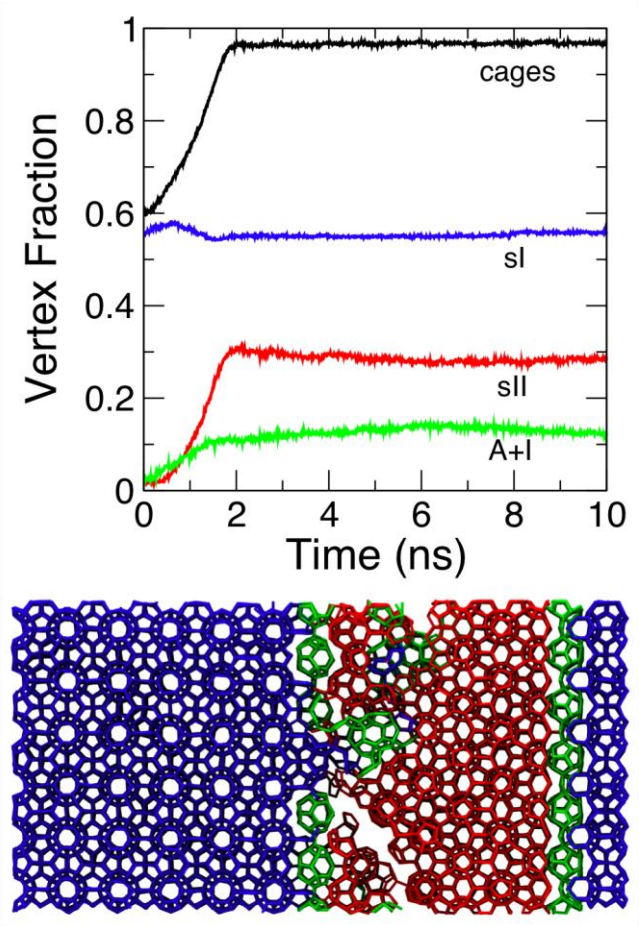

Figure 7.5. Cross nucleation of sI to grow sII from supercooled water. Upper panel: Evolution of order parameters during the growth of guest-free clathrate from supercooled water in a simulation that starts with about half of the water in a sI slab, but grows sII crystal. The fractions of water molecules in vertices that correspond to any clathrate cage type (black), sI clathrate crystal (blue), sII clathrate crystal (green) and interfacial or amorphous clathrate (green) are shown as a function of time. Lower panel: The structure of the simulation cell at t = 10 ns analyzed with the vertex OP distinguishes between sI (blue), sII (red), and amorphous/interfacial (green) regions. The few water molecules that did not crystallize are not shown.

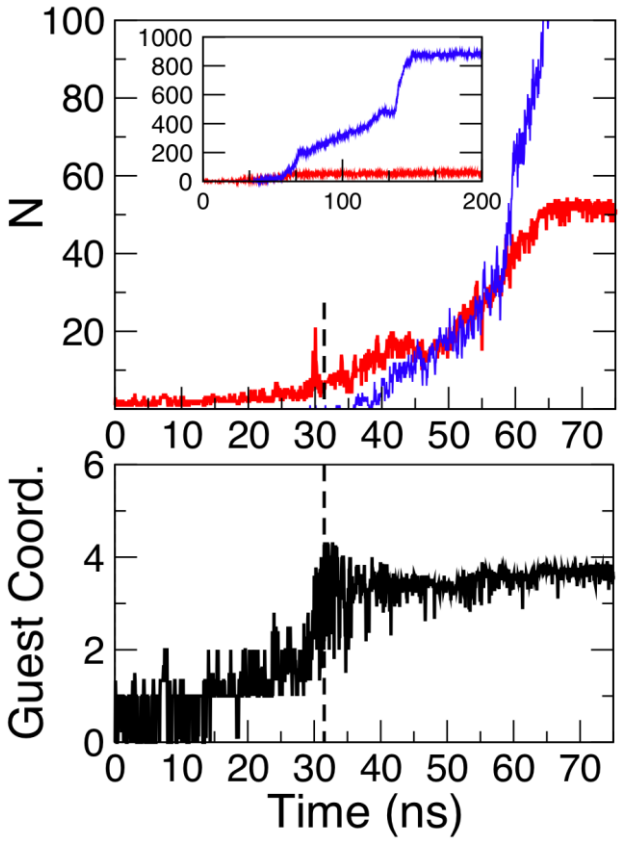

Figure 7.6. Top panel: Number of guests in the largest cluster of solvent-separated guests (LCSSG OP, red line) and the number of total polyhedral cages (cage OP, blue line) as a function of time near the onset of nucleation and for the entire trajectory (inset). The presence of empty polyhedral cages and the growth of the empty sII clathrate result in the number of cages far surpassing the number of guests in the largest SSG cluster. Lower panel: average coordination number of guests in the SSG cluster (GC OP). The vertical dashed line at 31.5 ns signals the time at which the average guest-guest coordination reaches a maximum. Nucleation takes place only when both LCSSG and GC are large enough. Once nucleation gives way to growth, the rate of cage formation outpaces that of guests attaching to the SSG cluster and most cages form empty.

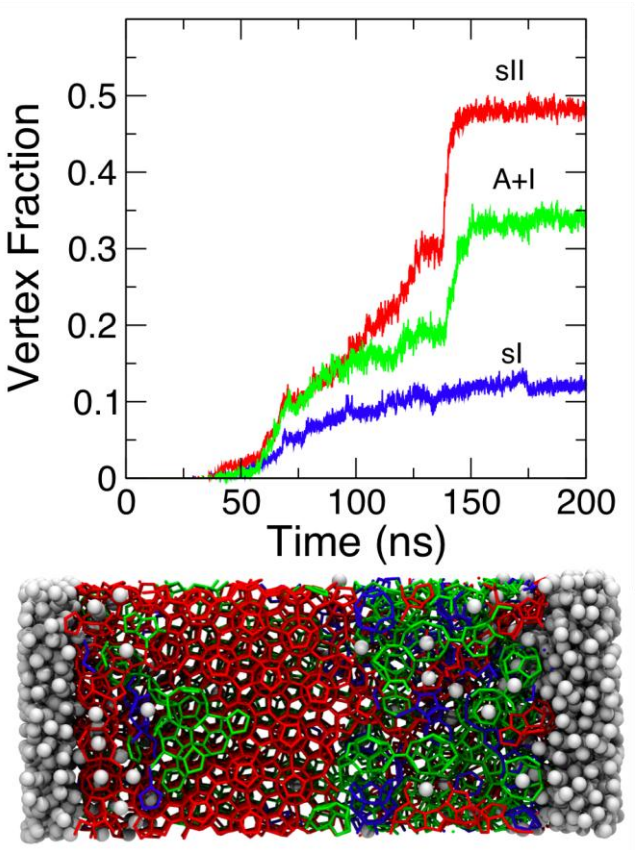

Figure 7.7. Evolution of the normalized vertex OP during the formation of clathrate. Upper panel: Fraction of water molecules identified as sI crystal (blue), sII crystal (red), and amorphous or interfacial clathrate (green) as a function of time for the same nucleation trajectory shown in Figure 6. The clathrate cages formed after ~70 ns are mostly empty. Lower panel: The structure of the simulation cell at the end of the simulation analyzed with the vertex OP distinguishes between sI (blue), sII (red), and amorphous/interfacial (green) regions.